NASA CR-121129

THE PREDICTION OF THREE-DIMENSIONAL LIQUID-PROPELLANT ROCKET NOZZLE ADMITTANCES

by

W. A. Bell and B. T. Zinn

GEORGIA INSTITUTE OF TECHNOLOGY

prepared for

NATIONAL AERONAUTICS AND SPACE ADMINISTRATION

NASA Lewis Research Center
Grant NGL 11-002-085
Richard J. Priem, Project Manager

Requests for copies of this report should be referred to:

National Aeronautics and Space Administration
Scientific and Technical Information Facility
P. O. Box 33
College Park, Md. 20740

Report No.	2. Government Accession No.	3. Recipient's Catalog No.
NASA CR-121129		

Title and Subtitle	5. Report Date
THE PREDICTION OF THREE-DIMENSIONAL LIQUID-PROPELLANT ROCKET NOZZLE ADMITTANCES	February 1973
	6. Performing Organization Code
Author(s)	8. Performing Organization Report No.
W. A. Bell and B. T. Zinn	
	10. Work Unit No.
Performing Organization Name and Address	11. Contract or Grant No.
Georgia Institute of Technology Atlanta, Georgia 30332	NGL 11-002-085
	13. Type of Report and Period Covered
Sponsoring Agency Name and Address	Contractor Report
National Aeronautics and Space Administration Washington, D. C. 20546	14. Sponsoring Agency Code

Supplementary Notes

Technical Officer, Richard J. Priem, NASA Lewis Research Center, 21000 Brookpark Road, Cleveland, Ohio 44135

Abstract

Crocco's three-dimensional nozzle admittance theory is extended to be applicable when the amplitudes of the combustor and nozzle oscillations increase or decrease with time. An analytical procedure and a computer program for determining nozzle admittance values from the extended theory are presented and used to compute the admittances of a family of liquid-propellant rocket nozzles. The calculated results indicate that the nozzle geometry, entrance Mach number and temporal decay coefficient significantly affect the nozzle admittance values. The theoretical predictions are shown to be in good agreement with available experimental data.

Key Words (Suggested by Author(s))	18. Distribution Statement
Combustion instability Liquid rockets Nozzles	Unclassified - unlimited

Security Classif. (of this report)	20. Security Classif. (of this page)	21. No. of Pages	22. Price*
Unclassified	Unclassified	55	$3.00

* For sale by the National Technical Information Service, Springfield, Virginia 22151

ABSTRACT

Crocco's three-dimensional nozzle admittance theory is extended to be applicable when the amplitudes of the combustor and nozzle oscillations increase or decrease with time. An analytical procedure and a computer program for determining nozzle admittance values from the extended theory are presented and used to compute the admittances of a family of liquid-propellant rocket nozzles. The calculated results indicate that the nozzle geometry, entrance Mach number and temporal decay coefficient significantly affect the nozzle admittance values. The theoretical predictions are shown to be in good agreement with available experimental data.

TABLE OF CONTENTS

INTRODUCTION 1

SYMBOLS 2

ANALYSIS 4

Derivation of the Wave Equations 4

Method of Solution 9

RESULTS AND DISCUSSION 12

Admittances for Longitudinal Modes 12

Admittances for Mixed First Tangential-Longitudinal Modes 14

Effect of Decay Coefficient upon Admittance Data 15

SUMMARY AND CONCLUSIONS 15

FIGURES 16

APPENDIX 26

REFERENCES 55

LIST OF ILLUSTRATIONS

Figure	Title	Page
1	Typical Mathematical Model Used in Combustion Instability Analyses of Liquid Rocket Engines	16
2	Nozzle Contour	17
3	The Effect of Nozzle Half-Angle on the Theoretical and Experimental Nozzle Admittance Values for Longitudinal Modes	18
4	The Effect of Entrance Mach Number on the Theoretical and Experimental Nozzle Admittance Values for Longitudinal Modes	19
5	The Effect of the Radii of Curvature on the Theoretical and Experimental Nozzle Admittance Values for Longitudinal Modes	20
6	The Effect of the Nozzle Half-Angle on the Theoretical and Experimental Nozzle Admittance Values for Mixed First Tangential-Longitudinal Modes	21
7	The Effect of Entrance Mach Number on the Theoretical and Experimental Nozzle Admittance Values for Mixed First Tangential-Longitudinal Modes	22
8	The Effect of the Radii of Curvature on the Theoretical and Experimental Nozzle Admittance Values for Mixed First Tangential-Longitudinal Modes	23
9	Effect of the Temporal Decay Coefficient on the Theoretical Nozzle Admittance Values for Longitudinal Modes	24
10	Effect of the Temporal Decay Coefficient on the Theoretical Nozzle Admittance Values for Mixed First Tangential-Longitudinal Modes	25
A-1	Flow Chart for the Nozzle Admittance Computer Program	45

LIST OF TABLES

Table	Title	Page
1	Values of Transverse Mode Eigenvalues, S_{mn}	13
A-1	List of Subroutines in the Computer Program Used to Determine the Irrotational Nozzle Admittance	27
A-2	Definition of FORTRAN Variables	28
A-3	Input Parameters	32
A-4	Output Parameters	33
A-5	Listing of the Computer Program Used to Determine the Irrotational Nozzle Admittance	34
A-6	Sample Output	44

INTRODUCTION

The interaction between the pressure oscillations inside an unstable rocket combustion chamber and the wave motion in the convergent section of the exhaust nozzle can have a significant effect on the stability characteristics of the rocket motor and is an important consideration in analytical studies concerned with the prediction of the stability of liquid-propellant rocket engines. This report is concerned with the investigation of this interaction.

To determine the stability of a liquid-propellant rocket engine, the equations describing the behavior of the oscillatory flow field throughout the rocket motor must be solved. To simplify the problem, it is convenient to analyze the oscillations in the combustion chamber and the nozzle separately. For such an analysis, the combustion chamber extends from the injector face to the nozzle entrance as shown in Fig. 1. All the combustion is assumed to take place in the combustion chamber where the mean flow Mach number is generally assumed to be low. On the other hand, no combustion is assumed to take place in the nozzle and its mean flow Mach number increases from a low value at the nozzle entrance to unity at the throat. Downstream of the throat the flow is supersonic and disturbances in this region cannot propagate upstream and affect the chamber conditions. Therefore, in combustion instability studies it is only necessary to consider the behavior of the oscillations in the converging section of the nozzle since only these oscillations can influence the conditions in the combustion chamber.

The nozzle admittance[1,2] is the boundary condition that must be satisfied by the combustor flow oscillations at the nozzle entrance. Defined as the ratio of the axial velocity perturbation to the pressure perturbation at the nozzle entrance, the nozzle admittance can also be used to determine whether wave motion in the nozzle under consideration adds or removes energy from the combustor oscillations. Furthermore, this boundary condition influences the structures and resonant frequencies of the natural modes of the combustor under investigation.

To theoretically determine the nozzle admittance, the equations which describe the behavior of the waves in the convergent section of the exhaust nozzle must be solved. These equations have been developed by

Crocco[2] and were solved numerically to obtain admittance values for one- and three-dimensional oscillations. These values were tabulated over a wide range of frequencies and entrance Mach numbers for a specific nozzle geometry. By applying the scaling technique developed in Ref. 2, the admittances of related nozzles can be determined. It was pointed out,[2] however, that interpolation of the tabulated values can result in large errors in the predicted nozzle admittances; furthermore, the accuracy of the scaling procedure is open to question. In addition, Crocco's theory is only applicable to constant amplitude periodic wave motions, and in its present form it cannot be applied to cases where the amplitude of the oscillations varies in time.

In this report, the equations needed for computing the nozzle admittance are presented and their solutions are outlined. Crocco's theory is extended to account for wave-amplitude variation with time. Typical theoretical predictions are shown and compared with available experimental data. The effects of the nozzle geometry and chamber Mach number on the nozzle admittance are presented in plots showing frequency dependence of the real and imaginary parts of the nozzle admittance. The effects of the decay coefficient are also assessed. A manual describing the use of the computer program which calculates nozzle admittance values along with a program listing is presented in the appendix.

SYMBOLS

A, B, C	variable coefficients defined below Eq. (14)
c	nondimensional speed of sound, $c^*/\bar{c}^*_o$
$\underset{\sim}{e}_\varphi$, $\underset{\sim}{e}_\psi$, $\underset{\sim}{e}_\theta$	unit vectors
i	$\sqrt{-1}$
J_m	Bessel function of the first kind of order m
$K(\psi,\theta,t)$	a function having the following space and time dependence:

$$J_m\left[S_{mn}\left(\frac{\psi}{\psi_w}\right)^{\frac{1}{2}}\right]e^{i\omega t \pm im\theta}$$

M	Mach number at the nozzle entrance

m	number of mode diametral nodal lines
n	number of mode tangential nodal lines
p	nondimensional pressure, $p^*/\bar{p}^*_o$
q	nondimensional velocity, $\underset{\rightarrow}{q}^*/\bar{c}^*_o$
r	nondimensional radius, r^*/r^*_c
r_{cc}	nondimensional radius of curvature at the nozzle entrance, r_{cc}^*/r^*_c
r_{ct}	nondimensional radius of curvature at the nozzle throat, r_{ct}^*/r^*_c
S	nondimensional frequency, $\omega^* r^*_c/\bar{c}^*$
S_{mn}	the nth root of the equation $$\frac{dJ_m(x)}{dx} = 0$$
t	nondimensional time, $t^*\bar{c}^*_o/r^*_o$
u	nondimensional axial velocity component, $u^*/\bar{c}^*_o$
v	nondimensional radial velocity component, $v^*/\bar{c}^*_o$
w	nondimensional tangential velocity component, $w^*/\bar{c}^*_o$
y	irrotational specific nozzle admittance defined in Eq. (13) $$y = \bar{\rho}^*\bar{c}^* \frac{u'^*}{p'^*} = \gamma\bar{\rho}\bar{c}\frac{u'}{p'}$$
z	nondimensional axial coordinate, z^*/r^*_c
γ	ratio of specific heats
ζ	a function used to compute the nozzle admittance; defined below Eq. (13)
θ	tangential coordinate, radians
θ_1	nozzle half-angle, degrees
λ	nondimensional temporal decay coefficient, $\lambda^* r^*_c/\bar{c}^*_o$
ρ	nondimensional density, $\rho^*/\bar{\rho}^*_o$
τ	a function used to compute the nozzle admittance; $\tau = 1/\zeta$
φ	nondimensional steady state velocity potential, $\varphi^*/\bar{c}^*_o r^*_c$
Φ	a function describing the φ-dependence of the radial velocity perturbation
ψ	nondimensional steady state stream function, $\frac{1}{2}\bar{\rho}(\varphi)\bar{q}(\varphi)r^2$
ω	nondimensional frequency, $\omega^* r^*_c/\bar{c}^*_o$

Subscripts:

c	evaluated at the chamber wall
i	imaginary part of a complex quantity
o	stagnation value
r	real part of a complex quantity
th	evaluated at the nozzle throat
w	evaluated at the nozzle wall
→	vector quantity

Superscripts:

′	perturbation quantity
—	steady state value
*	dimensional quantity

ANALYSIS

Derivation of the Wave Equations

The equations used by Crocco[2] to compute the nozzle admittance will be developed from the conservation equations. To keep the problem mathematically tractable and yet physically meaningful, the following assumptions were employed.

(1) The nozzle flow is a calorically perfect gas consisting of a single species.

(2) Viscosity and heat conduction are negligible.

(3) The steady state flow is one-dimensional; this assumption implies that the nozzle is slowly converging.

(4) The amplitudes of the waves are small so that only linear terms in the perturbed quantities need to be retained in the conservation equations.

(5) The oscillations are assumed to be irrotational.

Using these assumptions, the equations of motion in nondimensional form become

Continuity

$$\frac{\partial \rho}{\partial t} + \nabla \cdot (\rho q) = 0 \qquad (1)$$

Momentum

$$\frac{\partial \underset{\to}{q}}{\partial t} + \tfrac{1}{2}\nabla \bar{q}^2 = - \frac{1}{\rho}\nabla p \tag{2}$$

and, from the isentropic conditions, $c^2 = p/\rho$ and $p = \rho^{\gamma}$.

To obtain the linearized wave equations, the dependent variables are expressed in the following form:

$$\underset{\to}{q} = \bar{q} + q', \quad p = \bar{p} + p', \quad \rho = \bar{\rho} + \rho' \tag{3}$$

Substituting these expressions into Eqs. (1) and (2), neglecting all non-linear terms involving primed quantities, and separating the resulting system of equations into a set of steady state equations and a set of unsteady equations yield the system of steady state equations:

$$\nabla\cdot(\bar{\rho}\underset{\to}{\bar{q}}) = 0; \quad \bar{c}^2 = \bar{\rho}^{\gamma - 1} = 1 - \frac{\gamma - 1}{2}\bar{q}^2; \quad \bar{p} = \bar{\rho}^{\gamma} \tag{4}$$

and the following system of unsteady linear equations that describe the wave motion:

$$\frac{\partial \rho'}{\partial t} + \nabla\cdot(\underset{\to}{\bar{q}}\rho' + \bar{\rho}\underset{\to}{q'}) = 0 \tag{5}$$

$$\frac{\partial \underset{\to}{q'}}{\partial t} + \nabla(\bar{q}\cdot q') = - \nabla\left(\frac{p'}{\gamma\bar{\rho}}\right) \tag{6}$$

$$p' = \bar{c}^2\rho' \tag{7}$$

To simplify the application of the boundary conditions at the nozzle walls, these wave equations are solved in the orthogonal coordinate system shown in Fig. 1. In this coordinate system the steady state velocity potential φ replaces the axial coordinate z, the steady state stream function ψ replaces the radial coordinate r and the angle θ is used to denote azimuthal variations. Using this coordinate system the velocity vectors can be expressed as follows:

$$\underset{\rightarrow}{\bar{q}} = \bar{q}(\varphi)\,\underset{\rightarrow}{e}_{\varphi}$$

$$\underset{\rightarrow}{q}' = u'\underset{\rightarrow}{e}_{\varphi} + v'\underset{\rightarrow}{e}_{\psi} + w'\underset{\rightarrow}{e}_{\theta}$$

Using the definitions of the steady state velocity potential and stream function for a one-dimensional mean flow, it can be shown[2] that

$$q(\varphi) = \frac{d\varphi}{dz}$$

$$\psi = \tfrac{1}{2}\bar{\rho}(\varphi)\,\bar{q}(\varphi)\,r^2$$

Rewriting Eqs. (5) and (6) in the (φ,ψ,θ) coordinate system yields the following system of equations[2]:

Continuity

$$\frac{\partial}{\partial t}\left(\frac{p'}{\bar{p}}\right) + \bar{q}^2\,\frac{\partial}{\partial\varphi}\left(\frac{\rho'}{\bar{\rho}} + \frac{u'}{\bar{q}}\right) + 2\bar{\rho}\bar{q}\,\frac{\partial}{\partial\psi}\left(\frac{v'}{r\bar{\rho}\bar{q}}\right) + \frac{\bar{\rho}\bar{q}}{2\psi}\,\frac{\partial(rw')}{\partial\theta} = 0 \tag{8}$$

Momentum

φ-component

$$\frac{\partial\left(\frac{u'}{\bar{q}}\right)}{\partial t} + \frac{\partial}{\partial\varphi}\left(\bar{q}^2\,\frac{u'}{\bar{q}}\right) + \frac{\partial}{\partial\varphi}\left(\frac{p'}{\gamma\bar{p}}\right) = 0 \tag{9}$$

ψ-component

$$\frac{\partial}{\partial t}\left(\frac{v'}{r\bar{\rho}\bar{q}}\right) + \bar{q}^2\,\frac{\partial}{\partial\varphi}\left(\frac{v'}{r\bar{\rho}\bar{q}}\right) + \frac{\partial}{\partial\psi}\left(\frac{p'}{\gamma\bar{p}}\right) = 0 \tag{10}$$

θ-component

$$\frac{\partial}{\partial t}(rw') + \bar{q}^2\,\frac{\partial}{\partial\varphi}(rw') + \frac{\partial}{\partial\theta}\left(\frac{p'}{\gamma\bar{p}}\right) = 0 \tag{11}$$

Equations (7) through (11) constitute a system of five equations in the five unknowns -- $\rho'/\bar{\rho}$, $u'/\bar{q}$, $v'/r\bar{\rho}\bar{q}$, rw', and $p'/\gamma\bar{p}$. These equations are solved by the method of separation of variables and the solutions are

$$\frac{u'}{\bar{q}} = \frac{d\Phi(\varphi)}{d\varphi} K(\psi,\theta,t)$$

$$\frac{v'}{r\bar{\rho}\bar{q}} = \Phi(\varphi) \frac{\partial}{\partial\psi}\left[K(\psi,\theta,t)\right]$$

$$rw' = \Phi(\varphi) \frac{\partial}{\partial\theta}\left[K(\psi,\theta,t)\right]$$

$$\frac{p'}{\bar{p}} = -\left[i(\omega - i\lambda)\Phi(\varphi) + \bar{q}^2(\varphi) \frac{d\Phi(\varphi)}{d\varphi}\right] K(\psi,\theta,t)$$

$$\frac{\rho'}{\bar{\rho}} = -\frac{1}{\bar{c}^2}\left[i(\omega - i\lambda) \Phi(\varphi) + \bar{q}^2(\varphi) \frac{d\Phi(\varphi)}{d\varphi}\right] K(\psi,\theta,t)$$

where

$$K(\psi,\theta,t) = \begin{cases} J_m\left[S_{mn}\left(\frac{\psi}{\psi_w}\right)^{\frac{1}{2}}\right] \cos m\theta\, e^{i(\omega - i\lambda)t} & \text{for standing waves} \\ J_m\left[S_{mn}\left(\frac{\psi}{\psi_w}\right)^{\frac{1}{2}}\right] e^{\pm im\theta}\, e^{i(\omega - i\lambda)t} & \text{for spinning waves} \end{cases}$$

These solutions identically satisfy the momentum and energy equations. Substituting these solutions into Eq. (8) and eliminating variables give the following differential equation for the function Φ:

$$\bar{q}^2(\bar{c}^2 - \bar{q}^2) \frac{d^2\Phi}{d\varphi^2} - \bar{q}^2\left[\frac{1}{\bar{c}^2} \frac{d\bar{q}^2}{d\varphi} + 2i(\omega - i\lambda)\right] \frac{d\Phi}{d\varphi}$$

$$+ \left[(\omega - i\lambda)^2 - \frac{\gamma - 1}{2} i(\omega - i\lambda) \frac{\bar{q}^2}{\bar{c}^2} \frac{d\bar{q}^2}{d\varphi} - \frac{S_{mn}^2\bar{c}^2}{r_w^2}\right] \Phi = 0 \qquad (12)$$

The function Φ can be related to the specific acoustic admittance by the formula[2]

$$y = \gamma\bar{\rho}\bar{c} \frac{u'}{p'} = -\frac{\gamma\bar{\rho}\bar{c}\zeta}{\bar{q}^2\zeta + i(\omega - i\lambda)} \qquad (13)$$

where $\zeta = \frac{1}{\Phi}\frac{d\Phi}{d\varphi}$. Using the definition of ζ and Eq. (12), the following differential equation for ζ is derived:

$$\frac{d\zeta}{d\varphi} - \frac{B}{A}\zeta + \zeta^2 = -\frac{C}{A} \qquad (14)$$

where

$$A = \bar{q}^2(\bar{c}^2 - \bar{q}^2)$$

$$B = \bar{q}^2\left[\frac{1}{\bar{c}^2}\frac{d\bar{q}^2}{d\varphi} + 2i(\omega - i\lambda)\right]$$

$$C = \left[(\omega - i\lambda)^2 - \frac{S_{mn}^2\bar{c}^2}{r_w^2} - i(\omega - i\lambda)\ \frac{\gamma - 1}{2}\frac{\bar{q}^2}{\bar{c}^2}\frac{d\bar{q}^2}{d\varphi}\right]$$

Equation (14) is a complex Riccati equation which must be solved numerically to obtain ζ. Once the value of ζ is determined at the nozzle entrance, the nozzle admittance can be computed directly from Eq. (13). Inspection of Eq. (14) shows that the value of ζ depends upon its coefficients A, B, and C which in turn depend upon ω, λ, S_{mn}, and the space dependence of $\bar{q}$ and $\bar{c}$ in the nozzle. The behavior of $\bar{q}$ and $\bar{c}$ in the nozzle can be computed once the value of γ and the nozzle contour are specified.

To determine ζ for given values of ω, λ, S_{mn} and γ and a specific nozzle contour, Eq. (14) must be integrated numerically. A major difficulty which can occur during this integration is that ζ becomes unbounded whenever Φ approaches zero, which causes numerical difficulties in the integration scheme. Crocco and Sirignano[2] noted that this phenomenon occurred for low Mach numbers and high values of ω/S_{mn}. At these Mach numbers and frequencies they developed asymptotic solutions for ζ.

Instead of using the asymptotic solution, an exact numerical solution is obtained in this study. The problem is resolved by introducing a new dependent variable

$$\tau = \frac{1}{\zeta} = \frac{\Phi}{\frac{d\Phi}{d\varphi}}$$

As Φ approaches zero and the magnitude of ζ becomes large, τ becomes small. Introducing the definition of τ into Eq. (14) gives the following Riccati equation for τ

$$\frac{d\tau}{d\varphi} + \frac{B}{A}\tau - \frac{C}{A}\tau^2 = 1 \tag{15}$$

At those regions where ζ becomes unbounded, Eq. (15) is integrated instead of Eq. (14).

Method of Solution

To obtain the nozzle admittance from Eq. (13), values of ζ and τ are computed by numerically integrating Eq. (14) or (15). To evaluate the coefficients A, B, and C, a differential equation that describes the variations of the steady state velocity in the subsonic portion of the nozzle must be derived. Differentiating the continuity equation

$$\bar{\rho} r^2 \bar{q} = \bar{\rho}_{th}\, r_{th}^2\, \bar{q}_{th} = \text{constant} \tag{16}$$

where $\bar{q}_{th}^2 = \bar{c}_{th}^2 = 2/(\gamma + 1)$, and using Eq. (4) yield the following differential equation

$$\frac{d\bar{q}^2}{dr} = \frac{1}{dr/d\bar{q}^2} = -\frac{4}{r_{th}}\left(\frac{2}{\gamma+1}\right)^{\frac{-\gamma-1}{4(\gamma-1)}}\left[\frac{(\bar{q}^2)^{\frac{5}{4}}\left(1 - \frac{\gamma-1}{2}\bar{q}^2\right)^{\frac{2\gamma-1}{2(\gamma-1)}}}{1 - \frac{\gamma+1}{2}\bar{q}^2}\right] \tag{17}$$

Using Eq. (17) and the specified nozzle contour in terms of $r(z)$, the quantity $d\bar{q}/d\varphi$ can be obtained from the relationship

$$\frac{d\bar{q}^2}{d\varphi} = \frac{d\bar{q}^2}{dr}\frac{dr}{dz}\frac{dz}{d\varphi} = 2\frac{d\bar{q}}{dr}\frac{dr}{dz} \tag{18}$$

Once $\bar{q}^2$ is known the corresponding value of $\bar{c}^2(\varphi)$ can be obtained by use of Eq. (4). To evaluate dr/dz in Eq. (18), the nozzle contour shown in Fig. 2 is used. Starting at the combustion chamber the contour is generated by a circular arc of radius r_{cc} turned through an angle θ_1, the nozzle half-angle. This arc connects smoothly to a straight line which is inclined at an angle θ_1 to the nozzle axis. This straight line then joins with another circular arc of radius r_{ct} which turns through an angle θ_1 and ends at the throat. Using this nozzle contour, in regions I, II and III of Fig. 2

$$\left.\frac{dr}{dz}\right|_{I} = - \frac{\left[2r_{ct}(r - r_{th}) - (r - r_{th})^2\right]^{\frac{1}{2}}}{r_{ct} + r_{th} - r}$$

$$\left.\frac{dr}{dz}\right|_{II} = - \tan \theta_1$$

$$\left.\frac{dr}{dz}\right|_{III} = \frac{\left[2r_{cc}(1 - r) - (1 - r)^2\right]^{\frac{1}{2}}}{1 - r_{cc} - r}$$

Utilizing the appropriate expression for dr/dz, Eq. (18) can now be solved simultaneously with Eq. (14) or (15) to determine the nozzle admittance.

The numerical integration of these equations must start at some initial point where the initial conditions are known. Since the equation for ζ is singular at the throat[2], the integration is initiated at a point that is located a short distance upstream of the throat. The needed initial conditions are obtained by expanding the dependent variables in a Taylor series about the throat. To obtain this Taylor series, its coefficients $\zeta(0) = \zeta_0$ and $\zeta_1 = \left.\frac{d\zeta}{d\varphi}\right|_{\varphi = 0}$ must be evaluated at the throat where $\varphi = 0$. These coefficients are evaluated by substituting the series

$$\zeta = \zeta_0 + \zeta_1\varphi + \ldots$$

into Eq. (14) and taking the limit as $\varphi \to 0$. The results are

$$\zeta_0 = \zeta(0) = \frac{C_0}{B_0}$$

$$\zeta_1 = \left.\frac{d\zeta}{d\varphi}\right|_{\varphi = 0} = \left[B_1\left(\frac{C_0}{B_0}\right) - A_1\left(\frac{C_0}{B_0}\right)^2 - C_1\right]/(A_1 - B_0)$$

where

$$C_0 = C\Big|_{\varphi = 0} = \left[(\omega - i\lambda)^2 - i\,\frac{2(\gamma - 1)(\omega - i\lambda)}{(\gamma + 1)\sqrt{r_{th} r_{ct}}} - \frac{S_{mn}^2}{r_{th}^2}\left(\frac{2}{\gamma + 1}\right)\right]$$

$$B_0 = B\Big|_{\varphi = 0} = \frac{4}{\gamma + 1}\left[\frac{1}{\sqrt{r_{th} r_{ct}}} + i(\omega - i\lambda)\right]$$

$$B_1 = \frac{dB}{d\varphi}\Big|_{\varphi = 0} = \frac{4}{\gamma + 1}\left[\frac{6 + \gamma}{3r_{th} r_{ct}} + i\,\frac{2(\omega - i\lambda)}{\sqrt{r_{th} r_{ct}}}\right]$$

$$A_1 = \frac{dA}{d\varphi}\Big|_{\varphi = 0} = \frac{-4}{(\gamma + 1)\sqrt{r_{th} r_{ct}}}$$

$$C_1 = \frac{dC}{d\varphi}\Big|_{\varphi = 0} = 2\left(\frac{\gamma - 1}{\gamma + 1}\right)\left[\frac{S_{mn}^2}{r_{th}^2\sqrt{r_{th} r_{ct}}} - \frac{i(\omega - i\lambda)}{3r_{th} r_{ct}}\,(6 + \gamma)\right]$$

The following relations are used in the evaluation of the above quantities:

$$\bar{q}^2\Big|_{\varphi = 0} = \frac{2}{\gamma + 1}$$

$$\frac{d\bar{q}^2}{d\varphi}\Big|_{\varphi = 0} = \frac{4}{(\gamma + 1)\sqrt{r_{th} r_{ct}}}$$

Once ζ_0 and ζ_1 are known, the initial condition at $\varphi = \varphi_1$ is obtained from the expression $\zeta(\varphi_1) = \zeta_0 + \zeta_1 \varphi_1$.

The numerical solution is obtained by use of a modified Adams predictor-corrector scheme, and employing a Runge-Kutte scheme of order four to start the numerical integration. Initially, Eqs. (14) and (18) are integrated to determine ζ; if the magnitude of ζ exceeds a specified value at which numerical difficulties can occur, the integration of Eq. (14) is terminated. Using the value of ζ at that point, τ is computed and the integration proceeds using Eq. (15). Similarly, should the magnitude of τ become excessively large, the integration of Eq. (15) is terminated, ζ is computed from the value of τ at that point, and the integration proceeds using Eq. (14). This process is repeated until the nozzle entrance is reached. A computer program utilizing this procedure has been written in FORTRAN V for use on the UNIVAC 1108 computer and it is presented in the Appendix.

RESULTS AND DISCUSSION

Using the previously mentioned computer program, theoretical values of the real and imaginary parts of the nozzle admittance have been computed for several nozzle configurations having contours similar to the one presented in Fig. 2. In these computations the radii of curvature, r_{cc} and r_{ct}, are assumed to be equal. The admittance values are presented as functions of the nondimensional frequency S in Figs. 3 through 9 where they are compared with available experimental data obtained from Ref. 3. In these figures, the frequency has been nondimensionalized by the ratio of the steady state speed of sound at the nozzle entrance to the chamber radius r_c.

Admittances for Longitudinal Modes

Longitudinal-type instabilities in general occur in the range of S from 0 to approximately 1.8 which is in the vicinity of the cutoff frequency of the first tangential modes. The cutoff frequency of a particular transverse mode is $S_{mn}\sqrt{(1 - M^2)}$ where S_{mn} is the transverse mode eigenvalue and the subscripts m and n respectively denote the number of diametral nodal lines and the number of tangential nodal lines. Values of S_{mn} are given in Table 1 for several values of m and n.

For longitudinal modes good agreement exists between the experimental and theoretical values of the real and imaginary parts of the admittance as shown in Figs. 3 through 5. The effect of changing the nozzle half-angle is presented in Fig. 3 for a nozzle with an entrance Mach number M of 0.08 and $r_{cc}/r_c = 0.44$. The data indicate that increasing θ_1 increases the frequency at which the real and imaginary parts of the admittance attain maximum values. These data also indicate that the assumption of a one-dimensional mean flow

Table 1. Values of Transverse Mode Eigenvalues; S_{mn}

Transverse Wave Pattern	m	n	S_{mn}
Longitudinal	0	0	0
First Tangential (1T)	1	0	1.8413
Second Tangential (2T)	2	0	3.0543
First Radial (1R)	0	1	3.8317
Third Tangential (3T)	3	0	4.2012
Fourth Tangential (4T)	4	0	5.3175
First Tangential, First Radial (1T,1R)	1	1	5.3313
Fifth Tangential (5T)	5	0	6.4154
Second Tangential, First Radial (2T,1R)	2	1	6.7060
Second Radial (2R)	0	2	7.0156

used in the development of the theory appears to be valid. Even for nozzles with half-angles as high as 45 degrees, for which it has been shown that the mean flow is two-dimensional,[4] the experimental and theoretical nozzle admittance values are in good agreement.

Examination of Fig. 4 shows that the entrance Mach number M has a significant effect on the admittance values for $\theta_1 = 15$ degrees and $r_{cc}/r_c = 0.44$. However, increasing the nozzle half-angle appears to decrease the influence of the entrance Mach number, and for $\theta_1 = 45$ degrees variations in M has little effect.[3] The dependence of the nozzle admittance upon the radius of curvature for a nozzle with $M = 0.16$ and $\theta_1 = 30$ degrees is shown in Fig. 5.

The data presented in Figs. 3 through 5 show that for longitudinal modes the real part of the nozzle admittance is always positive. As indicated by Crocco[1,2] positive values of the real part of the nozzle admittance imply that the nozzle removes acoustic energy from the combustor wave system which implies that the nozzle exerts a stabilizing influence upon the chamber oscillations.

In combustion instability analyses of liquid-propellant rocket motors, it is often assumed that the nozzle is short. This assumption implies that the nozzle length and throat diameter are much smaller than the chamber length and diameter so that the wave travel time in the nozzle is much shorter than the wave travel time in the chamber. For a short nozzle the real and imaginary parts of the admittance are independent of frequency and are given by the expressions[5]

$$y_r = \frac{\gamma - 1}{2} M ; \quad y_i = 0$$

These theoretical short nozzle admittance results do not agree with the results obtained for typical liquid rocket nozzles presented in Figs. 3 through 5. The disagreement is especially evident for nozzles with low values of θ_1, which imply that the nozzle is long, and for high values of S where the wave length of the oscillation becomes of the same order of magnitude as a characteristic nozzle dimension.

Admittances for Mixed First Tangential-Longitudinal Modes

The mixed first tangential-longitudinal modes are those three-dimensional modes which exist between the cutoff frequencies of the first tangential ($S \simeq 1.8$) and second tangential ($S \simeq 3.0$) modes. Theoretical and experimental nozzle admittance data for these modes are presented in Figs. 6 through 8.

In Fig. 6 the influence of the nozzle half-angle on the admittance values is shown. The theoretical and experimental results are in good agreement and they indicate that increasing θ_1 increases the frequency at which the real and imaginary parts of the admittance reach maximum values.

The effect of Mach number on the admittance values is presented in Fig. 7 for $\theta_1 = 15$ degrees and $r_{cc}/r_c = 0.44$. Mach number effects are especially significant at the higher frequencies. However, as shown in Ref. 3, increasing the nozzle half-angle decreases the dependence of the admittance values on the Mach number. The effect of changing the radii of curvature on the admittance values is presented in Fig. 8.

The results presented in Figs. 6 through 8 show that for mixed first tangential-longitudinal modes the real part of the nozzle admittance can be negative which means that the nozzle radiates wave energy back into the combustor; this process exerts a destabilizing influence on the oscillations in the chamber.[2] These negative values occur only for three-dimensional modes and, as shown by Crocco,[2] their cause can be traced to the term involving S_{mn} in Eq. (12). For longitudinal modes, for which S_{mn}

is zero, the real part of the nozzle admittance is always positive, and for those modes the nozzle always exerts a stabilizing influence upon the combustor oscillations.

Effect of Decay Coefficient upon Admittance Data

The nozzle admittance theory has been modified to include the effects of a temporal decay coefficient, λ. Typical results are shown in Figs. 9 and 10 for values of λ of -0.05, 0, and 0.05. These results indicate that varying λ affects both the real and imaginary parts of the admittance. Therefore, the decay coefficient should be included in the nozzle admittance computations when the oscillations are not neutrally stable.

SUMMARY AND CONCLUSIONS

The equations necessary to determine the nozzle admittance for one- and three-dimensional oscillations have been developed. The analytical approach used in solving the nozzle wave equations is outlined and employed to obtain nozzle admittance data for typical nozzle configurations. These data show the dependence of the nozzle admittance values upon nozzle geometry, nozzle Mach number, mode of oscillation, and the temporal damping coefficient.

The results can be summarized as follows for longitudinal and mixed first tangential-longitudinal modes. Decreasing the nozzle length by increasing the nozzle half-angle and Mach number or by decreasing the throat and entrance radii of curvature decreases the frequency dependence of the nozzle admittance. Good agreement exists between the theoretical predictions and available experimental data. However, the nozzle admittance values for typical liquid rocket nozzles are not in agreement with the values obtained from short nozzle theory. Including the effects of a temporal damping coefficient in the nozzle admittance computations changes the admittance values. Therefore, when the oscillations are not neutrally stable, the temporal decay coefficient should be accounted for in the computations.

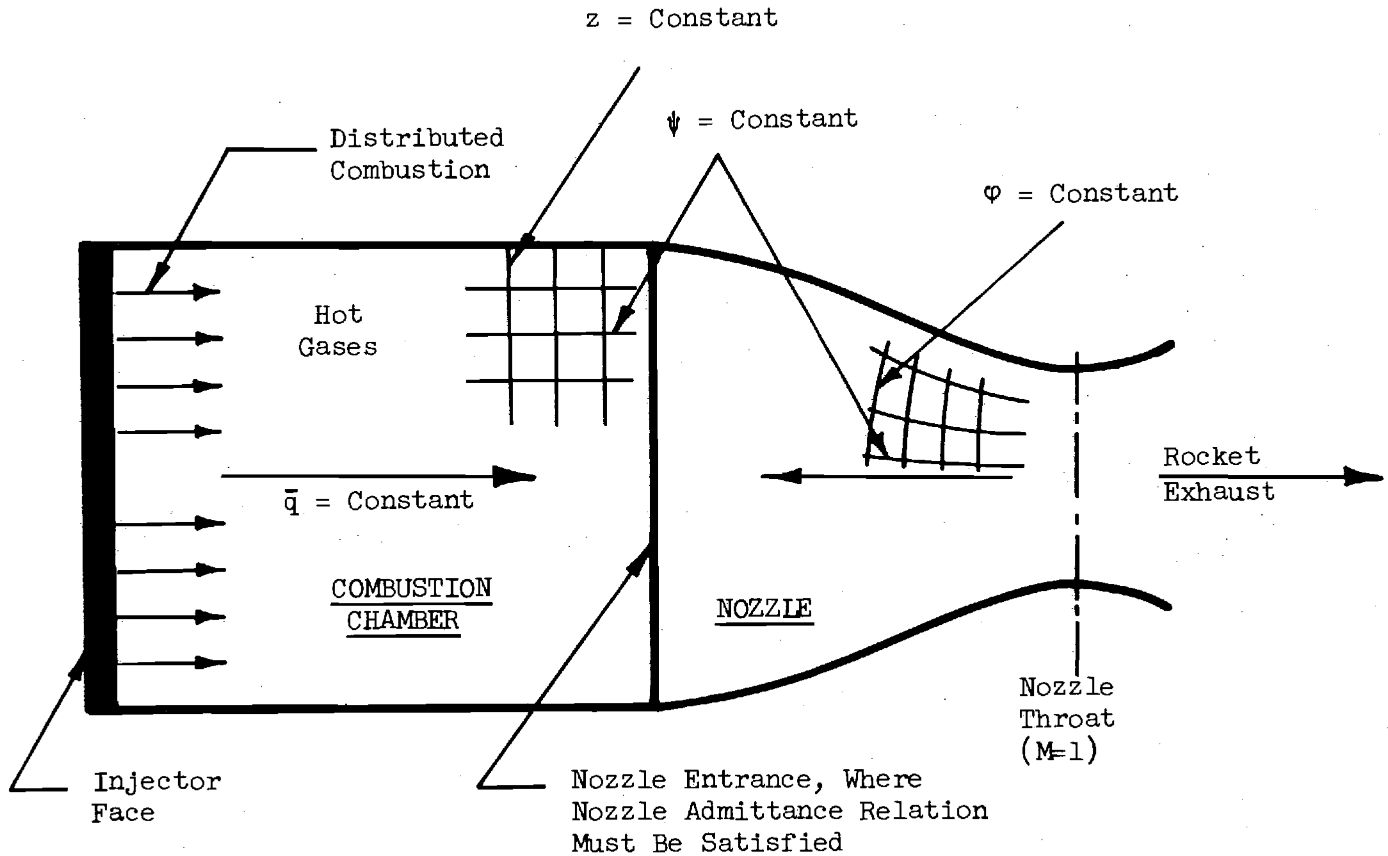

Figure 1. Typical Mathematical Model of a Liquid Rocket Engine

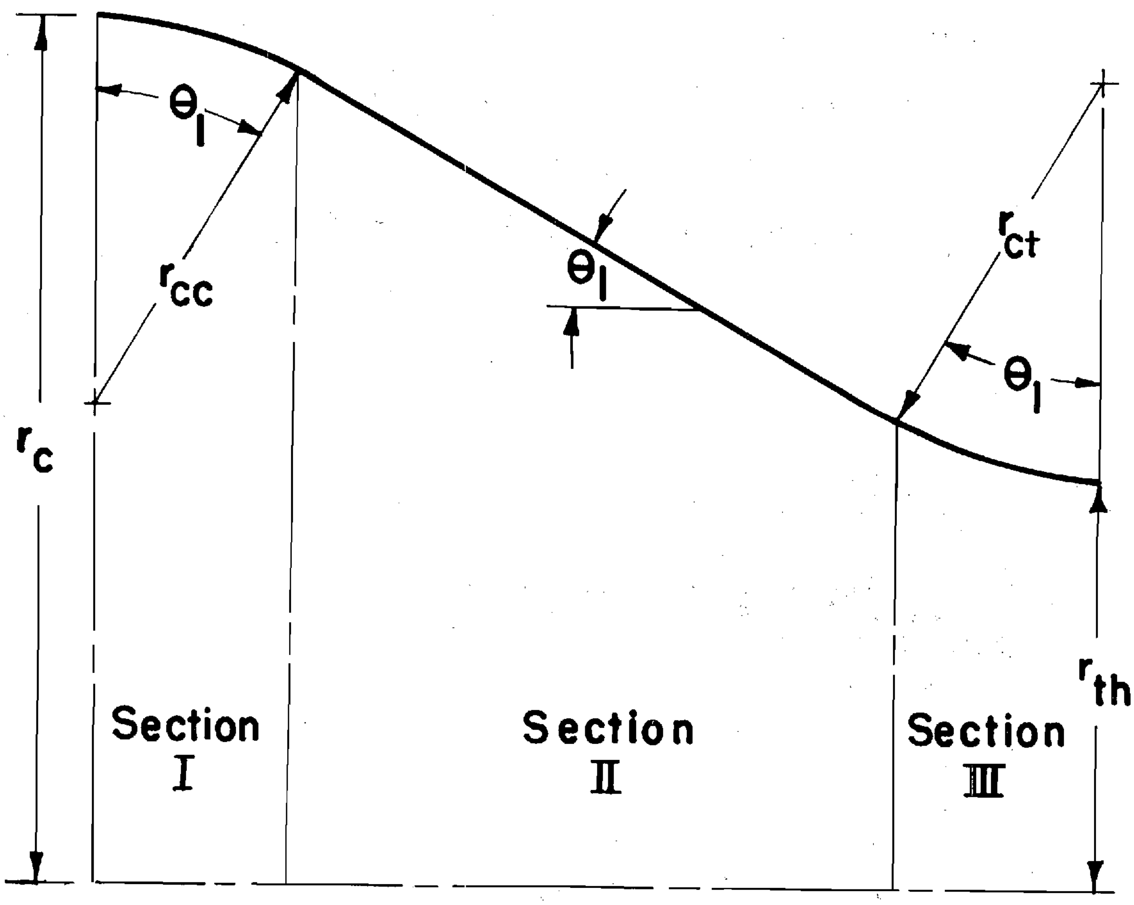

Figure 2. Nozzle Contour

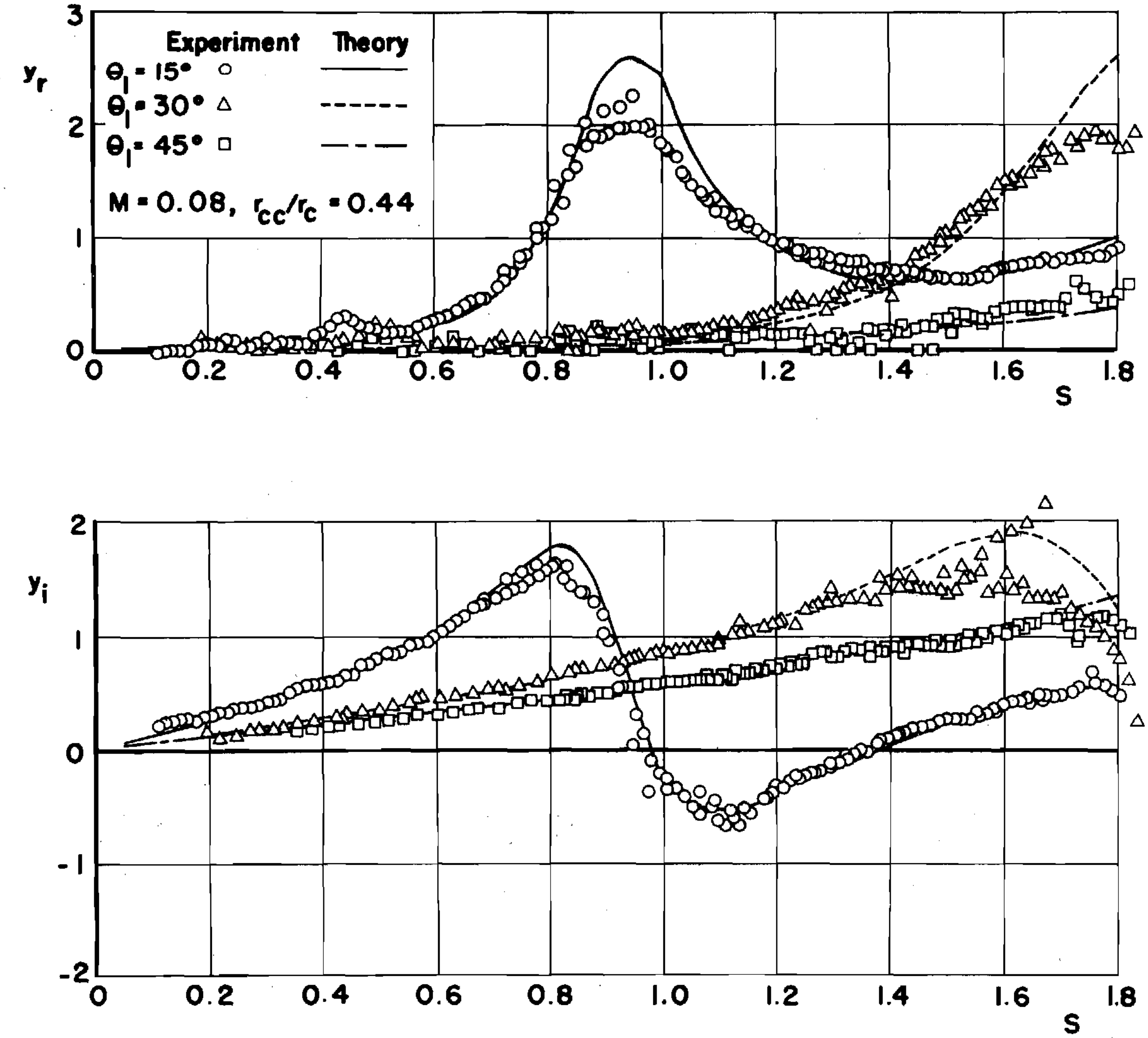

Figure 3. The Effect of Nozzle Half-Angle on the Theoretical and Experimental Nozzle Admittance Values for Longitudinal Modes

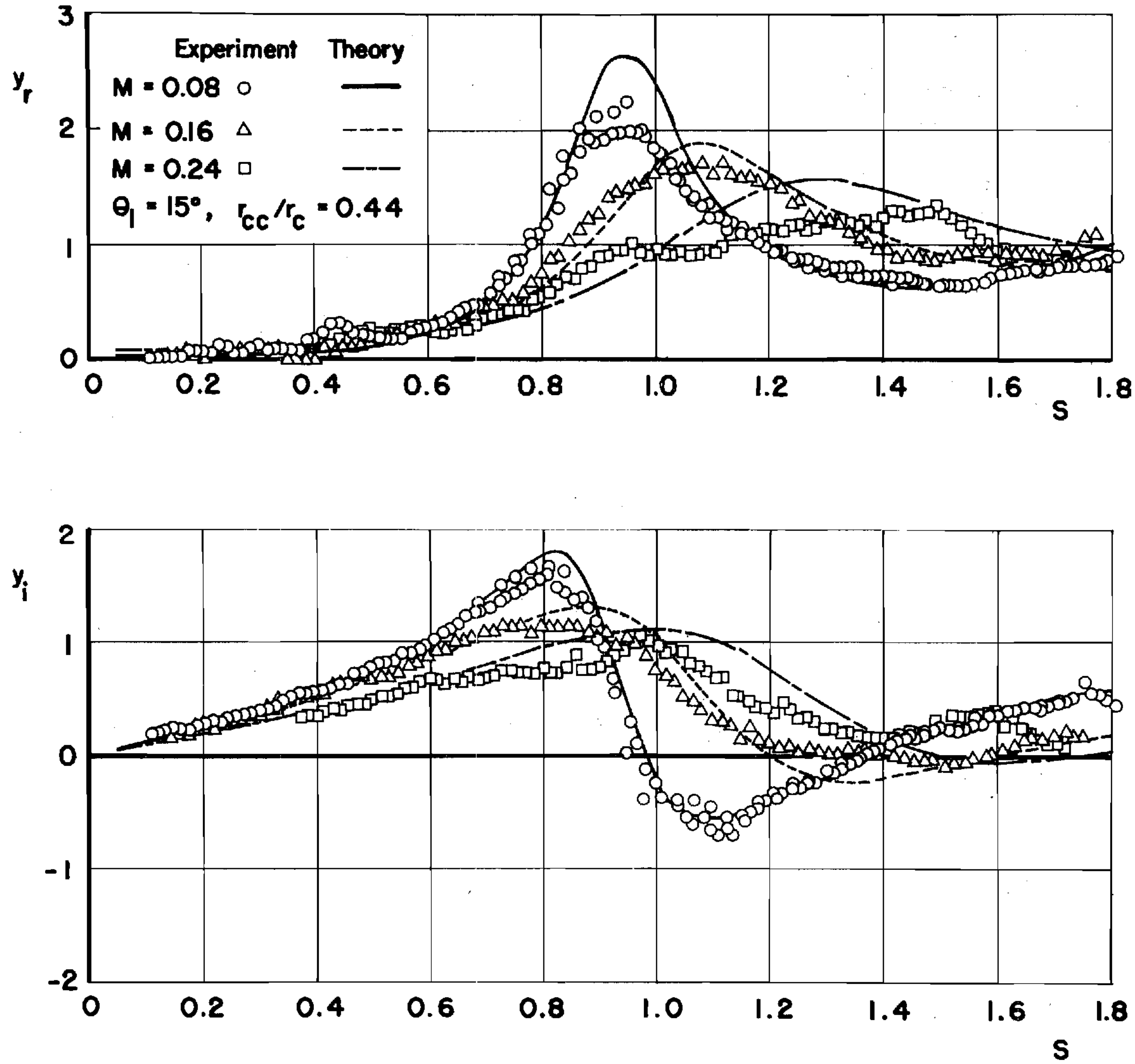

Figure 4. The Effect of Entrance Mach Number on the Theoretical and Experimental Nozzle Admittance Values for Longitudinal Modes

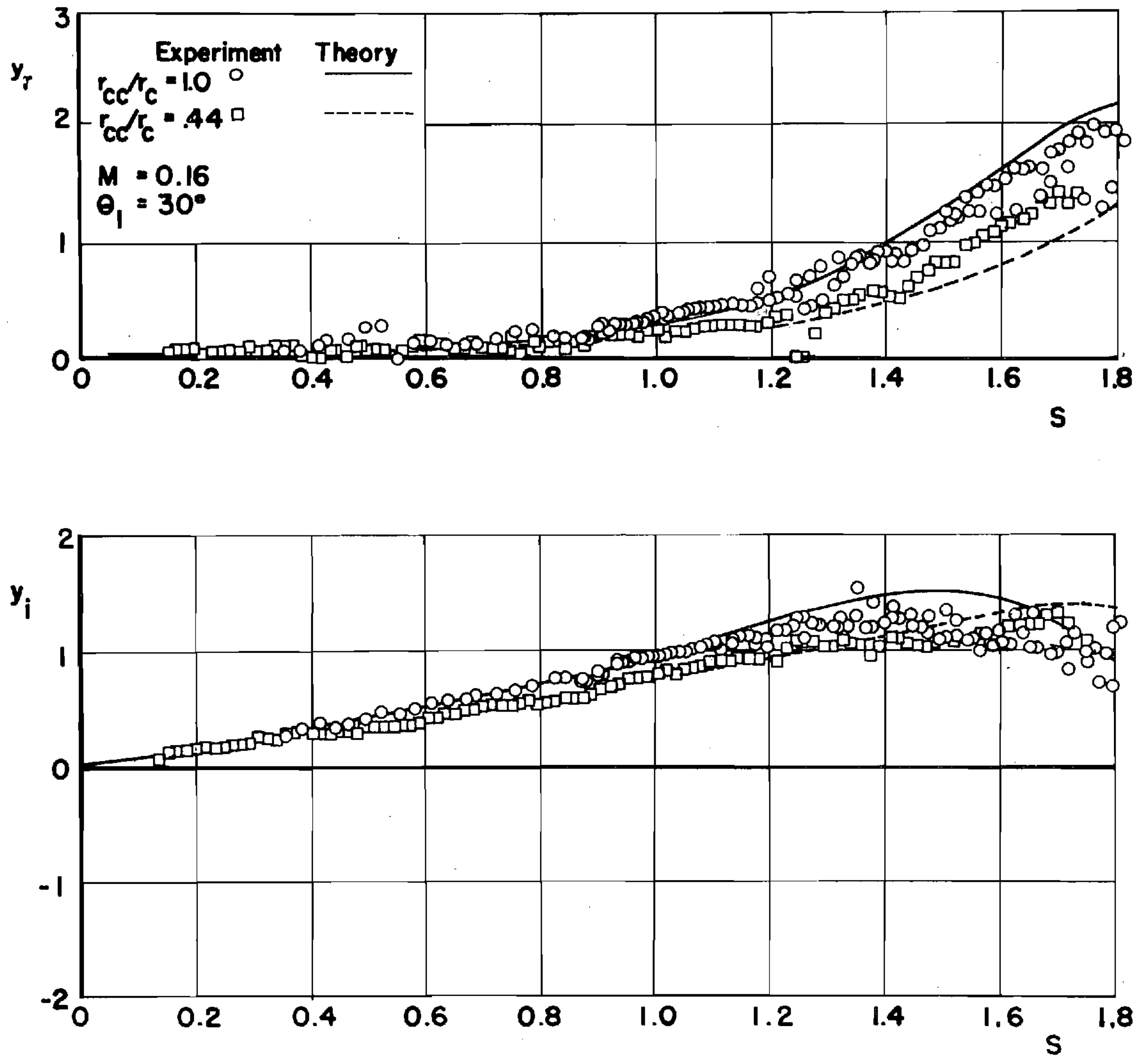

Figure 5. The Effect of the Radii of Curvature on the Theoretical and Experimental Nozzle Admittance Values for Longitudinal Modes

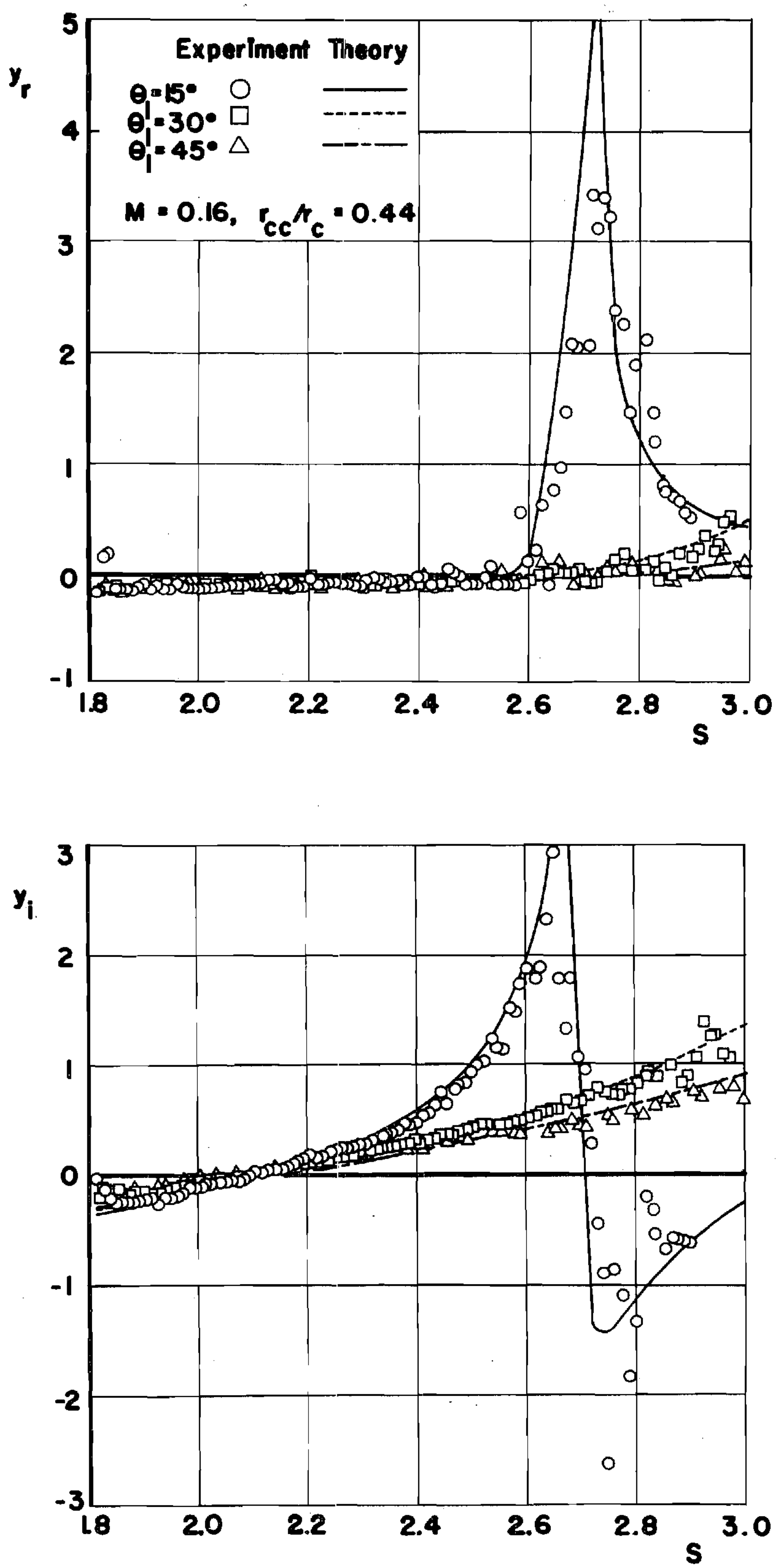

Figure 6. The Effect of the Nozzle Half-Angle on the Theoretical and Experimental Nozzle Admittance Values for Mixed First Tangential-Longitudinal Modes

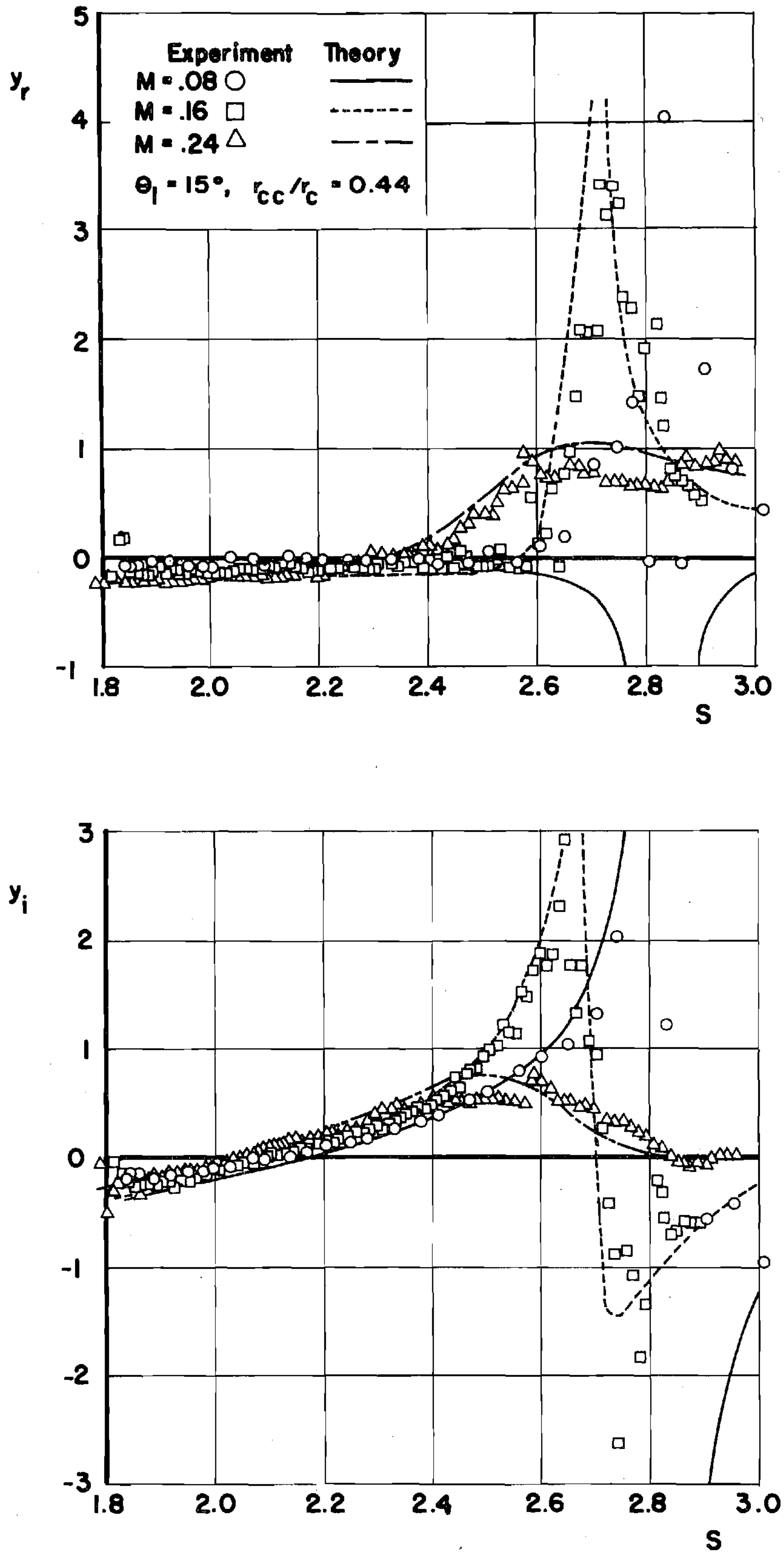

Figure 7. The Effect of Entrance Mach Number on the Theoretical and Experimental Nozzle Admittance Values for Mixed First Tangential-Longitudinal Modes

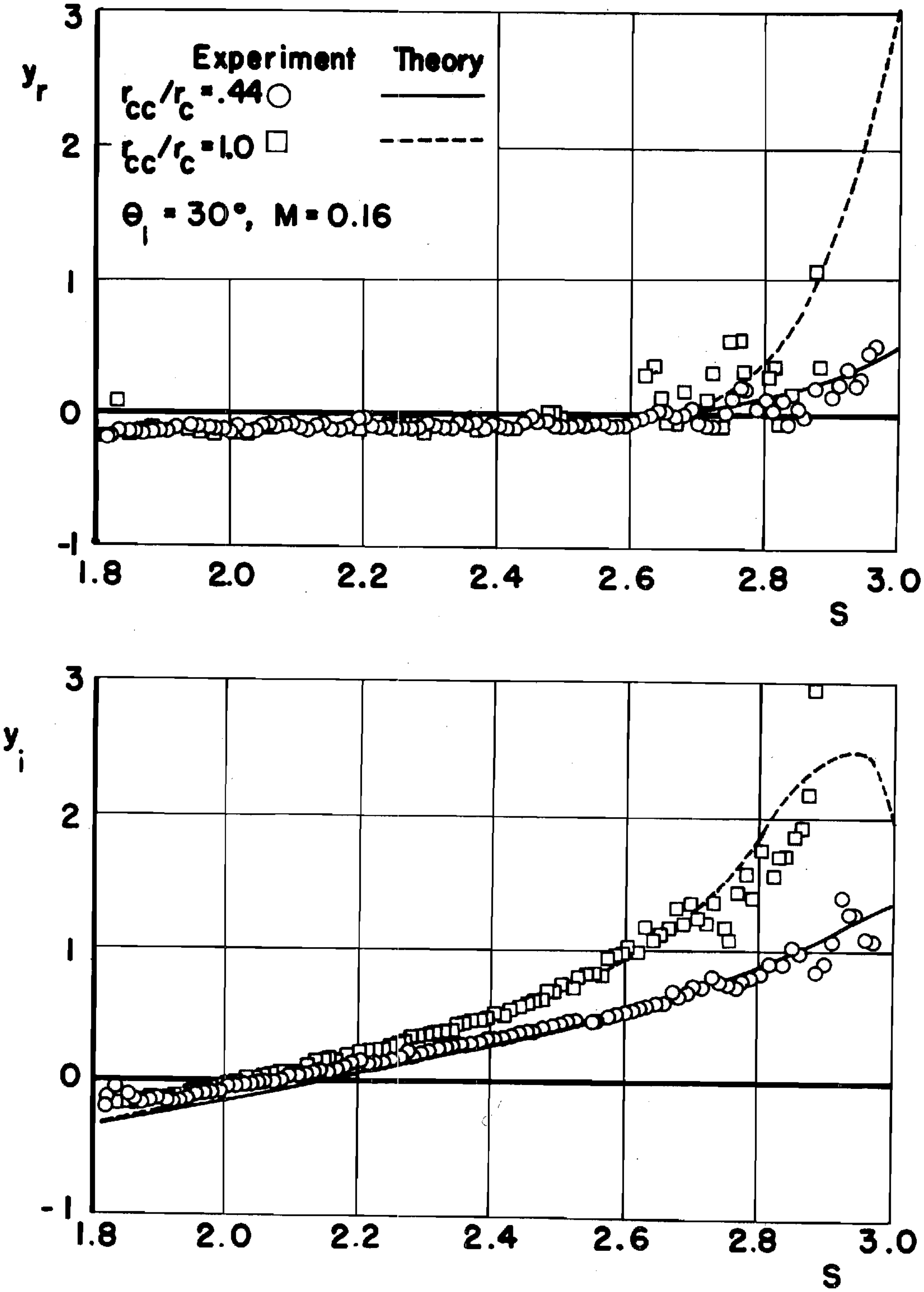

Figure 8. The Effect of the Radii of Curvature on the Theoretical and Experimental Nozzle Admittance Values for Mixed First Tangential-Longitudinal Modes

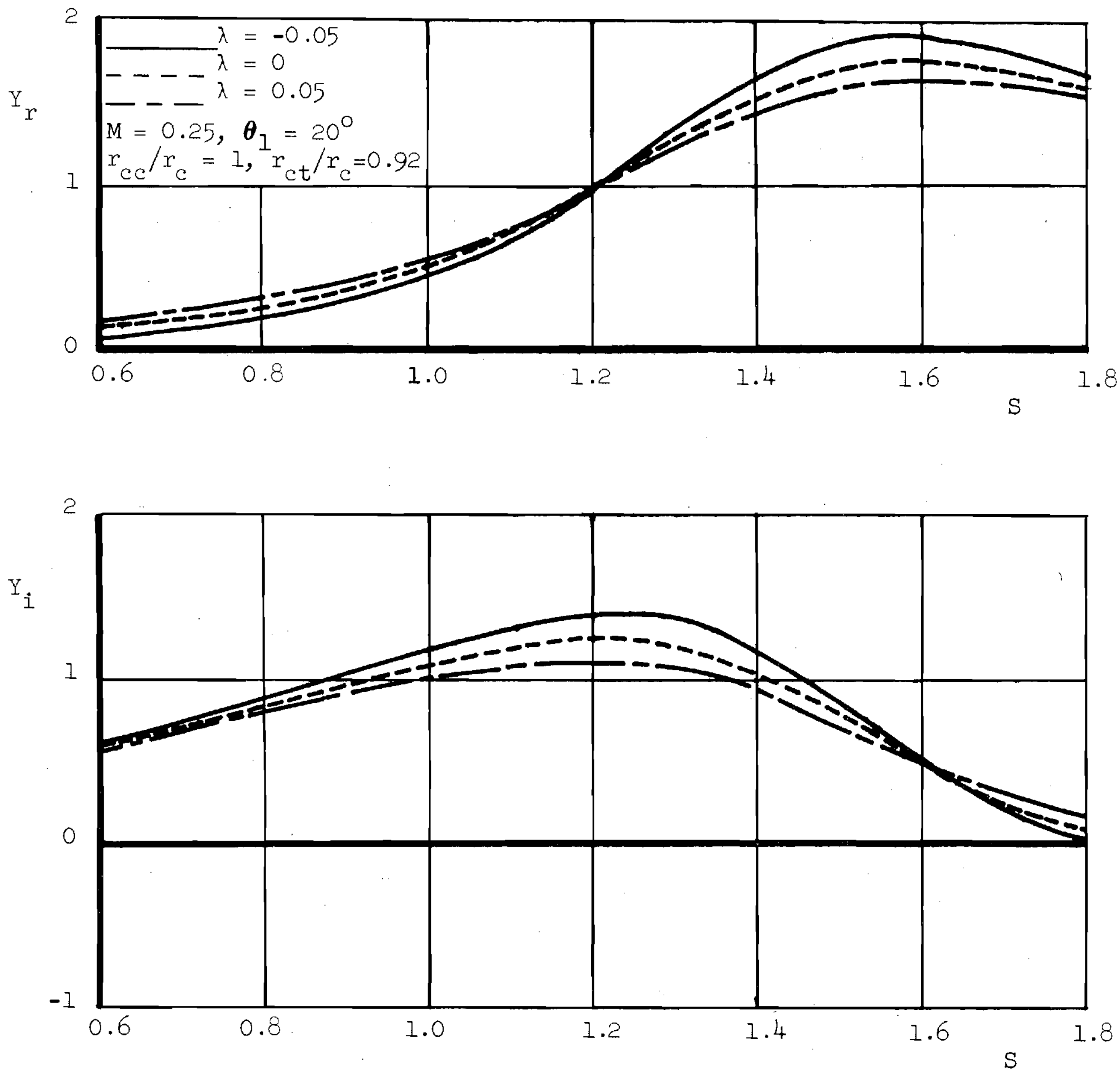

Figure 9. Effect of the Temporal Decay Coefficient on the Theoretical Nozzle Admittance Values for Longitudinal Modes

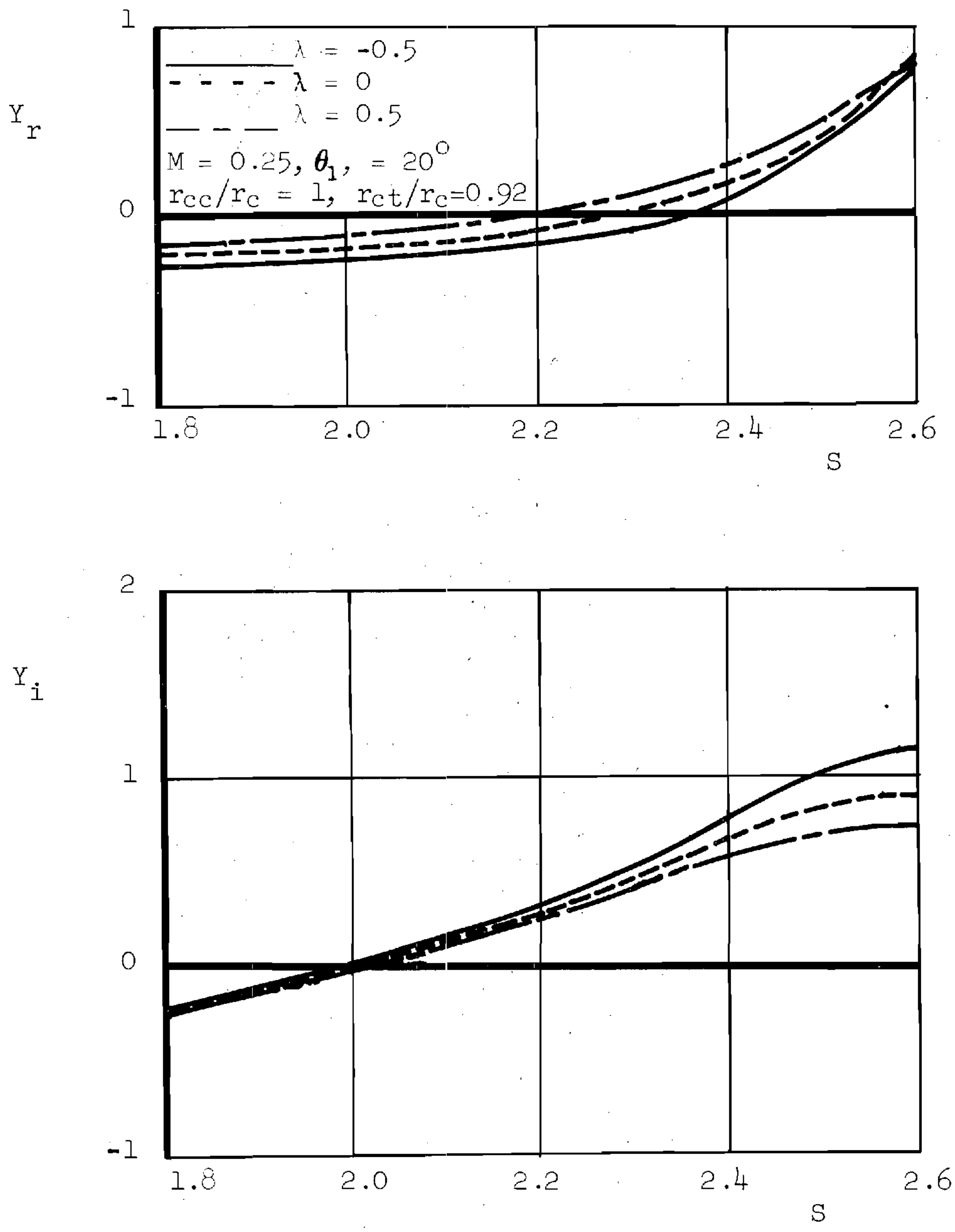

Figure 10. Effect of the Temporal Decay Coefficient on the Theoretical Nozzle Admittance Values for Mixed First Tangential-Longitudinal Modes

APPENDIX

COMPUTER PROGRAM USED TO DETERMINE THE IRROTATIONAL NOZZLE ADMITTANCE

The computer program for calculating the irrotational nozzle admittance from Crocco's theory[2] which is extended to account for temporal damping is written in FORTRAN V interpretive language compatible with the UNIVAC 1108 machine language compiler. This program consists of seven routines - the main or control program and six subroutines. The names of the routines are listed in Table A-1 in sequential order. The FORTRAN symbols used in these routines and their definitions are presented in Table A-2 in alphabetical order. The input parameters necessary for the admittance computations must be specified in the main program and are listed in Table A-3. The output parameters and their definitions are listed in Table A-4. A detailed flow chart of the computer program is shown in Fig. A-1, and the program listing and sample output are presented in Tables A-5 and A-6, respectively.

This computer program has been written to predict nozzle admittances for nozzle contours shown in Fig. 2. The run time required depends upon the number of admittance values desired and the nozzle length. To obtain 40 admittance values at different frequencies for the nozzles investigated in this study, one to two minutes of run time on the UNIVAC 1108 computer are required.

Table A-1. List of Subroutines in the Computer Program Used to Determine the Irrotational Nozzle Admittance

Subroutine	Description
MAIN	Specifies the nozzle geometry and operating conditions in the converging section of the nozzle
NOZADM	Specifies initial conditions at the throat, computes the final nozzle admittance values, and contains all output formats
RKTZ	Uses the Runge-Kutta of order four to obtain initial values for the modified Adams integration routine
RKZDIF	Computes the differential element in the converging section of the nozzle used to solve Eq. (14)
RKTDIF	Computes the differential element in the converging section of the nozzle used to solve Eq. (15)
ZADAMS	Numerically integrates Eq. (14) using the modified Adams numerical integration scheme
TADAMS	Numerically integrates Eq. (15) using the modified Adams numerical integration scheme

Table A-2. Definition of FORTRAN Variables
(Page 1 of 4)

Variable	Definition
A	Real coefficient A of Eqs. (14) and (15)
A(5)	Coefficients of the Runge-Kutta formulas of order four
AF	Nondimensional temporal damping coefficient λ
ANGLE	Nozzle half-angle, degrees
A1R	Derivative of the coefficient A evaluated at the throat
BI	Imaginary part of the coefficient B in Eqs. (14) and (15)
BR	Real part of the coefficient B in Eqs. (14) and (15)
BOI	Value of BI at the throat
BOR	Value of BR at the throat
B1I	Derivative of BI evaluated at the throat
B1R	Derivative of BR evaluated at the throat
C	Nondimensional speed of sound squared, c^2
CI	Imaginary part of the coefficient C in Eqs. (14) and (15)
CM	Mach number at the nozzle entrance
COR(5)	Formula for the corrector in the modified Adams integration routine
CR	Real part of the coefficient C in Eqs. (14) and (15)
COI	Value of CI at the throat
COR	Value of CR at the throat
C1I	Derivative of CI evaluated at the throat
C1R	Derivative of CR evaluated at the throat
DP	Integration stepsize
DP(5)	Derivative used in the corrector formula in the modified Adams integration routine
DR	Derivative of the local wall radius with respect to axial distance
DU	Derivative of the nondimensional velocity $\bar{q}^2$ with respect to the wall radius r
DWC	Increment of the nondimensional frequency ω

Table A-2. Definition of FORTRAN Variables
(Page 2 of 4)

Variable	Definition
DY(5,4)	Derivative used in the modified Adams integration scheme
F	Constant given as $\bar{q}/\gamma\bar{p}$ evaluated at the nozzle entrance
FZ(4,5)	Derivative used in the Runge-Kutta method
F1	Lumped parameter determined by the conditions at the throat
F2	Lumped parameter determined by the conditions at the throat
GAM	Ratio of specific heats γ
G(5)	Dependent variable in the Runge-Kutta integration routine
H	Integration stepsize
I	Integer counter
IP	Integer constant. If IP = 0 the nozzle admittance is output. If IP $\neq$ 0 the amplitude and phase of the pressure oscillation are output along the length of the nozzle
IQ	If IQ = 2, the integration of Eq. (15) for τ is complete
IQZ	= 1: Eq. (15) for τ is integrated = 2: Eq. (14) for ζ is integrated
J	Integer variable
JOPT	= 1: Eq. (15) for τ is integrated = 2: Eq. (14) for ζ is integrated
K	Integer variable
N	Integer variable
NU	Number of differential equations to be solved by the Runge-Kutta or the modified Adams integration routine
NWC	Number of frequency points
P	Value of the steady state velocity potential
PARG	Phase of the pressure oscillation in the nozzle
PHII	Imaginary part of Φ
PHIR	Real part of Φ

Table A-2. Definition of FORTRAN Variables
(Page 3 of 4)

Variable	Definition
PI	Imaginary part of the pressure oscillation
PMAG	Magnitude of the pressure oscillation
PR	Real part of the pressure oscillation
PRED(5)	Predictor formula for the modified Adams integration routine
Q	Constant given as $(r_{th}/4)\left(\frac{2}{\gamma + 1}\right)^{\frac{\gamma + 1}{4(\gamma - 1)}}$
QBAR	Nondimensional steady state velocity $\bar{q}$
R	Local wall radius r
RCC	Ratio of the radius of curvature at the nozzle entrance to the radius at the nozzle entrance
RCT	Ratio of the radius of curvature at the throat to the radius at the nozzle entrance
RHO	Nondimensional, steady-state density $\bar{\rho}$
RT	Nondimensional throat radius
R1	Nondimensional radius at the entrance to Section 2 of the converging portion of the nozzle
R2	Nondimensional radius at the entrance to Section 3 of the converging portion of the nozzle
SRTR	Constant give as $\sqrt{r_{th} r_{cc}}/r_c$
SVN	S_{mn}
SVNR	$S_{mn} r_c / r_{th}$
SYI	Imaginary part of the specific admittance y
SYR	Real part of the specific admittance y
T	Nozzle half-angle, in radians
TDN	Inverse of the square of the magnitude of ζ
TI	Imaginary part of τ
TMAG	Magnitude of τ
TPI	Derivative of TI with respect to φ

Table A-2. Definition of FORTRAN Variables
(Page 4 of 4)

Variable	Definition
TPR	Derivative of TR with respect to φ
TR	Real part of τ
TZ	Value of φ at the nth integration point
T2	Square of the magnitude of τ
U	Steady state velocity squared, $\bar{q}^2$
UZ	Dependent variable in the Runge-Kutta integration scheme
W	Nondimensional frequency S
WC	Nondimensional frequency ω
X	Value of φ at the nth integration point
Y(5)	Dependent variable used in the modified Adams integration scheme
YI	Imaginary part of the irrotational nozzle admittance defined by Crocco in Ref. 2
YR	Real part of the nozzle admittance defined by Crocco in Ref. 2
ZDN	Inverse of the square of the magnitude of ζ
ZI	Imaginary part of ζ
ZMAG	Magnitude of ζ
ZPI	Derivative of ZI with respect to φ
ZPR	Derivative of ZR with respect to φ
ZR	Real part of ζ
ZOI	Value of ZI at the throat
ZOR	Value of ZR at the throat
Z1I	Value of ZPI at the throat
Z1R	Value of ZPR at the throat
Z2	Square of the magnitude of ζ

Table A-3. Input Parameters

Variable	Definition
GAM	Ratio of specific heats, γ
CM	Mach number at the nozzle entrance
SVN	Nth root of the equation $\frac{dJ_V(x)}{dx} = 0$. Corresponds to S_{mn}. Values of S_{mn} are given in Table 1 for various acoustic modes
WC	Initial value of ω
DWC	Increment of frequency
NWC	Number of frequency points desired
ANGLE	Nozzle half-angle, degrees
RCT	Radius of curvature at the throat nondimensionalized with respect to the chamber radius
RCC	Radius of curvature at the nozzle entrance nondimensionalized with respect to the chamber radius
IP	$= 0$: nozzle admittances are printed $\neq 0$: pressure magnitude and phase are printed at each point along the nozzle
AF	Temporal damping coefficient λ

Table A-4. Output Parameters

Variable	Definition
WC	Nondimensional frequency, ω
YR	Real part of the admittance as defined by Crocco in Ref. 2
YI	Imaginary part of the admittance as defined by Crocco in Ref. 2
W	Nondimensional frequency
SYR	Real part of the specific admittance y
SYI	Imaginary part of the specific admittance y

Table A-5. Listing of the Computer Program Used to Determine the Irrotational Nozzle Admittance (Page 1 of 10)

```
      COMMON/X1/GAM, SVN, ANGLE, RCT, RCC /X2/T,RT, Q, R1, R2, IP, WC,AF
      COMMON/X3/Z1R, Z1I
      COMMON/X4/ CM
      GAM = 1.233
      AF = 0
      IP=0
      RCC = 1
      RCT = 5.457*2/11.82
      NWC = 40
      DWC = 0.05
      ANGLE = 20
      CM = .25
      DO 100 I = 1,2
      IF(I.EQ.2) GO TO 5
      SVN = 0
      NWC = 27
      GO TO 20
    5 SVN = 1.84129
      NWC = 20
   20 CONTINUE
      DO 200 J = 1,3
      AF = 0.05*(J-2)
      IF (I .EQ.2) GO TO 25
      WC = 0.55
      GO TO 30
   25 WC = 1.55
   30 CONTINUE
      IF(IP .EQ. 0) GO TO 10
      WRITE(6, 1000) CM, SVN, GAM, ANGLE, RCT, RCC
   10 CALL NOZADM(CM,      NWC, DWC)
  200 CONTINUE
  100 CONTINUE
 1000 FORMAT(46X, 28HPRESSURE MAGNITUDE AND PHASE, //, 38X,
     1       14HMACH NUMBER = , F3.2, 7H SVN = , F6.4, 9H GAMMA = , F3.1
     2       , /, 22X, 15HNOZZLE ANGLE = , F4.1, 21H RADII OF CURVATURE:
     3       , 9HTHROAT = , F6.4, 12H ENTRANCE = , F6.4, //, 46X,
     4       2H X, 7X, 4HPMAG, 10X, 4HPARG, /)
      STOP
      END
```

Table A-5. Continued (Page 2 of 10)

```
      SUBROUTINE NOZADM(CM,     NWC, DWC)
      DIMENSION DY(5,4), G(5), GP(5), Y(5)
      COMMON/X1/GAM,SVN,ANGLE,RCT,RCC/X2/T,RT,Q,R1,R2,IP,WC, AF
      COMMON/X3/Z1R,Z1I
      DP = -0.001
       T = 3.1415927 * ANGLE / 180
      WRITE(6,1000) CM, SVN, GAM, AF, ANGLE, RCT, RCC
      DO 10 N = 1, NWC
   20         WC = WC + DWC
   25         RT =(CM**0.5)*((1+ (GAM-1)*CM*CM/2)**((-GAM-1)/(4*(GAM-1)))
     1            )*((2/(GAM+1))**((-GAM-1)/(4*(GAM-1))))
               Q = (0.25*RT)*((2/(GAM+1))**((GAM+1)/(4*(GAM-1))))
            PHIR = 1
            PHII = 0
              R1 = RT + RCT*(1 - COS(T))
              R2 = 1  - RCC*(1 - COS(T))
               R = RT
               P = 0
               U = 2 / (GAM+1)
            SRTR = (RT * RCT)**0.5
             A1R = -4 /((GAM+1)*SRTR)
             B0R = -A1R +4*AF/(GAM+1)
             B0I = 4 * WC /(GAM+1)
            SVNR = SVN/RT
             C0R = WC * WC -((SVNR*SVNR) * 2 / (GAM+1))
     1             - AF*AF - 2*AF*(GAM-1)/((GAM+1)*SRTR)
             C0I = -2 * WC * (GAM-1) / ((GAM+1)*SRTR) - 2*AF*WC
             B1R = (24 + 4*GAM)/(3*RCT*RT*(GAM+1)) - 8*AF/(SRTR*(GAM+1))
             B1I = 8 * WC / (SRTR*(GAM+1))
             C1R = 2 * (GAM - 1) * SVNR * SVNR /(SRTR * (GAM+1))
     1             - AF* (B1R+8*AF/(SRTR*(GAM+1)))*(GAM-1)*0.5
             C1I = -B1R * WC * (GAM - 1) * 0.5
             Z0R = (B0R*C0R + B0I*C0I) / (B0R*B0R + B0I*B0I)
             Z0I = (B0R*C0I - B0I*C0R) / (B0R*B0R + B0I*B0I)
              F1 = B1R*Z0R - B1I*Z0I - Z0R*Z0R*A1R + A1R*Z0I*Z0I - C1R
              F2 = B1I*Z0R + B1R*Z0I - 2*A1R*Z0I*Z0R - C1I
             Z1R = (F1*(A1R - B0R) - F2*B0I) / ((A1R-B0R)*(A1R-B0R) +
     1              B0I*B0I)
             Z1I = (F2*(A1R - B0R) + F1*B0I) / ((A1R-B0R)*(A1R-B0R) +
     1              B0I*B0I)
               C = U
            G(1) = U
            G(2) = Z0R
            G(3) = Z0I
            G(4) = PHIR * Z0R - PHII * Z0I
            G(5) = PHII * Z0R + Z0I * PHIR
        DY(1,1) = -A1R
        DY(2,1) = Z1R
        DY(3,1) = Z1I
        DY(4,1) = PHIR
        DY(5,1) = PHII
             IQZ = 2
            DO 30 I = 2,4
                 CALL RKTZ(5,DP,P,G,GP,IQZ)
                    P = P + DP
                    U = G(1)
                   ZR = G(2)
                   ZI = G(3)
                 PHIR = G(4)
                 PHII = G(5)
```

```
                 DY(1,I) = GP(1)
                 DY(2,I) = GP(2)
                 DY(3,I) = GP(3)
                 DY(4,I) = GP(4)
      30         DY(5,I) = GP(5)
               Y(1) = U
               Y(2) = ZR
               Y(3) = ZI
               Y(4) = PHIR
               Y(5) = PHII
               CALL ZADAMS(5,DP,P,Y,DY,IQZ)
               IF(IP .EQ. 1) GO TO 10
                  U = Y(1)
                 ZR = Y(2)
                 ZI = Y(3)
          PHIR = Y(4)
          PHII = Y(5)
               QBAR = U**0.5
                  C = 1 - U*0.5*(GAM-1)
                RHO = C**(1/(GAM-1))
                  F = QBAR / (GAM*RHO)
               IF(IQZ .EQ. 1) GO TO 35
                ZDN = (U*ZR+AF)*(U*ZR+AF) + (WC+U*ZI)*(WC+U*ZI)
                 YR = -(ZR*(U*ZR+AF) + ZI*(WC+U*ZI))*F/ZDN
                 YI = F*(WC*ZR - AF*ZI)/ZDN
               GO TO 40
      35         TR = Y(2)
                 TI = Y(3)
                TDN = (U+AF*TR-WC*TI)*(U+AF*TR-WC*TI)+(WC*TR)*(WC*TR)
                 YR = -F*(U-WC*TI+AF*TR)/TDN
                 YI = F*(WC*TR+AF*TI)/TDN
                 YI = F * WC * TR / TDN
      40        SYR = GAM*(C**((GAM+1)/(2*(GAM-1))))*YR
                SYI = GAM*(C**((GAM+1)/(2*(GAM-1))))*YI
                  W = WC *(C**-.5)
      50       WRITE(6,1005) WC, YR, YI, W, SYR, SYI
      10 CONTINUE
    1000 FORMAT(1H1, 45X, 30HTHEORETICAL NOZZLE ADMITTANCES, //, 25X,
       1         14HMACH NUMBER = , F3.2, 7H SVN = , F6.4, 9H GAMMA = , F3.1
       1        ,21H DECAY COEFFICIENT = , F6.4, //,
       2         22X, 15HNOZZLE ANGLE = , F4.1, 2X, 21HRADII OF CURVATURE:
       3         ,   9HTHROAT = , F6.4, 12H ENTRANCE = , F6.4, //, 34X, 2HWC,
       4         7X, 2HYR, 8X, 2HYI, 8X, 1HW, 8X, 3HSYR, 8X, 3HSYI, /)
    1005 FORMAT(31X, F6.4, 5F10.5)
         RETURN
         END
```

```
      SUBROUTINE RKTZ(NU, H, T1, U, DUM, JOPT)
      COMMON/X2/T,RT,Q,R1,R2,IP,WC,AF
      DIMENSION U(5), A(5), UZ(5), FZ(4,5),DUM(5)
      A(1) = 0
      A(2) = 0
      A(3) = 0.5
      A(4) = 0.5
      A(5) = 1.0
        TZ = T1
      DO 10 J = 1, NU
          UZ(J) = U(J)
   10     DUM(J) = FZ(1,J)
      IF(JOPT .EQ. 2) GO TO 15
      CALL RKTDIF(TZ,UZ,DUM)
      GO TO 20
   15 CALL RKZDIF(TZ,UZ,DUM)
   20 DO 25 J = 1, NU
   25   FZ(1,J) = DUM(J)
      DO 30 I = 2,4
              TZ = T1 + A(I+1)*H
           DO 35 J = 1, NU
                UZ(J) = U(J) + A(I+1)*H*FZ(I-1,J)
   35          DUM(J) = FZ(I,J)
           IF(JOPT .EQ. 2) GO TO 40
           CALL RKTDIF(TZ,UZ,DUM)
           GO TO 45
   40      CALL RKZDIF(TZ,UZ,DUM)
   45      DO 50 J = 1, NU
   50         FZ(I,J) = DUM(J)
   30 CONTINUE
      DO 55 J = 1, NU
   55     U(J) = U(J) + H*(FZ(1,J)+2*(FZ(2,J)+FZ(3,J))+FZ(4,J)) / 6.0
      GO TO (60,65),JOPT
   60 CALL RKTDIF(TZ,U ,DUM)
      GO TO 70
   65 CALL RKZDIF(TZ,U ,DUM)
   70 IF(IP.EQ.0) GO TO 75
        PR = WC*U(5)- U(1)*DUM(4) - AF*U(4)
        PI = -WC*U(4) - U(1)*DUM(5) - AF*U(5)
      PMAG = SQRT(PR*PR + PI*PI)
      PARG = ATAN(PI/PR)
      WRITE(6,1000) TZ, PMAG, PARG
 1000 FORMAT(46X, F6.4, 1X, F10.5, 3X, F10.5)
   75 RETURN
      END
```

Table A-5. Continued (Page 5 of 10)

```
      SUBROUTINE RKZDIF(P,G,GP)
      COMMON/X1/GAM,SVN,ANGLE,RCT,RCC/X2/T,RT,Q,R1,R2,IP,WC,AF
      COMMON/X3/Z1R,Z1I
      DIMENSION G(5), GP(5)
         U = G(1)
        ZR = G(2)
        ZI = G(3)
      PHIR = G(4)
      PHII = G(5)
      IF(P) 15, 10, 15
   10 GP(1) = 4/((GAM+1)*((RCT*RT)**0.5))
      GP(2) = Z1R
      GP(3) = Z1I
      GP(4) = Z1R
      GP(5) = Z1I
      GO TO 20
   15    C = 1 - (GAM - 1) * U * 0.5
         R = Q * ((C)**(-1/(2*(GAM-1)))) * (U**-0.25) *4.0
      IF(R-1) 22, 22, 50
   22 IF(R - R1) 25, 30, 30
   25   DR = -((2*RCT*(R-RT) - (R-RT)*(R-RT))**0.5)/(RT+RCT-R)
      GO TO 45
   30 IF(R-R2) 35, 40, 40
   35   DR = -TAN(T)
      GO TO 45
   40   DR = ((2*RCC*(1-R) - (R-1)*(R-1))**0.5)/(1-R-RCC)
   45   DU = -(U**0.75)*(C**((2*GAM-1)/(2*(GAM-1))))/(Q*(1-(GAM+1)*U*.5)
     1     )
      GP(1)= DU*DR
      GO TO 55
   50 GP(1) = 0
   55    A = U*(C-U)
        BR = U*GP(1)/C + 2*AF*U
        BI = 2*WC*U
        CR = WC*WC - SVN*SVN*C/(R*R) - AF*AF
     1       -(GAM-1)*AF*U*GP(1)*0.5*(1/C)
        CI = -(GAM-1)*WC*U*GP(1)*0.5*(1/C) - 2*AF*WC
      GP(2)= ((BR*ZR - BI*ZI - CR) / A) - ZR*ZR + ZI*ZI
      GP(3)= ((BI*ZR + BR*ZI - CI) / A) - 2*ZR*ZI
      GP(4)= ZR*PHIR - ZI*PHII
      GP(5)= ZR*PHII + ZI*PHIR
   20 RETURN
      END
```

```
      SUBROUTINE RKTDIF(P,G,GP)
      COMMON/X1/GAM,SVN,ANGLE,RCT,RCC/X2/T,RT,Q,R1,R2,IP,WC,AF
      DIMENSION G(5), GP(5)
         U = G(1)
        TR = G(2)
        TI = G(3)
      PHIR = G(4)
      PHII = G(5)
         C = 1 - (GAM-1)*U*0.5
         R = Q * ((C)**(-1/(2*(GAM-1)))) * (U**-0.25) *4.0
      IF(R-1) 22,22,50
   22 IF(R-R1) 25, 30, 30
   25   DR = -((2*RCT*(R-RT) - (R-RT)*(R-RT))**0.5)/(RT+RCT-R)
      GO TO 45
   30 IF(R-R2) 35,40,40
   35   DR = -TAN(T)
      GO TO 45
   40   DR = ((2*RCC*(1-R) - (R-1)*(R-1))**0.5)/(1-R-RCC)
   45   DU = -(U**0.75)*(C**((2*GAM-1)/(2*(GAM-1)))) / (Q*(1-(GAM+1)*U*
     1      0.5))
      GP(1)= DU*DR
      GO TO 55
   50 GP(1) = 0
   55    A = U*(C-U)
        BR = U*GP(1)/C + 2*AF*U
        BI = 2*WC*U
        CR = WC*WC - SVN*SVN*C/(R*R) - AF*AF
     1         -(GAM-1)*AF*U*GP(1)*0.5*(1/C)
        CI = -(GAM-1)*WC*U*GP(1)*0.5*(1/C) - 2*AF*WC
      GP(2)= 1 - ((BR*TR-BI*TI) - (CR*(TR*TR-TI*TI)-2*CI*TR*TI))/ A
      GP(3)= (-BR*TI - BI*TR + CI*(TR*TR-TI*TI) + 2*CR*TR*TI) /A
        T2 = TR*TR + TI*TI
      GP(4)= (TR*PHIR - TI*PHII)/T2
      GP(5)= (TR*PHII + TI*PHIR)/T2
      RETURN
      END
```

```
      SUBROUTINE ZADAMS(N,H,X,Y,DY,IQZ)
      COMMON/X1/GAM,SVN,ANGLE,RCT,RCC/X2/T,RT,Q,R1,R2,IP,WC,AF
      COMMON/X4/ CM
      DIMENSION COR(5), DP(5), DY(5,4), PRED(5), Y(5), Q(5), GP(5)
   10 CONTINUE
      DO 15 I = 1,N
        PRED(I) = Y(I)+H*(55.*DY(I,4)-59.*DY(I,3)+37.*DY(I,2)-9.*DY(I,1)
     1                    )/24.0
   15 CONTINUE
         X = X+H
         U = PRED(1)
        ZR = PRED(2)
        ZI = PRED(3)
      PHIR = PRED(4)
      PHII = PRED(5)
         C = 1 - (GAM-1)*U*0.5
         R = Q * ((C)**(-1/(2*(GAM-1)))) * (U**-0.25) *4.0
      IF(R-1) 17,17,100
   17 IF(R-R1) 20, 25, 25
   20   DR = -((2*RCT*(R-RT)-(R-RT)*(R-RT))**0.5) / (RT+RCT-R)
      GO TO 40
   25 IF(R-R2) 30, 35, 35
   30   DR = -TAN(T)
      GO TO 40
   35   DR = ((2*RCC*(1-R) - (1-R)*(1-R))**0.5) / (1-R-RCC)
   40   DU = -(U**0.75)*(C**((2*GAM-1)/(2*(GAM-1))))/(Q*(1-(GAM+1)*U*0.5
     1         ))
      DP(1)= DR*DU
         A = U*(C-U)
        BR = U*DP(1)/C+ 2*AF*U
        BI = 2*WC*U
        CR = WC*WC - (SVN*SVN*C)/(R*R) - AF*AF
     1        -(GAM-1)*AF*U*DP(1)*0.5/C
        CI = -(GAM-1)*WC*U*DP(1)*0.5/C - 2*AF*WC
      DP(2)= ((BR*ZR - BI*ZI - CR)/A) - ZR*ZR + ZI*ZI
      DP(3)= ((BI*ZR + BR*ZI - CI)/A) - 2*ZR*ZI
      DP(4)= ZR*PHIR - ZI*PHII
      DP(5)= ZR*PHII + ZI*PHIR
      DO 45 I = 1,N
         COR(I) = Y(I)+H*(DY(I,2)-5.*DY(I,3)+19.*DY(I,4)+9.*DP(I))/24.0
   45      Y(I) = (251.*COR(I) + 19.*PRED(I)) / 270.
         U = Y(1)
        ZR = Y(2)
        ZI = Y(3)
      PHIR = Y(4)
      PHII = Y(5)
         C = 1 - (GAM-1)*U*0.5
   52 DO 55 I = 1,N
        DY(I,1) = DY(I,2)
        DY(I,2) = DY(I,3)
   55   DY(I,3) = DY(I,4)
      ZMAG = (ZR*ZR + ZI*ZI)**0.5
      IF(ZMAG - 10 ) 60, 90, 90
   60    R = Q * ((C)**(-1/(2*(GAM-1)))) * (U**-0.25) *4.0
      IF(R-1) 62, 62, 100
   62 IF(R-R1) 65,70,70
   65   DR = -((2*RCT*(R-RT) - (R-RT)*(R-RT))**0.5)/(RT+RCT-R)
      GO TO 85
   70 IF(R-R2) 75,80,80
   75   DR = -TAN(T)
      GO TO 85
```

```
      80   DR = ((2*RCC*(1-R) - (1-R)*(1-R))**0.5)/(1-R-RCC)
      85   DJ = -(U**0.75)*(C**((2*GAM-1)/(2*(GAM-1))))/(Q*(1-(GAM+1)*U/2))
         DY(1,4)= DR*DU
             A = U*(C-U)
            BR = U*DY(1,4)/C + 2*AF*U
            BI = 2*WC*U
            CR = WC*WC - (SVN*SVN*C)/(R*R) - AF*AF
     1           -(GAM-1)*AF*U*DY(1,4)*0.5/C
            CI = -(GAM-1)*WC*U*DY(1,4)*0.5/C -2*AF*WC
         DY(2,4)= (BR*ZR - BI*ZI -CR)/A - ZR*ZR + ZI*ZI
         DY(3,4)= (BI*ZR + BR*ZI -CI)/A - 2*ZR*ZI
         DY(4,4)= ZR*PHIR - ZI*PHII
         DY(5,4)= ZR*PHII + ZI*PHIR
         IF(IP .EQ. 0) GO TO 87
            PR = WC*PHII - U*DY(4,4) - AF*PHIR
            PI = -WC*PHIR -U*DY(5,4)   - AF*PHII
         PMAG = (PR*PR + PI*PI)**.5
         PARG = ATAN(PI/PR)
         WRITE(6,1000) X, PMAG, PARG
      87 GO TO 10
      90  IQZ = 1
           Z2 = ZMAG*ZMAG
         Y(2) = ZR/Z2
         Y(3) = -ZI/Z2
          ZPR = DY(2,4)
          ZPI = DY(3,4)
         DY(2,4)= -(ZPR*(ZR*ZR - ZI*ZI) + 2*ZR*ZI*ZPI)/(Z2*Z2)
         DY(3,4)= (2*ZPR*ZR*ZI - ZPI*(ZR*ZR - ZI*ZI))/(Z2*Z2)
         G(1) = U
         G(2) = Y(2)
         G(3) = Y(3)
         G(4) = PHIR
         G(5) = PHII
         DY(1,1)= DY(1,4)
         DY(2,1)= DY(2,4)
         DY(3,1)= DY(3,4)
         DY(4,1)= PHIR*ZR - PHII*ZI
         DY(5,1)= PHII*ZR + PHIR*ZI
         DO 95 I = 2,4
              CALL RKTZ(5,H,X,G,GP,IQZ)
                 X = X+H
                 U = G(1)
                TR = G(2)
                TI = G(3)
              PHIR = G(4)
              PHII = G(5)
           DY(1,I) = GP(1)
           DY(2,I) = GP(2)
           DY(3,I) = GP(3)
           DY(4,I) = GP(4)
      95   DY(5,I) = GP(5)
         Y(1) = U
         Y(2) = TR
         Y(3) = TI
         Y(4) = PHIR
         Y(5) = PHII
         CALL TADAMS(N,H,X,Y,DY,IQZ,IQ)
         GO TO (10, 100),IQ
    1000 FORMAT(46X,F6.4,1X,F10.5,3X,F10.5)
     100 RETURN
         END
```

```
      SUBROUTINE TADAMS(N,H,X,Y,DY,IQZ,IQ)
      COMMON/X1/GAM,SVN,ANGLE,RCT,RCC/X2/T,RT,Q,R1,R2,IP,WC,AF
      COMMON/X4/ CM
      DIMENSION COR(5), DP(5), DY(5,4), PRED(5), Y(5), G(5), GP(5)
   10 CONTINUE
      DO 15 I = 1,N
         PRED(I) = Y(I)+H*(55*DY(I,4)-59.*DY(I,3)+37.*DY(I,2)-9*DY(I,1))/
    1              24.0
   15 CONTINUE
          X = X+H
          U = PRED(1)
         TR = PRED(2)
         TI = PRED(3)
       PHIR = PRED(4)
       PHII = PRED(5)
          C = 1 - (GAM-1)*U*.5
          R = Q * ((C)**(-1/(2*(GAM-1)))) * (U**-0.25) *4.0
      IF(R-1) 17,17,100
   17 IF(R-R1) 20, 25, 25
   20    DR = -((2*RCT*(R-RT) - (R-RT)*(R-RT))**.5)/(RT+RCT-R)
      GO TO 40
   25 IF(R-R2) 30, 35, 35
   30    DR = -TAN(T)
      GO TO 40
   35    DR = ((2*RCC*(1-R) - (1-R)*(1-R))**.5)/(1-R-RCC)
   40    DU =-(U**.75)*(C**((2*GAM-1)/(2*(GAM-1))))/(Q*(1-(GAM+1)*U*.5))
      DP(1)= DR+DU
          A = U*(C-U)
         BR = U*DP(1)/C+ 2*AF*U
         BI = 2*WC*U
         CR = WC*WC - (SVN*SVN*C)/(R*R) - AF*AF
    1           -(GAM-1)*AF*U*DP(1)*0.5/C
         CI = -(GAM-1)*WC*U*DP(1)*0.5/C - 2*AF*WC
      DP(2)= 1 + (-BR*TR+BI*TI+CR*(TR*TR-TI*TI)-2*CI*TR*TI)/A
      DP(3)= (-BR*TI - BI*TR + CI*(TR*TR - TI*TI) + 2*CR*TR*TI)/A
         T2 = TR*TR + TI*TI
      DP(4)= (TR*PHIR - TI*PHII)/T2
      DP(5)= (TR*PHII + TI*PHIR)/T2
      DO 45 I = 1,N
          COR(I) = Y(I)+H*(DY(I,2)-5.*DY(I,3)+19.*DY(I,4)+9.*DP(I))/24.0
   45       Y(I) = (251.*COR(I) + 19.*PRED(I))/270.
          U = Y(1)
         TR = Y(2)
         TI = Y(3)
       PHIR = Y(4)
       PHII = Y(5)
          C = 1 - (GAM-1)*U*.5
   52 DO 55 I = 1,N
         DY(I,1) = DY(I,2)
         DY(I,2) = DY(I,3)
   55    DY(I,3) = DY(I,4)
         T2 = TR*TR + TI*TI
      TMAG = T2**.5
      IF(TMAG - 10 ) 60, 90, 90
   60     R = Q * ((C)**(-1/(2*(GAM-1)))) * (U**-0.25) *4.0
      IF(R-1) 62, 62, 100
   62 IF(R-R1) 65,70,70
   65    DR = -((2*RCT*(R-RT)-(R-RT)*(R-RT))**.5)/(RT+RCT-R)
      GO TO 85
   70 IF(R-R2) 75,80,80
   75    DR = -TAN(T)
      GO TO 85
```

```
80    DR = ((2*R*C*(1-R) - (1-R)*(1-R))**.5)/(1-R-RCC)
85    DU = -(U**.75)*(C**((2*GAM-1)/(2*(GAM-1))))/(Q*(1-(GAM+1)*U*.5))
      DY(1,4)= DR*DU
        A = U*(C-U)
       BR = U*DY(1,4)/C + 2*AF*U
       BI = 2*WC*U
       CR = WC*WC - (SVN*SVN*C)/(R*R) - AF*AF
     1         -(GAM-1)*AF*U*DY(1,4)*0.5/C
       CI = -(GAM-1)*WC*U*DY(1,4)*0.5/C -2*AF*WC
      DY(2,4)= 1 + (-BR*TR + BI*TI + CR*(TR*TR - TI*TI) - 2*CI*TR*TI)/A
      DY(3,4)= (-BR*TI - BI*TR + CI*(TR*TR - TI*TI) + 2*CR*TR*TI)/A
      DY(4,4)= (TR*PHIR - PHII*TI)/T2
      DY(5,4)= (TR*PHII + PHIR*TI)/T2
      IF(IP .EQ. 0) GO TO 87
       PR = WC*PHII - U*DY(4,4) - AF*PHIR
       PI = -WC*PHIR -U*DY(5,4)    - AF*PHII
      PMAG = (PR*PR + PI*PI)**.5
      PARG = ATAN(PI/PR)
      WRITE(6,1000) X, PMAG, PARG
87    GO TO 10
90     IQZ = 2
      Y(2) = TR/T2
      Y(3) = -TI/T2
       TPR = DY(2,4)
       TPI = DY(3,4)
      DY(2,4)= -(TPR*(TR*TR - TI*TI) + 2*TR*TI*TPI)/(T2*T2)
      DY(3,4)=(2*TPR*TR*TI-TPI*(TR*TR-TI*TI))/(T2*T2)
      G(1) = U
      G(2) = Y(2)
      G(3) = Y(3)
      G(4) = PHIR
      G(5) = PHII
      DY(1,1)= DY(1,4)
      DY(2,1)= DY(2,4)
      DY(3,1)= DY(3,4)
      DY(4,1)= (PHIR*TR - PHII*TI)/T2
      DY(5,1)= (PHII*TR - PHIR*TI)/T2
      DO 95 I = 2,4
           CALL RKTZ(5,H,X,G,GP,IQZ)
                 X = X+H
                 U = G(1)
                ZR = G(2)
                ZI = G(3)
              PHIR = G(4)
              PHII = G(5)
        DY(1,I) = GP(1)
        DY(2,I) = GP(2)
        DY(3,I) = GP(3)
        DY(4,I) = GP(4)
95      DY(5,I) = GP(5)
      Y(1) = U
      Y(2) = ZR
      Y(3) = ZI
      Y(4) = PHIR
      Y(5) = PHII
       IQ  = 1
      GO TO 105
100    IQ = 2
1000  FORMAT(46X, F6.4, 1X, F10.5, 3X, F10.5)
105   RETURN
      END
```

Table A-6. Sample Output

THEORETICAL NOZZLE ADMITTANCES

MACH NUMBER = .25 SVM = 1.8413 GAMMA = 1.2 DECAY COEFFICIENT = -.0500

NOZZLE ANGLE = 20.0 RADII OF CURVATURE: THROAT = .9234 ENTRANCE = 1.0000

NC	YR	YI	W	SYR	SYI
1.6000	-.28273	-.35883	1.60581	-.33670	-.42732
1.6500	-.27001	-.31495	1.65600	-.32154	-.37507
1.7000	-.25820	-.27057	1.70618	-.30749	-.32221
1.7500	-.24715	-.22543	1.75636	-.29433	-.26845
1.8000	-.23669	-.17922	1.80654	-.28186	-.21343
1.8500	-.22661	-.13161	1.85672	-.26986	-.15673
1.9000	-.21667	-.08219	1.90690	-.25803	-.09788
1.9500	-.20659	-.03048	1.95709	-.24603	-.03630
2.0000	-.19598	.02407	2.00727	-.23339	.02867
2.0500	-.18432	.08216	2.05745	-.21950	.09784
2.1000	-.17087	.14458	2.10763	-.20348	.17217
2.1500	-.15459	.21227	2.15781	-.18410	.25279
2.2000	-.13397	.28633	2.20799	-.15954	.34098
2.2500	-.10675	.36791	2.25818	-.12713	.43814
2.3000	-.06962	.45811	2.30836	-.08291	.54555
2.3500	-.01763	.55747	2.35854	-.02100	.66387
2.4000	.05634	.66508	2.40872	.06709	.79202
2.4500	.16198	.77657	2.45890	.19290	.92479
2.5000	.31059	.88672	2.50908	.36987	1.04883
2.5500	.49692	.94600	2.55927	.59165	1.12557

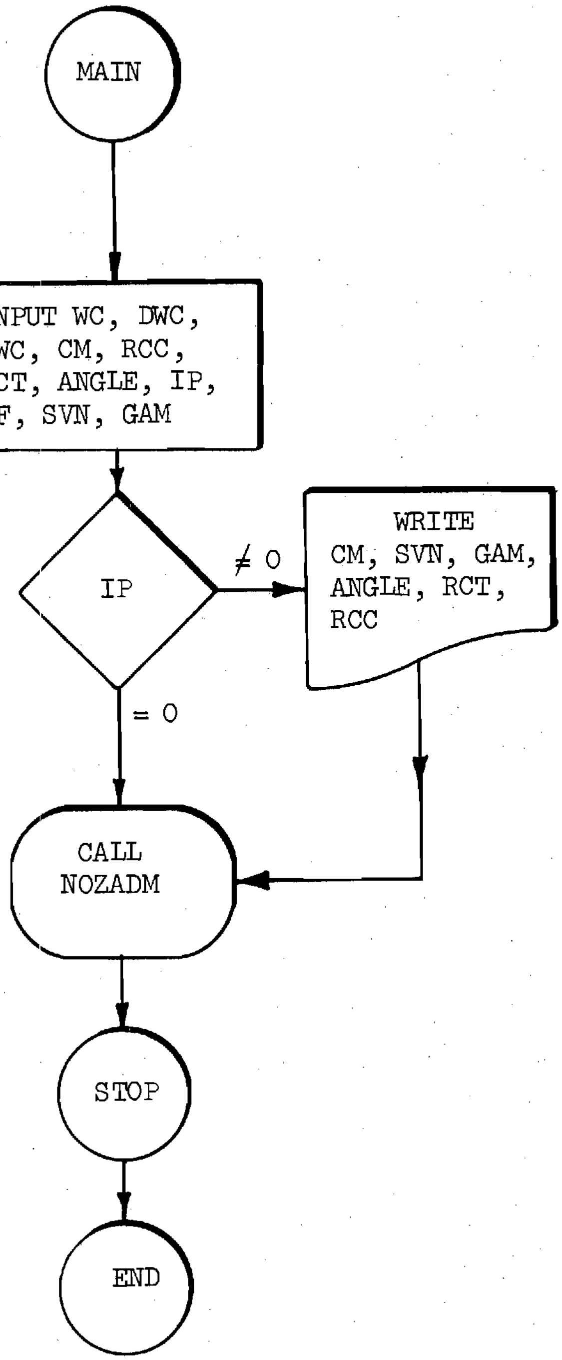

Figure A-1. Flow Chart for the Nozzle Admittance Computer Program (Page 1 of 10)

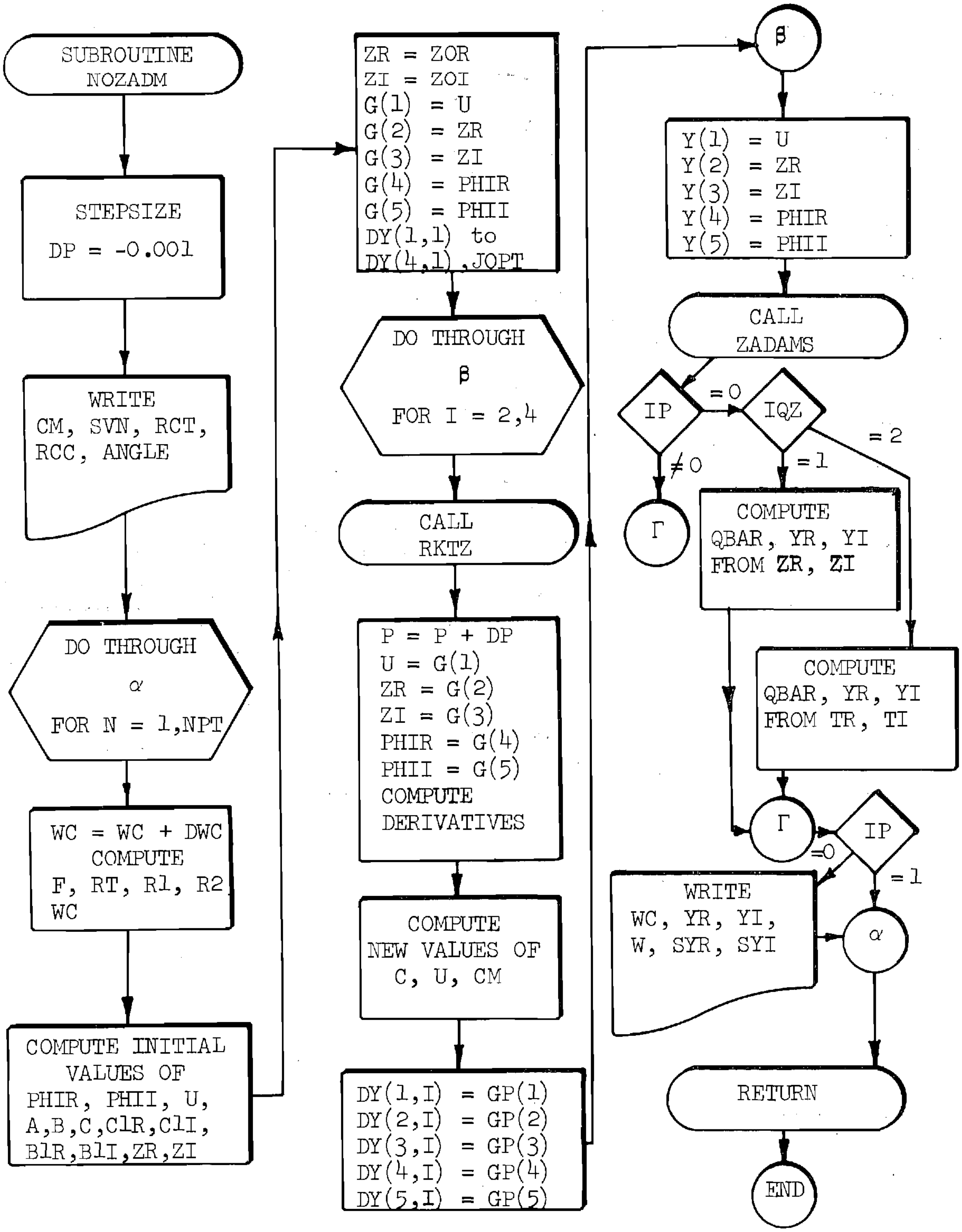

Figure A-1. Continued (Page 2 of 10)

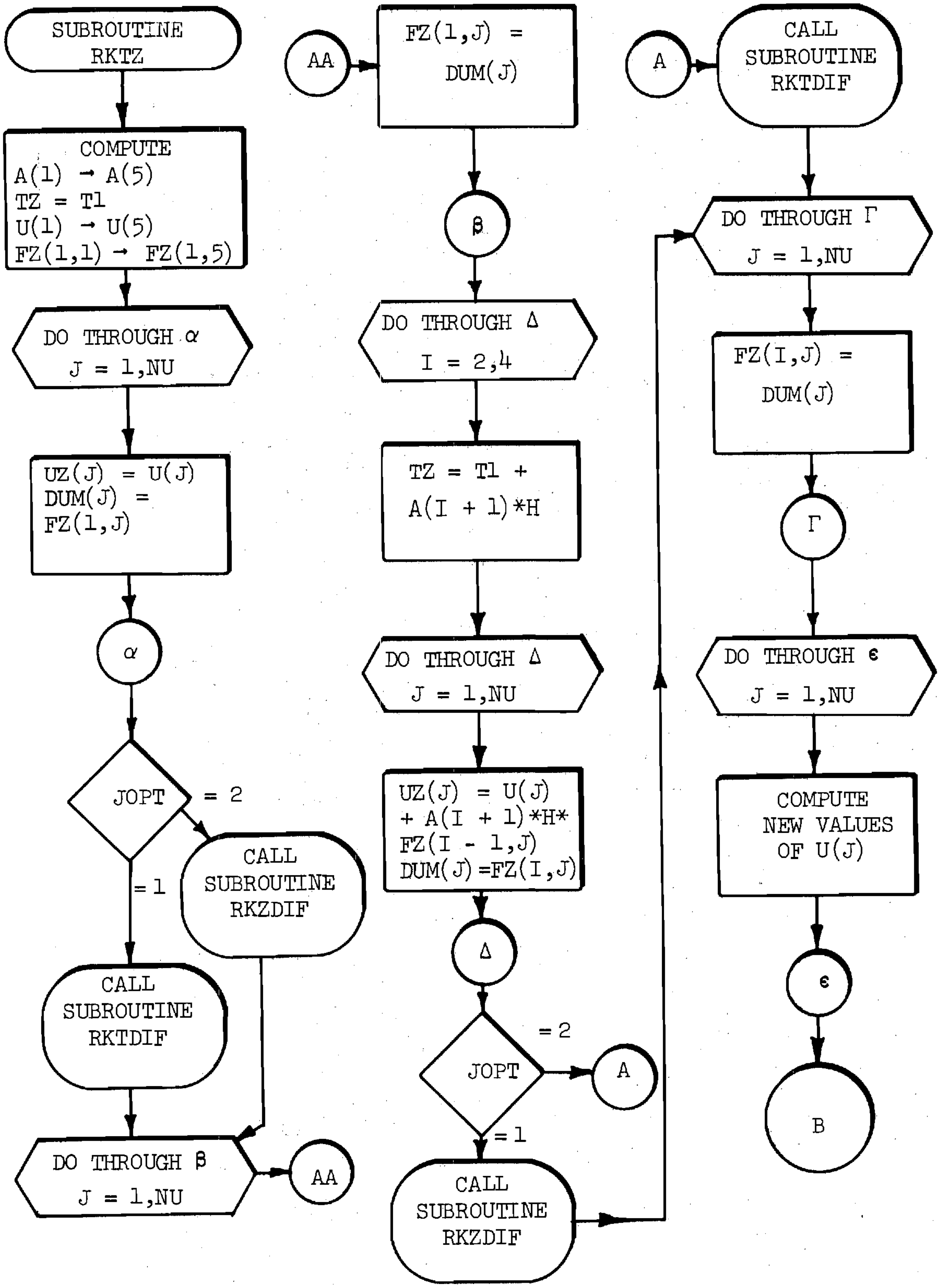

Figure A-1. Continued (Page 3 of 10)

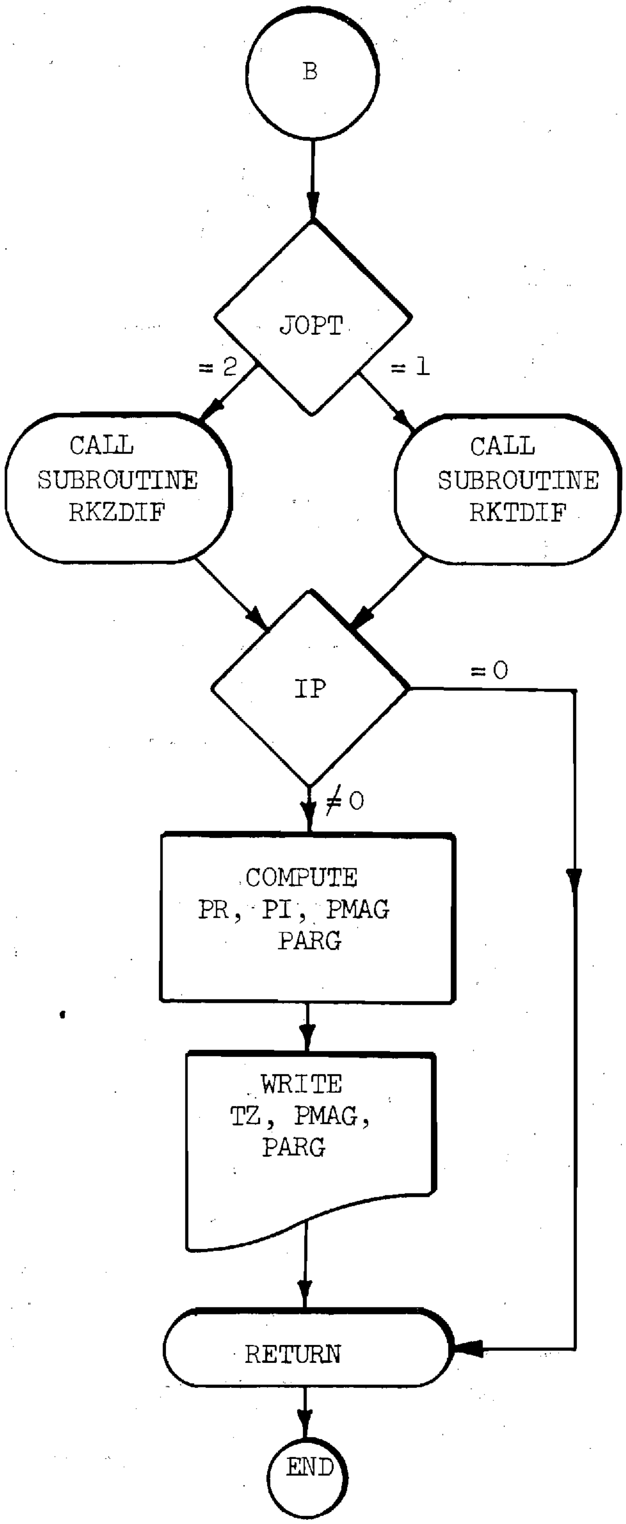

Figure A-1. Continued (Page 4 of 10)

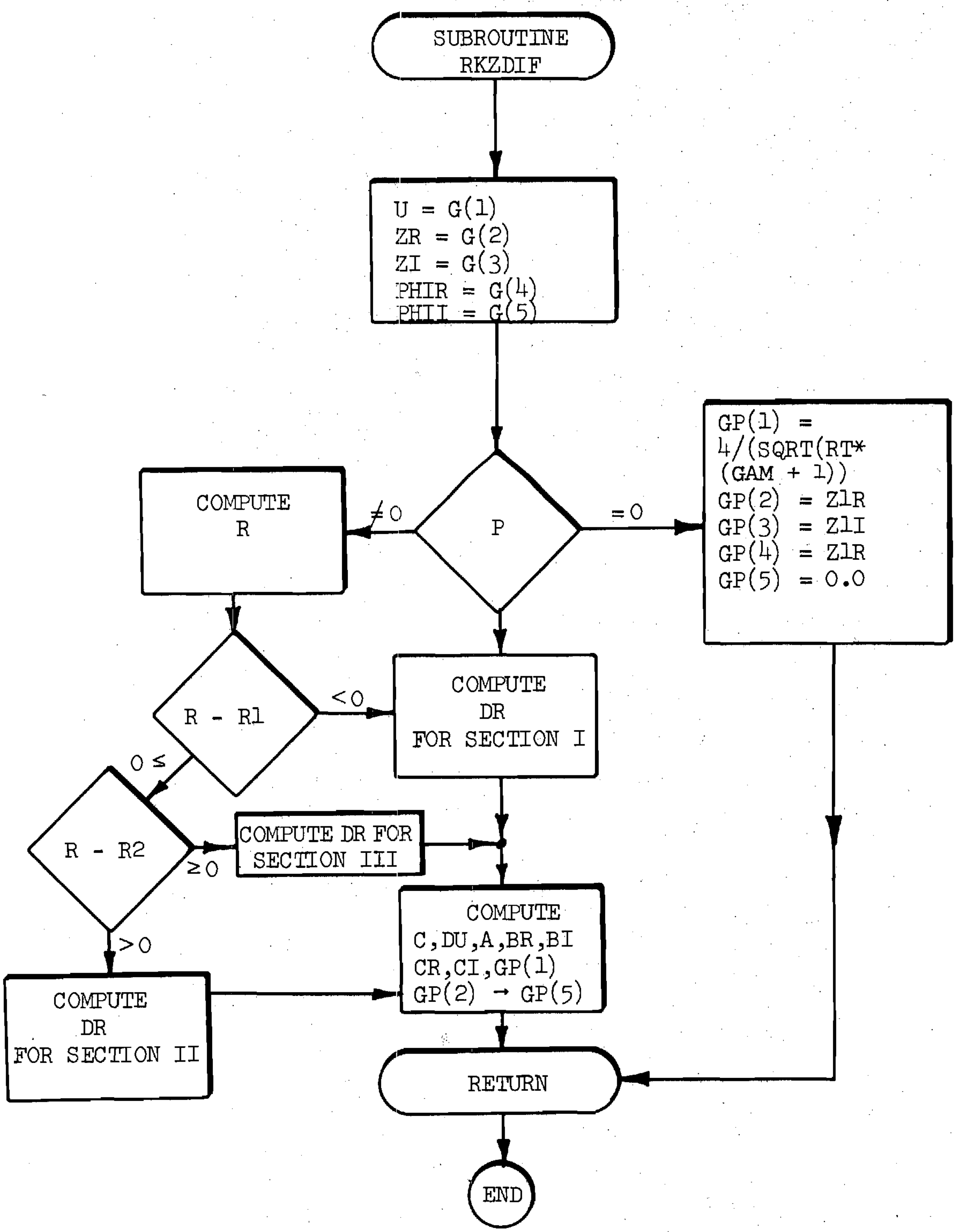

Figure A-1. Continued (Page 5 of 10)

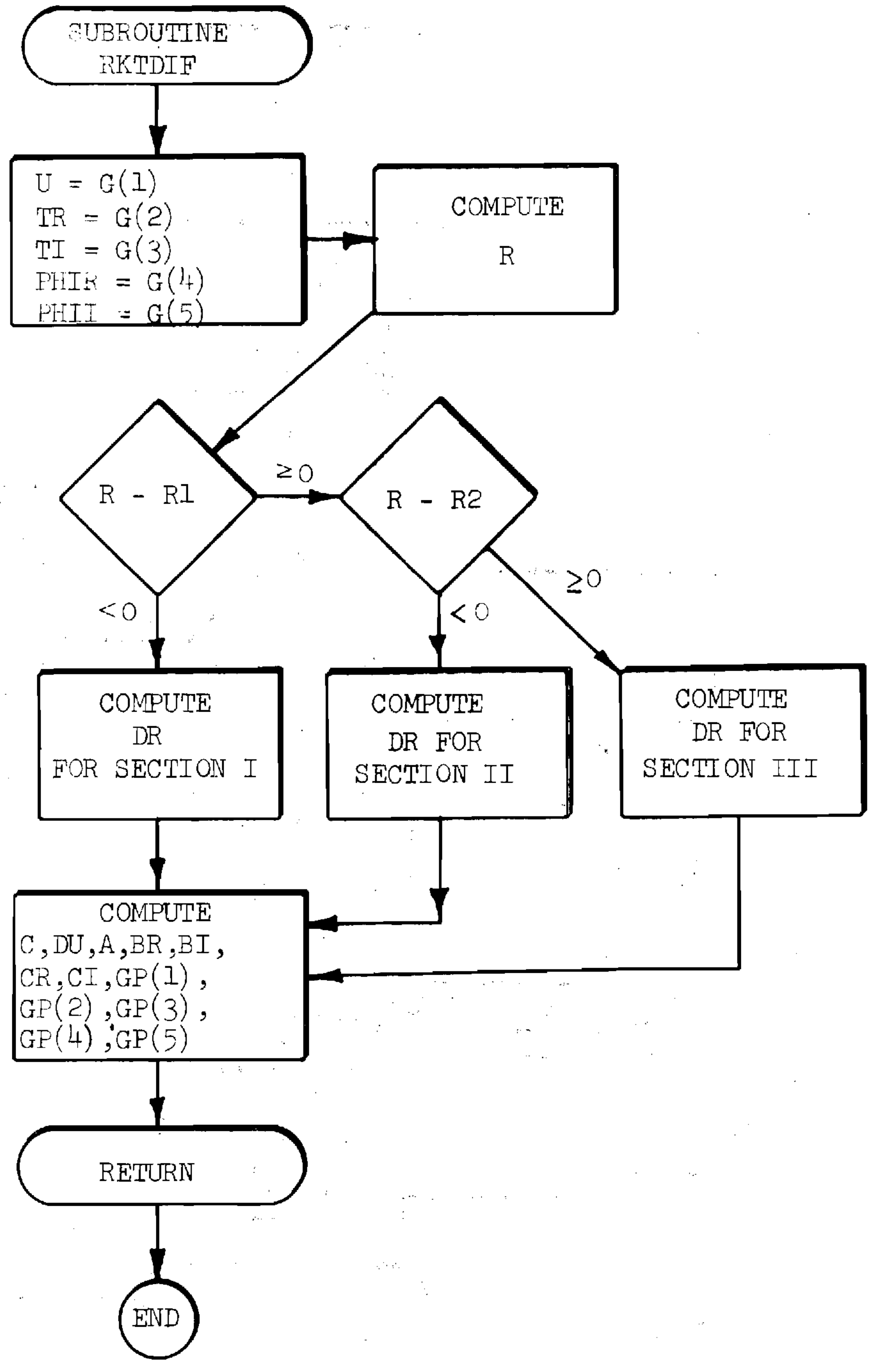

Figure A-1. Continued (Page 6 of 10)

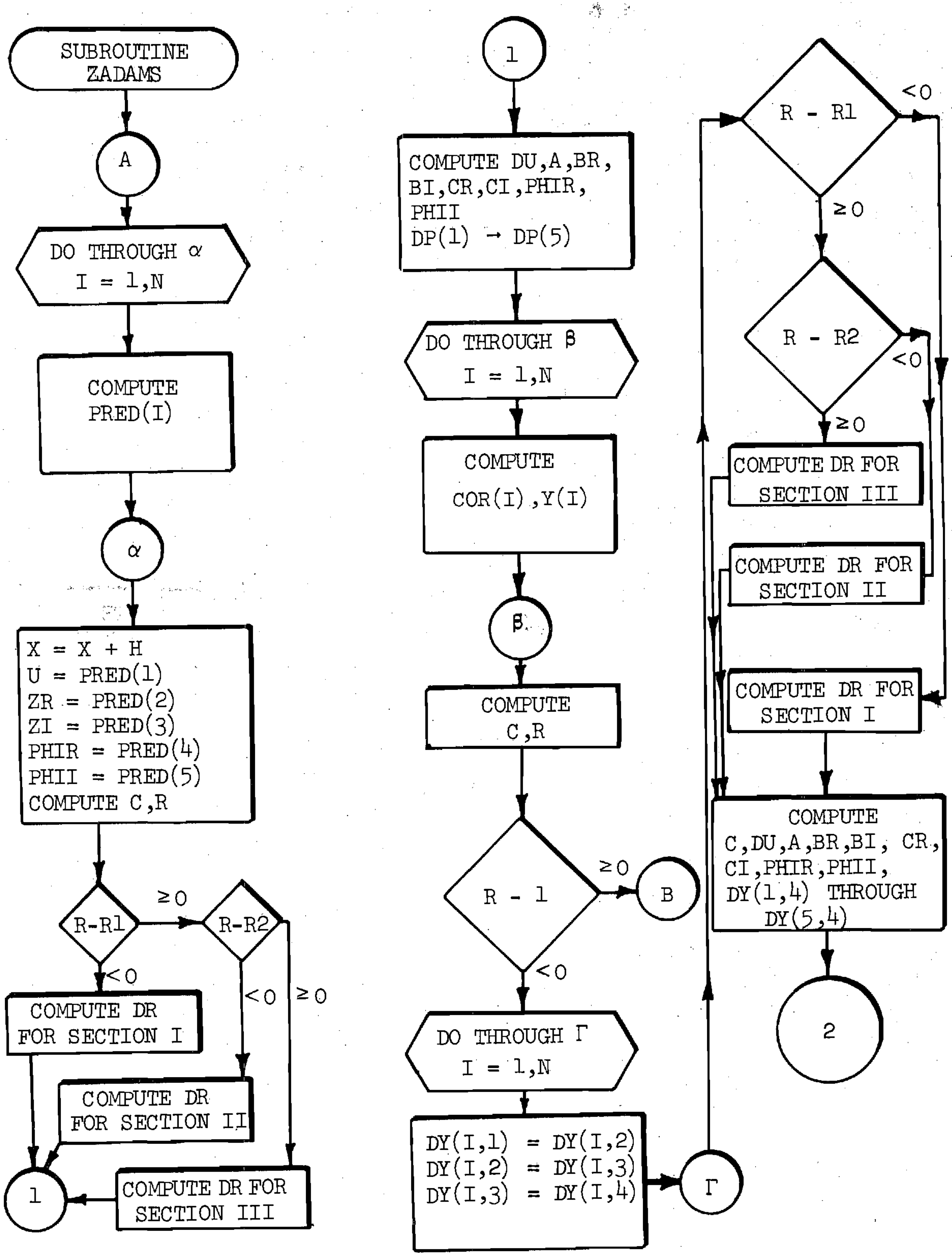

Figure A-1. Continued (Page 7 of 10)

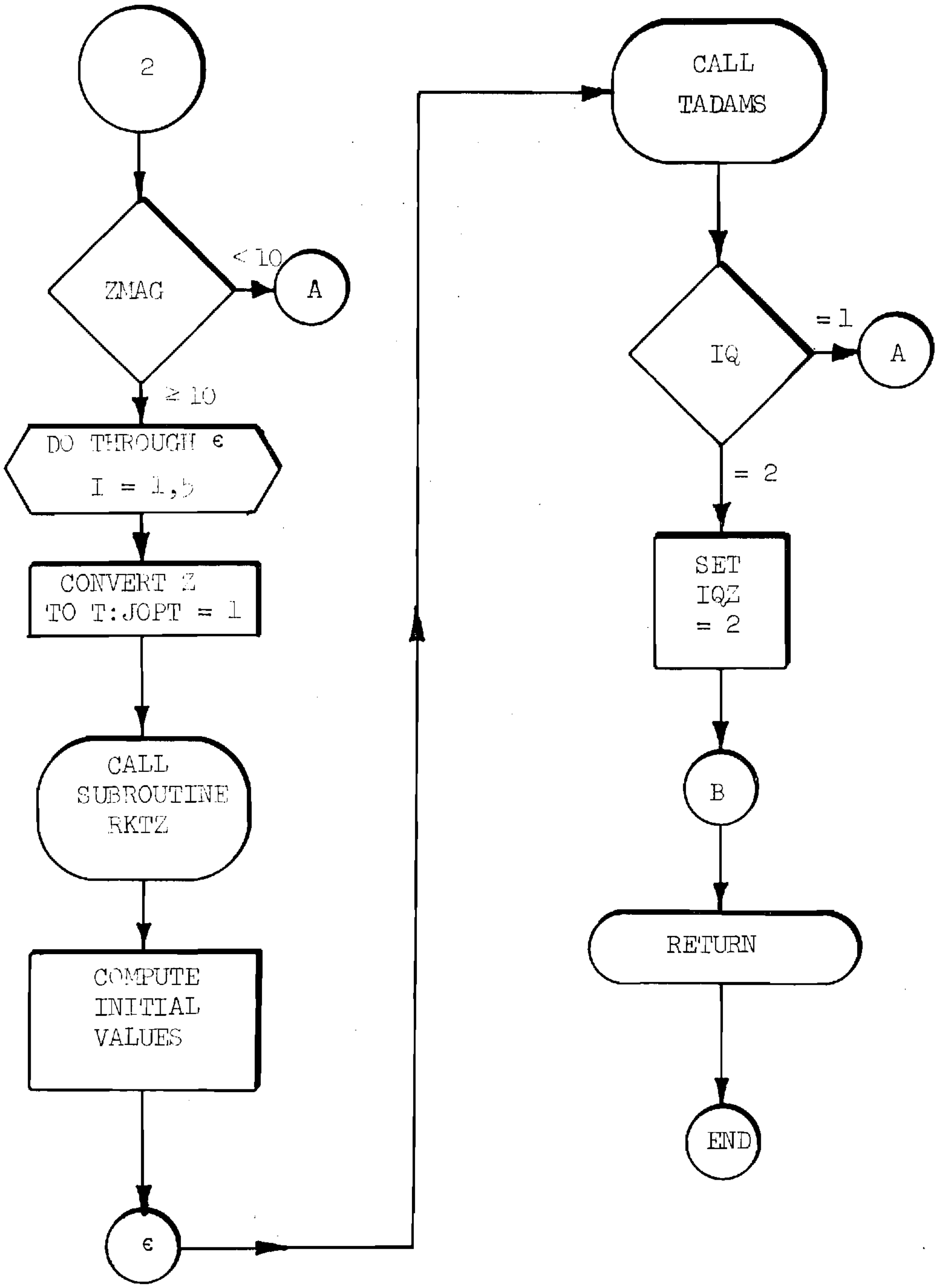

Figure A-1. Continued (Page 8 of 10)

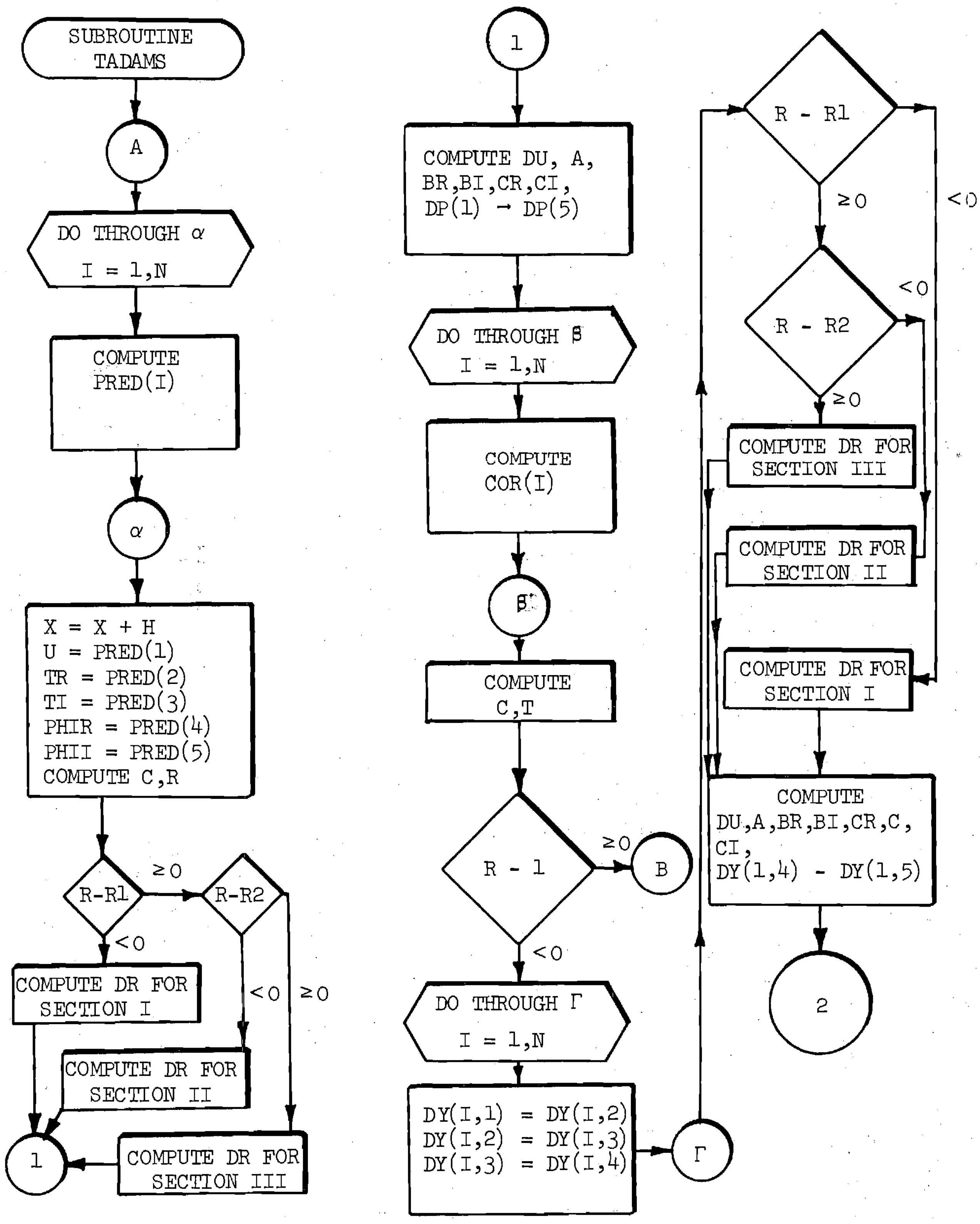
SUBROUTINE TADAMS
A
DO THROUGH α I = 1,N
COMPUTE PRED(I)
α
X = X + H
U = PRED(1)
TR = PRED(2)
TI = PRED(3)
PHIR = PRED(4)
PHII = PRED(5)
COMPUTE C,R
R-R1
≥0
<0
R-R2
<0
≥0
COMPUTE DR FOR SECTION I
COMPUTE DR FOR SECTION II
COMPUTE DR FOR SECTION III
1
1
COMPUTE DU, A, BR,BI,CR,CI, DP(1) → DP(5)
DO THROUGH β I = 1,N
COMPUTE COR(I)
β
COMPUTE C,T
R - 1
≥0
B
<0
DO THROUGH Γ I = 1,N
DY(I,1) = DY(I,2)
DY(I,2) = DY(I,3)
DY(I,3) = DY(I,4)
Γ
R - R1
≥0
<0
R - R2
<0
≥0
COMPUTE DR FOR SECTION III
COMPUTE DR FOR SECTION II
COMPUTE DR FOR SECTION I
COMPUTE DU,A,BR,BI,CR,C, CI, DY(1,4) - DY(1,5)
2

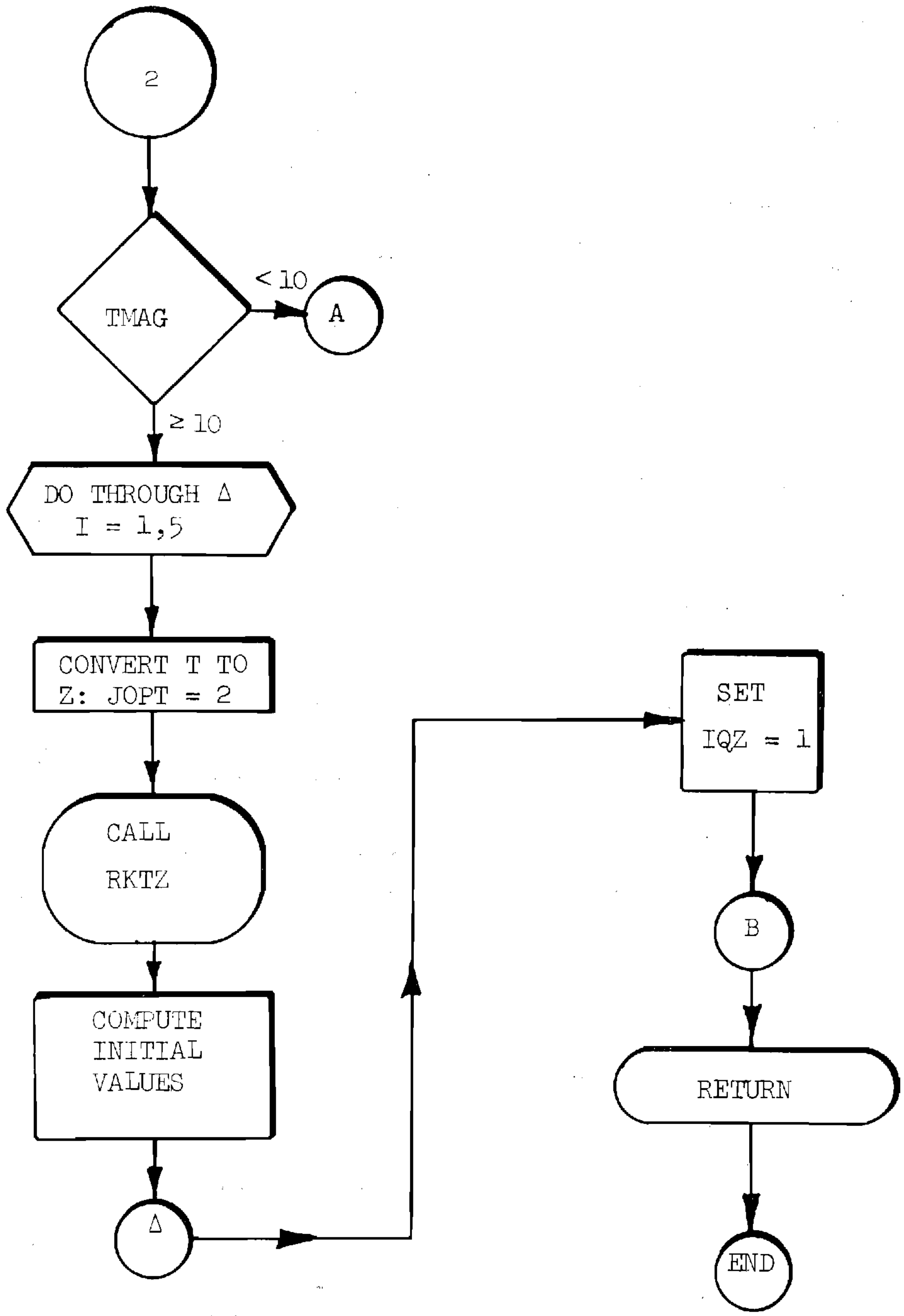

Figure A-1. Concluded (Page 10 of 10)

REFERENCES

1. Crocco, L., and Cheng, S. I., Theory of Combustion Instability in Liquid Propellant Rocket Motors, AGARDograph 8, Butterworth Publications Limited, London, 1956.
2. Crocco, L., and Sirignano, W. A., Behavior of Supercritical Nozzles under Three-Dimensional Oscillatory Conditions, AGARDograph 117, Butterworth Publications Limited, London, 1967.
3. Bell, W. A., "Experimental Determination of Three-Dimensional Liquid Rocket Nozzle Admittances," PH.D. Thesis, School of Aerospace Engineering, Georgia Institute of Technology, Atlanta, Georgia, July 1972.
4. Serra, R. A., "Determination of Internal Gas Flows by a Transient Numerical Technique," AIAA Journal, Vol. 10, May 1972, p. 603.
5. Zinn, B. T., "Longitudinal Mode Acoustic Losses in Short Nozzles," J. of Sound and Vibration, 22(1), pp. 93-105, 1972.

REPORT DISTRIBUTION LIST

Dr. R. J. Priem, MS 500-209
NASA Lewis Research Center
21000 Brookpark Road
Cleveland, Ohio 44135 (2)

Norman T. Musial
NASA Lewis Research Center
21000 Brookpark Road
Cleveland, Ohio 44135

Library
NASA Lewis Research Center
21000 Brookpark Road
Cleveland, Ohio 44135 (2)

Report Control Office
NASA Lewis Research Center
21000 Brookpark Road
Cleveland, Ohio 44135

Brooklyn Polytechnic Institute
Attn: V. D. Agosta
Long Island Graduate Center
Route 110
Farmingdale, New York 11735

Chemical Propulsion Information Agency
Johns Hopkins University/APL
Attn: T. W. Christian
8621 Georgia Avenue
Silver Spring, Maryland 20910

NASA
Lewis Research Center
Attn: E. W. Conrad, MS 500-204
21000 Brookpark Road
Cleveland, Ohio 44135

North American Rockwell Corporation
Rocketdyne Division
Attn: L. P. Combs, D/991-350, Zone 11
6633 Canoga Park, California 91304

National Technical Information Service
Springfield, Virginia 22151
(40 Copies)

Aerospace Corporation
Attn: O. W. Dykema
Post Office Box 95085
Los Angeles, California 90045

Ohio State University
Department of Aeronautical and Astronautical Engineering
Attn: R. Edse
Columbus, Ohio 43210

TRW Systems
Attn: G. W. Elverum
One Space Park
Redondo Beach, California 90278

Bell Aerospace Company
Attn: T. F. Ferger
Post Office Box 1
Mail Zone J-81
Buffalo, New York 14205

Pratt & Whitney Aircraft
Florida Research & Development Center
Attn: G. D. Garrison
Post Office Box 710
West Palm Beach, Florida 33402

NASA
Lewis Research Center
Attn: L. Gordon, MS 500-209
21000 Brookpark Road
Cleveland, Ohio 44135

Purdue University
School of Mechanical Engineering
Attn: R. Goulard
Lafayette, Indiana 47907

Air Force Office of Scientific Research
Chief Propulsion Division
Attn: Lt. Col. R. W. Haffner (NAE)
1400 Wilson Boulevard
Arlington, Virginia 22209

NASA Representative
NASA Scientific and Technical
Information Facility
P. O. Box 33
College Park, Maryland 20740
(2 Copies with Document Release
Authorization Form)

University of Illinois
Aeronautics/Astronautic Engineering
Department
Attn: R. A. Strehlow
Transportation Building, Room 101
Urbana, Illinois 61801

NASA
Manned Spacecraft Center
Attn: J. G. Thibadaux
Houston, Texas 77058

Massachusetts Institute of Technology
Department of Mechanical Engineering
Attn: T. Y. Toong
77 Massachusetts Avenue
Cambridge, Massachusetts 02139

Illinois Institute of Technology
Attn: T. P. Torda
Room 200 M. H.
3300 S. Federal Street
Chicago, Illinois 60616

AFRPL
Attn: R. R. Weiss
Edwards, California 93523

U. S. Army Missile Command
AMSMI-RKL, Attn: W. W. Wharton
Redstone Arsenal, Alabama 35808

University of California
Aerospace Engineering Department
Attn: F. A. Williams
Post Office Box 109
LaJolla, California 92037

Georgia Institute of Technology
School of Aerospace Engineering
Attn: B. T. Zinn
Atlanta, Georgia 30332

Pennsylvania State University
Mechanical Engineering Department
Attn: G. M. Faeth
207 Mechanical Engineering Bldg.
University Park, Pennsylvania 16802

TISIA
Defense Documentation Center
Cameron Station
Building 5
5010 Duke Street
Alexandria, Virginia 22314

Office of Assistant Director
(Chemical Technician)
Office of the Director of Defense
Research and Engineering
Washington, D. C. 20301

D. E. Mock
Advanced Research Projects Agency
Washington, D. C. 20525

Dr. H. K. Doetsch
Arnold Engineering Development Center
Air Force Systems Command
Tullahoma, Tennessee 37389

Library
Air Force Rocket Propulsion
Laboratory (RPR)
Edwards, California 93523

Library
Bureau of Naval Weapons
Department of the Navy
Washington, D. C.

Library
Director (Code 6180)
U. S. Naval Research Laboratory
Washington, D. C. 20390

APRP (Library)
Air Force Aero Propulsion Laboratory
Research and Technology Division
Air Force Systems Command
United States Air Force
Wright-Patterson AFB, Ohio 45433

Marshall Industries
Dynamic Science Division
2400 Michelson Drive
Irvine, California 92664

Mr. Donald H. Dahlene
U. S. Army Missile Command
Research, Development, Engineering
and Missile Systems Laboratory
Attn: AMSMI-RK
Redstone Arsenal, Alabama 35809

Library
Bell Aerosystems, Inc.
Box 1
Buffalo, New York 14205

Report Library, Room 6A
Battelle Memorial Institute
505 King Avenue
Columbus, Ohio 43201

D. Suichu
General Electric Company
Flight Propulsion Laboratory
Department
Cincinnati, Ohio 45215

Library
Ling-Temco-Vought Corporation
Post Office Box 5907
Dallas, Texas 75222

Marquardt Corporation
16555 Saticoy Street
Box 2013 - South Annex
Van Nuys, California 91409

P. F. Winternitz
New York University
University Heights
New York, New York

R. Stiff
Propulsion Division
Aerojet-General Corporation
Post Office Box 15847
Sacramento, California 95803

Technical Information Department
Aeronutronic Division of Philco
Ford Corporation
Ford Road
Newport Beach, California 92663

Library-Documents
Aerospace Corporation
2400 E. El Segundo Boulevard
Los Angeles, California 90045

Library
Susquehanna Corporation
Atlantic Research Division
Shirley Highway and Edsall Road
Alexandria, Virginia 22314

STL Tech. Lib. Doc. Acquisitions
TRW System Group
One Space Park
Redondo Beach, California 90278

Dr. David Altman
United Aircraft Corporation
United Technology Center
Post Office Box 358
Sunnyvale, California 94088

Library
United Aircraft Corporation
Pratt & Whitney Division
Florida Research and Development
Center
Post Office Box 2691
West Palm Beach, Florida 33402

Library
Air Force Rocket Propulsion
Laboratory (RPM)
Edwards, California 93523

Allan Hribar, Assistant Professor
Post Office Box 5014
Tennessee Technological University
Cookeville, Tennessee 38501

NASA
Lewis Research Center
Attn: E. O. Bourke, MS 500-209
21000 Brookpark Road
Cleveland, Ohio 44135

Library, Department 596-306
Rocketdyne Division of Rockwell
North American Rockwell, Inc.
6633 Canoga Avenue
Canoga Park, California 91304

Library
Stanford Research Institute
333 Ravenswood Avenue
Menlo Park, California 94025

Rudy Reichel
Aerophysics Research Corp.
Post Office Box 187
Bellevue, Washington 98009

Princeton University
James Forrestal Campus Library
Attn: D. Harrje
Post Office Box 710
Princeton, New Jersey 08540

U. S. Naval Weapons Center
Attn: T. Inouye, Code 4581
China Lake, California 93555

Office of Naval Research
Navy Department
Attn: R. D. Jackel, 473
Washington, D. C. 20360

Air Force Aero Propulsion Laboratory
Attn: APTC Lt. M. Johnson
Wright-Patterson AFB, Ohio 45433

Naval Underwater Systems Center
Energy Conversion Department
Attn: Dr. R. S. Lazar, Code TB 131
Newport, Rhode Island 02840

NASA
Langley Research Center
Attn: R. S. Levine, MS 213
Hampton, Virginia 23365

Aerojet General Corporation
Attn: David A. Fairchild, Mech. Design
Post Office Box 15847 (Sect. 9732)
Sacramento, California 95809

NASA
Lewis Research Center, MS 500-313
Rockets & Spacecraft Procurement Section
21000 Brookpark Road
Cleveland, Ohio 44135

NASA
Lewis Research Center
Attn: H. W. Douglass, MS 500-205
21000 Brookpark Road
Cleveland, Ohio 44135

University of Michigan
Aerospace Engineering
Attn: J. A. Nicholls
Ann Arbor, Michigan 48104

Tulane University
Attn: J. C. O'Hara
6823 St. Charles Avenue
New Orleans, Louisiana 70118

University of California
Department of Chemical Engineering
Attn: A. K. Oppenheim
6161 Etcheverry Hall
Berkeley, California 94720

Army Ballistics Laboratories
Attn: J. R. Osborn
Aberdeen Proving Ground, Maryland 21005

Sacramento State College
School of Engineering
Attn: F. H. Reardon
6000 J. Street
Sacramento, California 95819

Purdue University
School of Mechanical Engineering
Attn: B. A. Reese
Lafayette, Indiana 47907

NASA
George C. Marshall Space Flight Center
Attn: R. J. Richmond, SNE-ASTN-PP
Huntsville, Alabama 35812

Colorado State University
Mechanical Engineering Department
Attn: C. E. Mitchell
Fort Collins, Colorado 80521

University of Wisconsin
Mechanical Engineering Department
Attn: P. S. Myers
1513 University Avenue
Madison, Wisconsin 53706

North American Rockwell Corporation
Rocketdyne Division
Attn: J. A. Nestlerode,
AC46 D/596-121
6633 Canoga Avenue
Canoga Park, California 91304

Jet Propulsion Laboratory
California Institute of Technology
Attn: J. H. Rupe
4800 Oak Grove Drive
Pasadena, California 91103

University of California
Mechanical Engineering Thermal Systems
Attn: Professor R. Sawyer
Berkeley, California 94720

ARL (ARC)
Attn: K. Scheller
Wright-Patterson AFB, Ohio 45433

E-16-601
Final Tech.

NASA CR-134788

CHARACTERISTICS OF RESPONSE FACTORS OF COAXIAL GASEOUS ROCKET INJECTORS

by

B. A. Janardan
B. R. Daniel
B. T. Zinn

GEORGIA INSTITUTE OF TECHNOLOGY
ATLANTA, GEORGIA 30332

prepared for

NATIONAL AERONAUTICS AND SPACE ADMINISTRATION

NASA Lewis Research Center
Grant NGL 11-002-085
Richard J. Priem, Project Manager

Requests for copies of this report should be referred to:

National Aeronautics and Space Administration
Scientific and Technical Information Facility
P.O. Box 33
College Park, Md. 20740

1. Report No.	2. Government Accession No.	3. Recipient's Catalog No.
NASA CR-134788		

4. Title and Subtitle	5. Report Date
CHARACTERISTICS OF RESPONSE FACTORS OF COAXIAL GASEOUS ROCKET INJECTORS	March 1975
	6. Performing Organization Code
7. Author(s) B. A. Janardan, B. R. Daniel and B. T. Zinn	8. Performing Organization Report No.
	10. Work Unit No.
9. Performing Organization Name and Address Georgia Institute of Technology Atlanta, Georgia 30332	11. Contract or Grant No. NGL 11-002-085
	13. Type of Report and Period Covered Contractor Report
12. Sponsoring Agency Name and Address National Aeronautics and Space Administration Washington, D. C. 20546	14. Sponsoring Agency Code

15. Supplementary Notes

Technical Monitor, Richard J. Priem, NASA Lewis Research Center, 21000 Brookpark Road, Cleveland, Ohio 44135

16. Abstract

In this report the results of an experimental investigation undertaken to determine the frequency dependence of the response factors of various gaseous propellant rocket injectors subject to axial instabilities are presented. The injector response factors were determined, using the modified impedance-tube technique, under cold-flow conditions simulating those observed in unstable rocket motors. The tested injectors included a gaseous-fuel injector element, a gaseous-oxidizer injector element and a coaxial injector with both fuel and oxidizer elements. Emphasis was given to the determination of the dependence of the injector response factor upon the open-area ratio of the injector, the length of the injector orifice, and the pressure drop across the injector orifices. The measured data are shown to be in reasonable agreement with the corresponding injector response factor data predicted by the Feiler and Heidmann model.

17. Key Words (Suggested by Author(s))	18. Distribution Statement
Combustion instability Gaseous rocket Injector Response factor	Unclassified - unlimited

19. Security Classif. (of this report)	20. Security Classif. (of this page)	21. No. of Pages	22. Price*
Unclassified	Unclassified	36	$3.00

* For sale by the National Technical Information Service, Springfield, Virginia 22151

SUMMARY

In this report the results of an experimental investigation undertaken to determine the frequency dependence of the response factors of various gaseous propellant rocket injectors subject to axial instabilities are presented. The injector response factors were determined, using the modified impedance-tube technique, under cold-flow conditions simulating those observed in unstable rocket motors. The tested injectors included a gaseous-fuel injector element, a gaseous-oxidizer injector element and a coaxial injector with both fuel and oxidizer elements. Emphasis was given to the determination of the dependence of the injector response factor upon the open-area ratio of the injector, the length of the injector orifice, and the pressure drop across the injector orifices. The measured data are shown to be in reasonable agreement with the corresponding injector response factor data predicted by the Feiler and Heidmann model.

TABLE OF CONTENTS

INTRODUCTION 1

NOMENCLATURE 3

ANALYTICAL CONSIDERATIONS 4

RESPONSE FACTOR DETERMINATION 7

TEST INJECTORS 10

RESULTS 11

Introduction 11

Comparison of Measured and Predicted Injector Admittances 13

Effect of Injector Design Parameters Upon Injector Response Factors 14

CONCLUSIONS 16

REFERENCES 17

FIGURES 19

LIST OF ILLUSTRATIONS

Figure	Title	Page
1	Gaseous Hydrogen Injector	19
2	Experimental Apparatus	20
3	Description of Injector Configuration 1	21
4	Description of Injector Configuration 2	22
5	Description of Injector Configurations 3, 4 and 5	23
6	Description of Injector Configuration 6	24
7	Repeatability of the Measured Response Factor Data	25
8	Predicted Admittances for the Injector Configuration 1	26
9	Feiler and Heidmann Predicted Response Factor Data with and without Orifice Length Correction	27
10	Frequency Dependence of the Surface Admittances of Injector Configuration 1	28
11	Frequency Dependence of the Surface Admittances of Injector Configuration 2	29
12	Frequency Dependence of the Surface Admittances of Injector Configuration 3	30
13	Frequency Dependence of the Surface Admittances of Injector Configuration 4	31
14	Frequency Dependence of the Surface Admittances of Injector Configuration 5	32
15	Generalized Response Factor Data Plotted Against Reactance	33

16	Effect of Open-Area Ratio on Injector Response Factor	34
17	Effect of Orifice Length on Injector Response Factor	35
18	Frequency Dependence of Response Factors of Injector Configuration 6	36

INTRODUCTION

The stability of the combustor of a rocket motor depends upon the wave-energy balance between the various gain and loss mechanisms that are present in the system. The primary source of wave-energy gain is the combustion process. Wave-energy losses are provided by the mean flow, the nozzle, and mechanical damping devices (e.g., acoustic liners) which may be present in the system. As the stability of a rocket motor depends upon the difference between the gain and loss mechanisms, it is of utmost importance that quantitative data capable of describing the damping provided by the loss mechanisms and the driving provided by the unsteady combustion process must be available. Furthermore, an understanding of the dependence of these gain and loss mechanisms upon engine design parameters and operating conditions is needed. The investigation described in this report was undertaken for the purpose of obtaining a better understanding of the driving provided by the unsteady combustion process; specifically, this investigation was concerned with the acquisition of experimental data that quantitatively describes the manner in which various injector designs affect the energy gain provided by the unsteady combustion process.

The injector elements of a gaseous rocket motor control the steady state gas flow and heat transfer patterns inside the combustion chamber. In addition, the injector design influences the response of the flow rate through the injector to combustion chamber disturbances. The characteristics of this response have a profound effect upon engine stability. Customarily, the influence of the injector upon the chamber stability is described by an injector response factor which describes the manner in which the propellants' burning rate responds to a given pressure oscillation in the chamber. The injector response factor basically accounts for the dependence of the unsteady burning rate upon both the unsteady combustion process and unsteady flow of propellants through the injector elements. This response factor can be used to evaluate the energy added by the combustion process into the disturbance in the combustion chamber. It can also be used as the injector end boundary condition that needs to be satisfied in a stability analysis of a gaseous rocket combustion chamber.

Most of the available experimental investigations[1-7] on the behavior of gaseous propellant injectors were concerned with the steady operation of these devices with little or no consideration being given to the corresponding unsteady problem. In contrast, the analytical studies of Feiler and Heidmann were concerned with the predictions of the characteristics of the response factor of a gaseous injector element. In the Feiler and Heidmann analysis,[8,9] a single gaseous hydrogen injector element is modeled as a combination of lumped flow elements. The desired expressions for the injector response factor are then obtained by solving the conservation equations that describe the unsteady flow inside the various components of the injector. The resulting expressions describe the dependence of the injector response factor upon the injector geometry and the flow conditions in the chamber and the injector. In this analytical model, combustion is assumed to be concentrated in front of the injector face and the effects of mixing and chemical reactions are accounted for by the introduction of an as yet unknown time delay τ_b^*. The period τ_b^* describes the time required for the gaseous oxidizer and fuel streams to mix and burn. In Ref. 10, the Feiler and Heidmann predictions[8] have been modified to account for the compressibility of the gaseous streams flowing through the injector elements.

The results of Refs. 8 and 10 indicate that for a given frequency range and for certain ranges of the parameter τ_b^*, various injector designs can indeed result in the amplification of chamber disturbances. When τ_b^* is identically zero, which corresponds to the case of no combustion present in the system, the results of Refs. 8 and 10 indicate that under these conditions the injector acts as a mechanical damping device; a situation that is to be expected from related studies of Helmholtz resonators and acoustic liners.

Although the predictions of the Feiler and Heidmann analysis have been known for a number of years, they have never been verified experimentally. It is one of the objectives of this investigation to provide experimental data that could be used to check the validity of the Feiler and Heidmann model. In addition, this investigation is concerned with providing experimental data that will quantitatively describe the manner in which various coaxial injector designs affect the stability of gaseous propellant rocket motors. In pursuit of the above-mentioned objectives, the response factors of a number of gaseous rocket injector configurations have been measured under cold-flow conditions simulating those observed in rocket motors experiencing axial instabilities. Specifically, the response factor of configurations that simulate the flow conditions in a gaseous-fuel injector element, a gaseous-oxidizer injector element, and a coaxial injector with both fuel and oxidizer elements have been determined using the modified impedance-tube technique. The measured injector response factor data are presented and the results discussed in this report.

NOMENCLATURE

A	area
C	Capacitance, defined by Eq. (4)
c	speed of sound
I	Inductance, defined by Eq. (4)
L	length of the injector orifice
l_{eff}	effective orifice length given by Eq. (14)
M	Mach number
N	nondimensional injector response factor
P	pressure
R	Resistance, defined by Eq. (4)
V	injector dome volume
W	mass flow rate of propellant
Y	admittance
y	nondimensional admittance
α	admittance parameter defined by Eq. (7)
β	admittance parameter defined by Eq. (8)

γ	specific heat ratio
δ	equal to $(\bar{P}_d^* - \bar{P}_c^*)/\bar{P}_c^*$
λ	wavelength
ρ	density
σ	open-area ratio of the injector
τ	time lag
ω	angular frequency

Superscripts

$(\bar{\ })$	steady state quantity
$(\ )^*$	dimensional quantity
$(\ )'$	perturbation quantity

Subscripts

$(\ )_b$	associated with the combustion process
$(\ )_c$	evaluated in the chamber
$(\ )_d$	evaluated in the injector dome
$(\ )_f$	associated with the fuel
$(\ )_{ox}$	associated with the oxidizer
$(\ )_s$	evaluated at the injector surface
$(\ )_1$	evaluated at injector orifice entrance
$(\ )_2$	evaluated at injector orifice exit

ANALYTICAL CONSIDERATIONS

The ability to quantitatively describe the injector response factor is of great practical importance since the combined response of the injector flow rate and the combustion process to chamber disturbances is the mechanism responsible for amplifying and maintaining combustion instability oscillations. In an effort to develop an analytical technique for the prediction of the response factor of a gaseous injector, Feiler and Heidmann [8, 9] analyzed in detail the unsteady flow through the gaseous hydrogen injector element shown in Fig. 1. Combustion is assumed to occur a certain distance downstream of the injector exit plane and the response of the injector flow rate to a small amplitude pressure oscillation in the chamber is determined by analyzing the linearized conservation equations for each of the injector components. Assuming that each of the injector components behaves as a lumped element, and applying the Laplace transform to the linearized conservation equations, the relationships presented in Fig. 1 are obtained. By appropriate manipulations of these equations and setting the Laplace operator s equal to iω, which implies a sinusoidal time dependence of the perturbations, the following expression for the injector response factor was obtained:

$$N = \frac{W_b'}{P_c'} = \left(\frac{W'_{b_{max}}}{P'_{c_{max}}}\right)e^{i\theta} \tag{1}$$

where

$$\frac{W'_{b_{max}}}{P'_{c_{max}}} = \frac{-1}{R_2\left\{\left[\frac{R_1}{C^*\omega^*} - I^*\omega^*\right]^2 + \left[2\left(\frac{R_1 \Delta P_1^*}{\bar{P}_d^*} + \frac{\Delta P_2^*}{\bar{P}_2^*}\right)\right]^2\right\}^{\frac{1}{2}}} \tag{2}$$

$$\theta = \frac{\pi}{2} - \omega^*\tau_b^* - \arctan\frac{2\left\{\frac{R_1\Delta P_1^*}{\bar{P}_d^*} + \frac{\Delta P_2^*}{\bar{P}_2^*}\right\}}{\left\{\frac{R_1}{C^*\omega^*} - I^*\omega^*\right\}} \tag{3}$$

and

$$C^*\omega^* = \left(\bar{\rho}_d^* V^*/\gamma\bar{W}^*\right)\omega^* \quad ; \quad I^*\omega^* = \left[\bar{W}^*\left(L^*/A_1^*\right)/g\bar{P}_2^*\right]\omega^* \tag{4a}$$

$$\frac{\Delta P_1^*}{\bar{P}_d^*} = \left(\bar{P}_d^* - \bar{P}_1^*\right)/\bar{P}_d^* \quad ; \quad \frac{\Delta P_2^*}{\bar{P}_2^*} = \left(\bar{P}_2^* - \bar{P}_c^*\right)/\bar{P}_2^* \tag{4b}$$

$$R_1 = \frac{\bar{P}_d^*}{\bar{P}_1^* - \left(\Delta P_1^*/\gamma\right)} \; ; \quad R_2 = \frac{\bar{P}_2^*}{\bar{P}_c^* - \left(\Delta P_2^*/\gamma\right)} \tag{4c}$$

The quantity τ_b^* appearing in Eq. (3) is the residence time of a propellant mass element in the combustor prior to its combustion; τ_b^* is identically zero when there is no combustion in the system. The parameters appearing in Eq. (4) depend upon the injector geometry and engine operating conditions, and their influence upon the injector element response factor is also of interest to rocket designers.

Expressions similar to those developed above for the gaseous-fuel injector element can also be developed for the gaseous-oxidizer injector element. The total response, N_t, of a coaxial gaseous injector element can then be obtained, by substituting the expressions for the fuel and oxidizer response factors into the following equation:

$$N_t = \frac{W_t'}{P'} = \frac{\left(W_t^*\right)'/\bar{W}_t^*}{(P^*)'/\bar{P}^*} = \frac{\left\{\left(W_{ox}^*\right)' + \left(W_f^*\right)'\right\}/\bar{W}_t^*}{(P^*)'/\bar{P}^*} \tag{5}$$

$$= \left[\frac{\bar{W}_{ox}^*}{\bar{W}_t^*}\right] N_{ox} + \left[\frac{\bar{W}_f^*}{\bar{W}_t^*}\right] N_f \tag{5}$$

where N_{ox} and N_f respectively represent the response factors of the oxidizer and fuel injector elements while $\bar{W}_{ox}^*/\bar{W}_t^*$ and $\bar{W}_f^*/\bar{W}_t^*$ represent the ratios of the mean oxidizer and fuel flow and the total mean flow, respectively.

RESPONSE FACTOR DETERMINATION

The required injector response factor data were determined in this investigation from injector admittance data measured by use of the modified impedance-tube technique. The impedance tube setup shown in Fig. 2, consists of a 6-inch diameter cylindrical tube with a sound source capable of generating harmonic waves of desired frequency placed at one end. The injector element under investigation is placed at the other end. During an experiment, the flow of a gaseous propellant through the injector is simulated by the flow of air. Regulating valves are provided to ensure that the pressure drop across the injector orifices is maintained at a required value. By means of an acoustic driver, a standing wave pattern of a given frequency is excited in the tube and a microphone probe is traversed along the tube to measure the axial variation of the standing pressure wave pattern. As explained in the next section, the admittance of the injector end of the impedance-tube is determined from the measured axial variation of the standing pressure wave. The frequency dependence of the admittance and the response factor of the injector is determined by repeating the experiment at different frequencies.

The first step in the determination of the injector response factor N consists of the measurement of the "average" surface admittance Y_s^* at the injector end of the modified impedance tube. The "average" surface admittance is defined as the ratio of the "average" normal velocity perturbation across the injector surface and the local pressure perturbation; that is:

$$Y_s^* = \frac{\vec{u}_s^{*\prime} \cdot \vec{n}}{P_s^{*\prime}} \tag{6}$$

The admittance Y_s^* is a complex number whose real and imaginary parts describe the relationships that exist at the location under consideration between the amplitudes and phases of the velocity and pressure perturbations.

From a physical point of view it is more satisfying to describe the admittance by means of two parameters α and β which respectively describe changes in amplitudes and phases between the incident and reflected pressure waves at the location under consideration; that is:

$$\left[\frac{\text{Amplitude of Reflected Pressure Wave}}{\text{Amplitude of Incident Pressure Wave}}\right]_{\substack{\text{Injector}\\ \text{Face}}} = e^{-2\pi\alpha} \tag{7}$$

$$\left[\begin{array}{l}\text{Phase change Between Incident and}\\ \text{Reflected Pressure Waves}\end{array}\right]_{\substack{\text{Injector}\\ \text{Face}}} = \pi(1 + 2\beta) \tag{8}$$

The parameter β appearing above satisfies the condition $|\beta| \leq 0.5$.

The expressions required for the calculation of the injector surface admittance are obtained from solutions of the system of conservation equations which describe the behavior of small amplitude, one-dimensional waves inside an impedance-tube containing a steady one-dimensional flow. These solutions are required to satisfy an admittance boundary condition at the injector surface in terms of the as yet unknown parameters α and β. The resulting expressions (See Ref. 12 for detailed derivations of these solutions), describing the time and space dependence of the pressure and velocity perturbations at the injector surface, are substituted into Eq. (6) to obtain an expression for the injector surface admittance. Normalizing the resulting expression with the characteristic admittance $Y_g^* = 1/\bar{\rho}^*\bar{c}^*$ of the gas medium, the following expression for the nondimensional injector surface admittance y_s is obtained[12]:

$$y_s = \frac{Y_s^*}{Y_g^*} = \Gamma + i\eta = \coth \pi(\alpha - i\beta) \tag{9}$$

It can also be shown[12] that the parameters α and β, which appear in Eqs. (7), (8) and (9) must satisfy the following relationships between variables describing the characteristics of the standing wave pattern:

$$\alpha = \frac{1}{\pi} \tanh^{-1}\left[\frac{|P^*_{min}|}{|P^*_{max}|}\right]; \quad \beta = \frac{2Z^*_{min}}{\lambda^*} \tag{10}$$

In impedance-tube experiments and in the present study, the relationships presented in Eq. (10) are used to determine the admittance variables α and β. The procedure leading to the determination of α and β consists of measuring (a) the distance Z^*_{min} from the injector surface to the first pressure amplitude minimum and (b) the ratio of $|P^*_{min}|/|P^*_{max}|$ of the minimum pressure amplitude to the maximum pressure amplitude. The resulting values of α and β are then substituted into Eq. (9) to obtain the injector surface admittance.

From the measured injector surface admittance y_s, the injector orifice admittance y_2 is determined by using the following relationship obtained from the perturbed form of mass conservation law:

$$(u^*)'_s A^*_s = (u^*)'_2 A^*_2$$

which upon dividing by $(P^*)'_s$ gives

$$y_2 = y_s/\sigma \tag{11}$$

where $\sigma = A^*_2/A^*_s$ is the injector open-area ratio. In deriving Eq. (11) the gas has been assumed to be incompressible; an allowable assumption for the situation under consideration.

An expression relating the nondimensional response factor N to the nondimensional admittance y is obtained from the definitions of these two quantities as follows:

$$N = \frac{\underset{\rightarrow}{W}^{*\prime} \cdot \underset{\rightarrow}{n}/\bar{W}^{*}}{P^{*\prime}/\bar{P}^{*}} = \frac{\bar{P}^{*}}{\bar{\rho}^{*}\bar{u}^{*}}\left[\bar{\rho}^{*} \frac{\underset{\rightarrow}{u}^{*\prime} \cdot \underset{\rightarrow}{n}}{P^{*\prime}} + \frac{\rho^{*\prime}}{P^{*\prime}} \underset{\rightarrow}{\bar{u}}^{*} \cdot \underset{\rightarrow}{n}\right]$$

$$= \frac{1}{\gamma\bar{M}}\left[\bar{\rho}^{*}\bar{c}^{*} \frac{\underset{\rightarrow}{u}^{*\prime} \cdot \underset{\rightarrow}{n}}{P^{*\prime}} + \underset{\rightarrow}{\bar{M}} \cdot \underset{\rightarrow}{n}\right]$$

$$= \frac{1}{\gamma\bar{M}} \left(y + \underset{\rightarrow}{\bar{M}} \cdot \underset{\rightarrow}{n}\right) \tag{12}$$

In deriving Eq. (12) it has been assumed that the gas is perfect and that the oscillations are isentropic. The response factor N of the test injectors is finally obtained by substituting the measured orifice admittance y_2 into Eq. (12) which can be rewritten in the following form for the experimental setup of this investigation:

$$N = \frac{1}{\gamma}\left[- \frac{y_2}{\bar{M}_2} + 1\right] \tag{13}$$

TEST INJECTORS

In order to obtain the needed data, the frequency dependence of the response factors of the injector configurations shown in Figs. 3 through 6 have been determined. The characteristic dimensions of these injectors, namely, the injector orifice open-area ratio, the orifice length, and the injector dome volume are also presented in the above-mentioned figures.

Injector configurations 1 and 2 were designed to simulate the flow behavior through gaseous-fuel injector elements. The dimensions of these configurations were chosen to provide data capable of determining the effect of the injector open-area ratio upon the injector response factor. Injector configurations 3 through 5 were designed to simulate the flow behavior in gaseous-oxidizer injector elements, and their dimensions were chosen to allow the determination of the dependence of the injector response factor upon the orifice length. Injector configuration 6, shown in Fig. 6, consists of a combination of configurations 1 and 3. This configuration was designed to simulate the flow behavior in a coaxial injector of a gaseous rocket motor. This injector configuration was tested to check the validity of Eq. (5) by comparing its measured response factors with predicted response factor data obtained by substituting the individually-predicted response factors of configurations 1 and 3 into Eq. (5).

RESULTS

Introduction

The results presented in this section were obtained by measuring the admittances and response factors of the test injectors over the frequency range of 150 to 800 Hz which included their resonant frequency. To establish the repeatability of the experimental data, the frequency dependence of the response factor one of the test injectors was measured on two different occasions and the response factor data obtained in these tests are presented in Fig. 7. An examination of this figure indicates that the measurement technique yields repeatable data. The scatter observed in the measured values of the imaginary part of the response factor is due to the fact that at the corresponding frequencies the standing wave in the impedance tube had a flat minima and hence its axial location could not be precisely measured.

Before presenting the results, it is necessary to point out a difference between the geometrical configurations of the injector elements whose admittances were measured in this study and the injector configurations considered in the theoretical model of Feiler and Heidmann.[8] The theoretical analysis considers the behavior of a single injector element and its predictions provide a response factor that is valid at the exit plane of the injector orifice. As it would be extremely difficult to directly measure the response factor of a single injector element, this study undertook the measurement of the response factors of configurations containing either 5 or 13 injector elements. As stated earlier, the admittances measured in this study represent "average" admittances over the tested injector surface. Hence, before any meaningful comparisons between the predicted and the measured sets of admittance data can be made, the above-mentioned difference must be suitably taken into consideration. This point was discussed in the previous section where it was shown that by using mass conservation considerations, this difference can be accounted for by multiplying the theoretically predicted orifice admittances by the open-area ratio σ of the injector configuration. This step "averages" the predicted orifice admittance over the injector surface. To illustrate this point, the theoretically predicted frequency dependence of the admittances of injector configuration 1 with a pressure drop δ of 0.068 across the injector orifices is presented in Fig. 8. The broken lines in this figure describe the admittances at the exit plane of the injector orifices while the solid lines represent the "average" admittances of the injector surface. It is this "average" data which has to be compared with the admittances measured during this investigation.

In the present study, the expressions provided by Feiler and Heidmann[8] have been slightly modified when used to compute the predicted admittances and response factors of the test injector configurations. This was necessitated by the observation that the measured resonant frequencies of the tested injectors did not coincide with their predicted values. This is illustrated by the data presented in Fig. 9. The broken line in this figure describes the theoretically predicted frequency dependence of the real and imaginary parts of the response factor of one of the test injectors. An examination of this figure indicates that while the two sets of data are similar in magnitude and shape, the observed injector resonant frequency is lower than its predicted value. In an effort to explain this frequency shift, use was made of knowledge developed in studies concerned with the behavior of Helmholtz resonators and acoustic liners[13, 14] where it has been well known that the effective length of the slug of the gaseous mass oscillating within the orifice is longer than the orifice length.

It is also well known that the resonant frequencies of Helmholtz resonators and acoustic liners are inversely proportional to the square root of the orifice length. This suggests that the actual length L^* of the injector orifices should be replaced by an effective length l^*_{eff} whenever it appears in the analytical expressions of the Feiler and Heidmann analysis. From experimental reactance data of acoustic liners with apertures of various thicknesses, Garrison[13] developed the following empirical relation for the effective length l^*_{eff}:

$$l^*_{eff} = L^* + 0.85\left[1 - 0.70\sqrt{\sigma}\right]\left(D^*_o - D^*_i\right) \quad (14)$$

where D^*_o and D^*_i are respectively the outer and inner diameters of the orifices. Computing the predicted response factor data of the test injector with L^* replaced by the effective length l^*_{eff}, the result indicated by the solid line in Fig. 9 was obtained. The experimental resonant frequency now is in better agreement with the predicted resonant frequency than the original Feiler and Heidmann prediction. Based on this result all of the theoretically predicted data presented in the remainder of this report was obtained by suitably incorporating Eq. (14) into the expressions of Ref. 8.

Comparison of Measured and Predicted Injector Admittances

The injector admittances measured during the course of the present study are presented in Figs. 10 through 14 along with admittance data predicted by the Feiler and Heidmann model. These figures describe, respectively, the frequency dependence of the real and imaginary parts of the surface admittances of injector configurations 1 through 5. An examination of these figures indicates a reasonable agreement between the measured and predicted admittances. The discrepancy observed in the data may be, among other factors, due to the fact that radial pressure gradients were measured in the domes of some of the tested injectors. These pressure gradients resulted in different pressure drops across different injector elements. The possibility of such pressure gradients is not considered in the theoretical model[8] and their effect cannot be accounted for in predicting the injectors' response factors. The theoretical admittances obtained in this study were computed assuming that the pressure drops across all of the injector orifices were equal to the pressure drop measured across one of the outer injector elements; an assumption that is contrary to the above-mentioned observations.

The response factors of injector configurations 1 through 5 were obtained by substituting the measured admittance data into Eq. (13). As suggested in Ref. 8, the response factor data for the injectors tested in this program, with different pressure drops, are plotted in Fig. 15 in terms of a generalized response factor φ defined as

$$\varphi = N_{Real}\left\{2R_2\left(\frac{R_1\Delta P_1^*}{\bar{P}_d^*} + \frac{\Delta P_2^*}{\bar{P}_2^*}\right)\right\} \tag{15}$$

and a generalized reactance Ψ defined as

$$\Psi = \left(\frac{R_1}{C^*\omega^*} - I^*\omega^*\right)/2\left(\frac{R_1\Delta P_1^*}{\bar{P}_2^*} + \frac{\Delta P_2^*}{\bar{P}_2^*}\right) \tag{16}$$

An examination of Fig. 15 indicates a reasonable agreement between the experimental data and the predictions of the Feiler and Heidmann model. Furthermore, this plot points to a convenient way for correlating and plotting injector response factor data.

Effect of Injector Design Parameters Upon Injector Response Factors

During this investigation, the dependence of the injector response factors upon the pressure drop across the injector orifices, the open-area ratio of the injector and the length of the injector orifices were investigated. The dependence of the injector response upon the pressure drop across the injector orifices is demonstrated by the data presented earlier in Figs. 10 through 14. An examination of these figures indicates that the injector admittances and response factors decrease rapidly in magnitude with increase in pressure drop across the orifices. Increase in pressure drop results in an increase in the resistance of the injector plate. This decreases the coupling between the pressure oscillation inside the injector dome and the pressure oscillation in the combustor in front of the injector plate. The increase in the injector pressure drop is observed, however, to have little effect upon the resonant frequency of the injector.

In order to determine the dependence of the injector response factor upon the injector characteristic dimensions, the admittance data measured with test configurations 1, 4 and 5 were substituted into Eq. (13) and the response factors obtained are presented in Figs. 16 and 17. The data presented in Fig. 16 describes the effect of the open-area ratio upon the injector response factor for a given orifice length and mass flux through the injector orifices. An examination of Fig. 16 indicates that an increase in the open-area ratio of the injector results in an increase in the damping provided by the injector. In addition, the data indicates an increase in the resonant frequency which is to be expected from results of studies on Helmholtz resonantors. The increase in the injector damping is due to the fact that for a given mass flux an increase in the open-area ratio results in a decrease in the pressure drop across the orifices. This in turn decreases the injector resistance. From a stability point of view this seems to suggest that, for a given mass flow across the injector plate, an injector should be designed with as large an open-area ratio as possible. However, in contemplating such changes in actual systems, one should also consider how an increase in the open-area ratio would affect other gain or loss mechanism in the system. For example, in an actual gaseous propellant rocket motor a decrease in the pressure drop across the injector orifices also affects the mixing rate and hence the propellants burning rate.

For a given open-area ratio and pressure drop across the orifices, data describing the effect of the orifice length upon the injector response factor is presented in Fig. 17. An examination of this figure indicates that an increase in the orifice length from 0.875" to 1.75" resulted in a decrease in the resonant frequency of the injector. Further examination of Fig. 17 indicates that although there is no observable change in the magnitude of the response factor at resonance, an increase in the orifice length decreases the band width of the response curve.

CONCLUSIONS

The measured data indicates that under the test conditions encountered in this study, there is reasonable agreement between the measured injector response factors and those predicted by the Feiler and Heidmann model. The good agreement observed between the measured and predicted total response factors of coaxial injectors containing both fuel and oxidizer elements suggests that the procedure suggested by Feiler and Heidmann for calculating the total response factors from individual injector response factor data is indeed valid.

The measured response factor data indicates that the orifice length can be varied to shift the resonant frequency of the injector without any change in the magnitude of the response factor at resonance. However, changes in pressure drop across the orifices and the open-area ratio of the injector were found to have a considerable effect on the injector response factor.

The injector configurations investigated in this program were similar to Helmholtz Resonators with a steady through flow. The interaction of such a configuration with a sound wave is not expected to produce any wave amplification, as was recognized by Feiler and Heidmann and confirmed by the data reported in this report. When a time delay, τ_b^*, due to combustion is added to the theoretical model, the phase relationship between the pressure and velocity perturbations required for wave amplification (and instability) is obtained. To test the latter hypothesis, and in the process measure the characteristic combustion time, τ_b^*, additional studies that will measure the response factors of "reacting" gaseous rocket injectors, under a variety of conditions simulating those observed in unstable engines, are needed.

REFERENCES

1. Falkenstein, G. L. and Domokos, S. J., "High Pressure Gaseous Hydrogen/Gaseous Oxygen Thrusters," AIAA/SAE 7th Propulsion Conference, Salt Lake City, Utah, AIAA Paper No. 71-737, June 1971.
2. Gregory, J. W. and Herr, P. N., "Hydrogen-Oxygen Space Shuttle ACPS Thruster Technology Review," AIAA/SAE 8th Propulsion Conference, New Orleans, Louisiana, AIAA Paper No. 72-1158, November 1972.
3. Paster, R. D., Lauffer, J. R., and Domokos, S. J., "Low Pressure Gaseous Hydrogen/Gaseous Oxygen Auxiliary Rocket Engines," AIAA/SAE 7th Propulsion Conference, Salt Lake City, Utah, AIAA Paper No. 71-738, June 1971.
4. Nagai, C. K., Gurnitz, R. N., and Clapp, S. D., "Cold-Flow Optimization of Gaseous Oxygen/Gaseous Hydrogen Injectors for the Space Shuttle APS Thrustor," AIAA/SAE 7th Propulsion Conference, Salt Lake City, Utah, AIAA Paper No. 71-673, June 1971.
5. Kors, D. L. and Calhoon, D. F., "Gaseous Oxygen/Gaseous Hydrogen Injector Element Modeling," AIAA/SAE 7th Propulsion Conference, Salt Lake City, Utah, AIAA Paper No. 71-674, June 1971.
6. Calhoon, D. F., Ito, J. I., and Kors, D. L., "Investigation of Gaseous Propellant Combustion and Associated Injector/Chamber Design Guidelines," NASA CR-121234, July 1973.
7. Burick, R. J., "Optimum Design of Space Storable Gas/Liquid Coaxial Injectors," Journal of Spacecraft and Rockets, Vol. 10, No. 10, pp. 663-670, October 1973.
8. Feiler, C. E. and Heidmann, M. F., "Dynamic Response of Gaseous Hydrogen Flow System and its Application to High Frequency Combustion Instability," NASA TN D-4040, June 1967.
9. Harrje, D. T., Editor, Liquid Propellant Rocket Combustion Instability, NASA SP-194, 1972.
10. Priem, R. J. and Yang, J. Y. S., "Technique for Predicting High Frequency Stability Characteristics of Gaseous Propellant Combustors," NASA TN D-7406, October 1973.
11. Morse, P. M. and Ingard, K. V., Theoretical Acoustics, McGraw Hill,

New York, 1968.

12. Bell, W. A., Daniel, B. R., and Zinn, B. T., "Experimental and Theoretical Determination of Admittances of a Family of Nozzles Subjected to Axial Instabilities," Journal of Sound and Vibration, Vol. 30, No. 2, pp. 179-190, September 1973.

13. Garrison, G. D., "Suppression of Combustion Oscillations with Mechanical Damping Devices," Interim Report PA FR-3299, Pratt and Whitney Aircraft Florida Research and Development Center, West Palm Beach, Florida, August 1969.

14. Lewis, G. D. and Garrison, G. D., "The Role of Acoustic Absorbers in Preventing Combustion Instability," AIAA/SAE 7th Propulsion Conferences, Salt Lake City, Utah, AIAA Paper No. 71-699, June 1971.

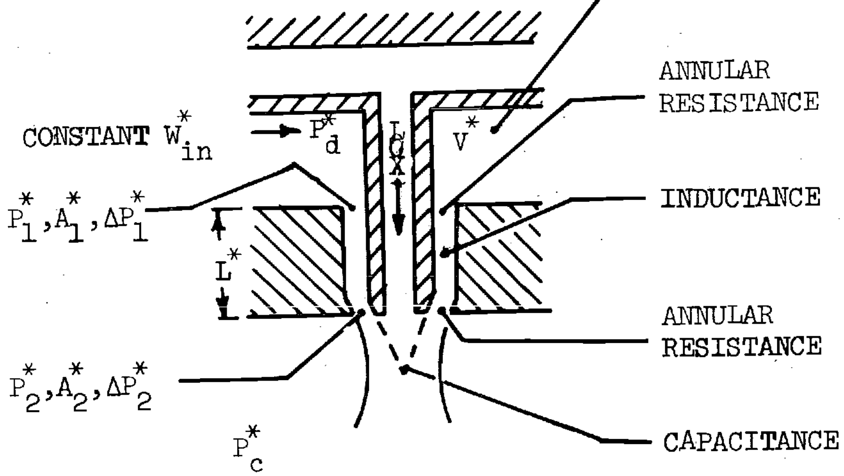

$$\frac{\bar{\rho}_d^* V^*}{\gamma \bar{W}^*} s P_d' = -W'$$

$$W' = \frac{1}{2}\left[\frac{\bar{P}_d^*}{\Delta P_1^*} P_d' + \left(\frac{1}{\gamma} - \frac{\bar{P}_1^*}{\Delta P_1^*}\right) P_1'\right]$$

$$P_1' - P_2' = \frac{\bar{W}^* L^*}{g \bar{P}_2^* A_1^*} s W'$$

$$W' = \frac{1}{2}\left[\frac{\bar{P}_2^*}{\Delta P_2^*} P_2' + \left(\frac{1}{\gamma} - \frac{\bar{P}_c^*}{\Delta P_2^*}\right) P_c'\right]$$

$$W_b' = W' e^{-\tau_b^* s}$$

Figure 1. Gaseous Hydrogen Injector.

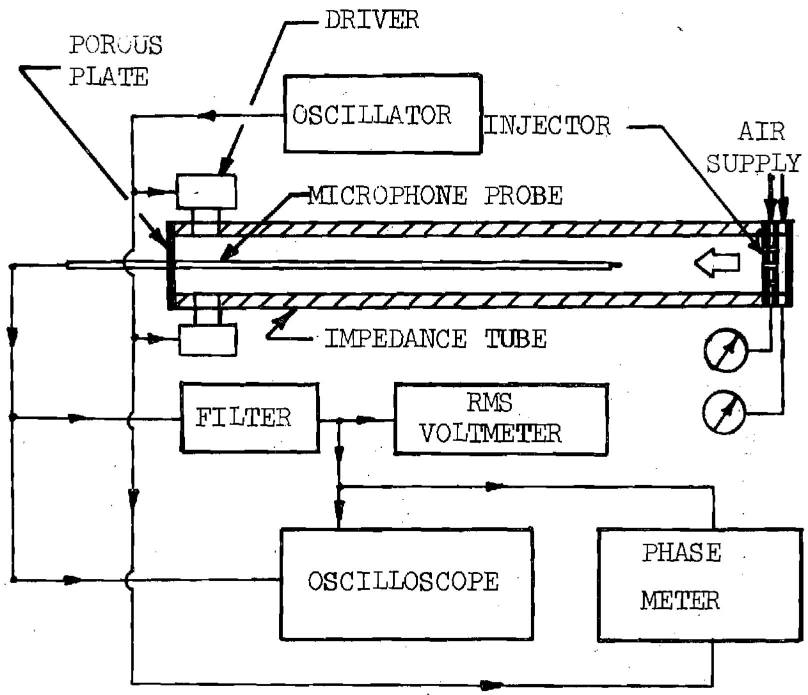

Figure 2. Experimental Apparatus

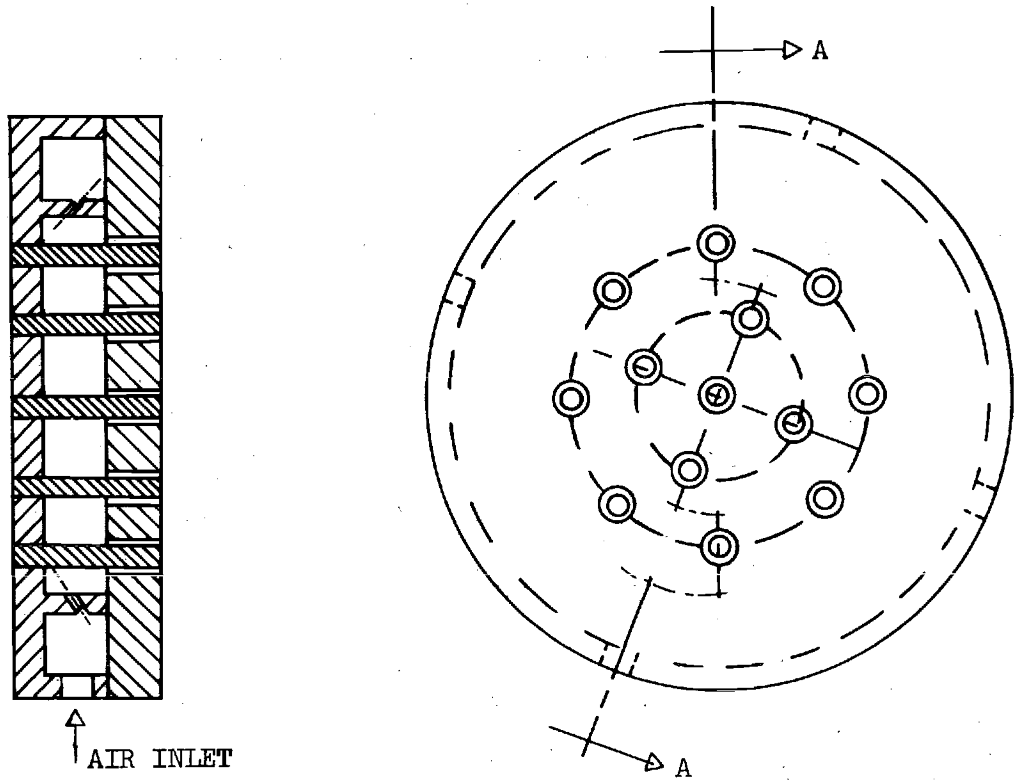

SECTION A-A

CONFIGURATION	σ (%)	L (IN.)	V (IN.^{3})
1	4.7	0.875	27.6

Figure 3. Description of Injector Configuration 1.

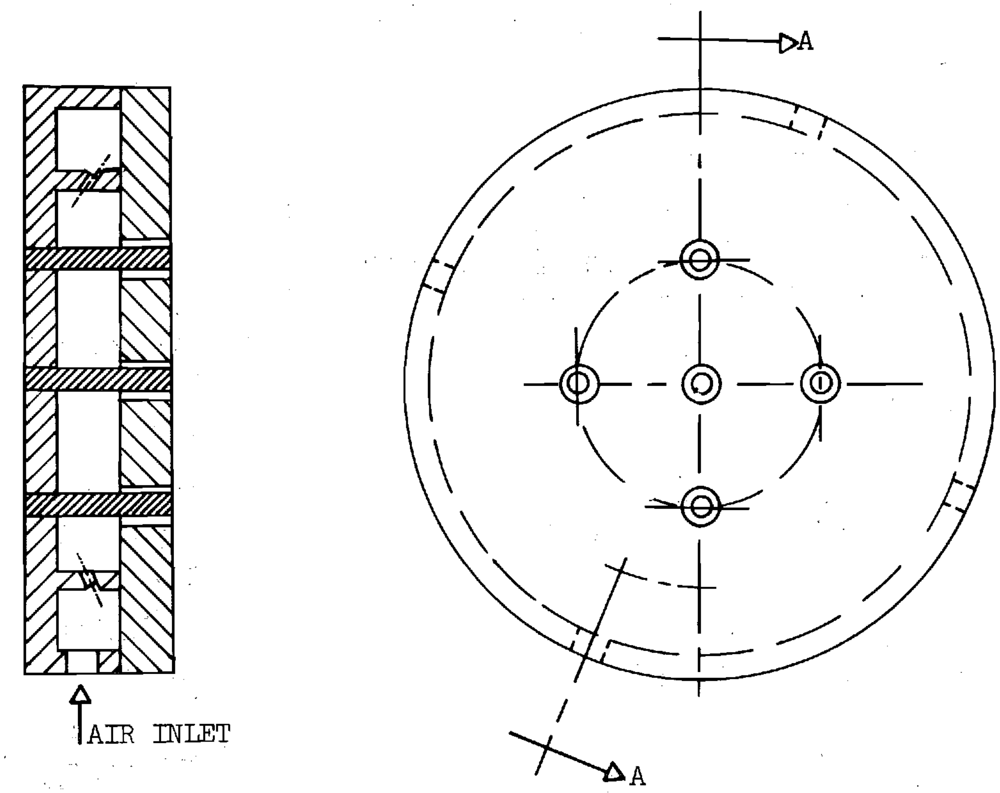

SECTION A-A

CONFIGURATION	σ (%)	L (IN.)	V (IN^3)
2	1.8	0.875	28.0

Figure 4. Description of Injector Configuration 2.

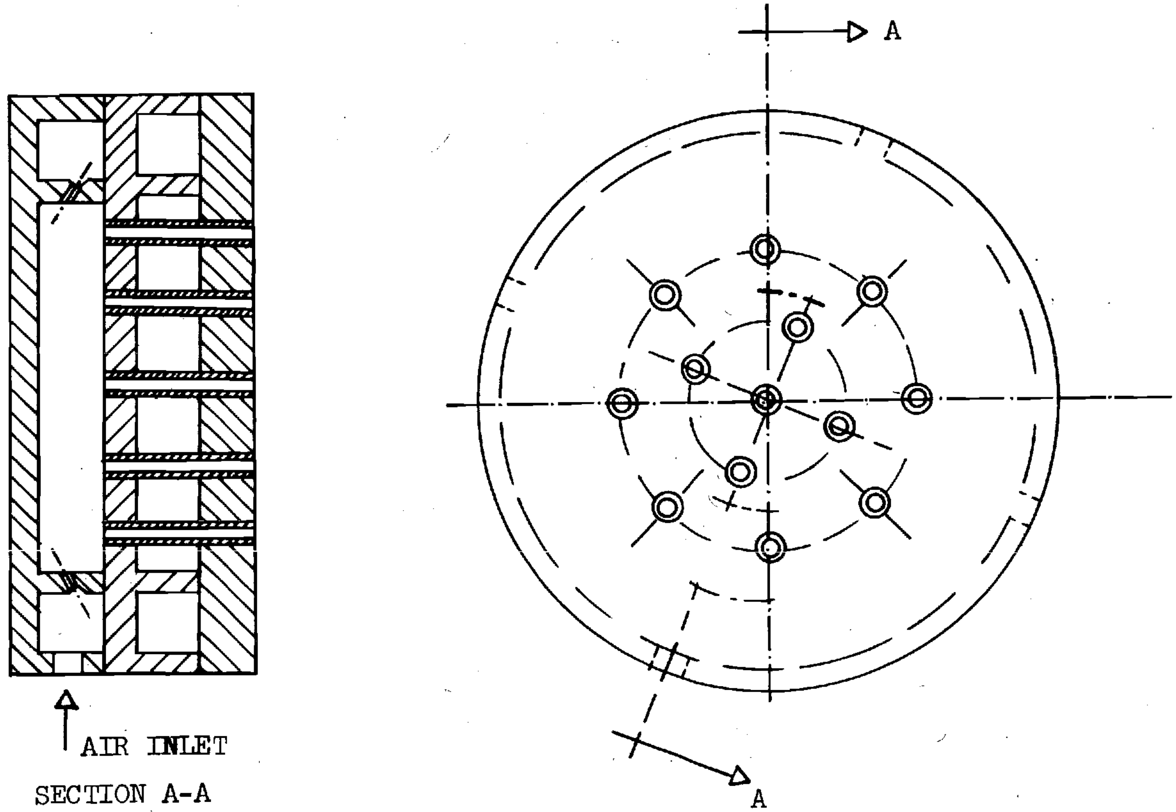

CONFIGURATION	σ (%)	L (IN.)	V(IN.^{3})
3	1.7	2.38	28.2
4	10.2	0.875	28.2
5	10.2	1.75	28.2

Figure 5. Descriptions of Injector Configurations 3, 4 and 5.

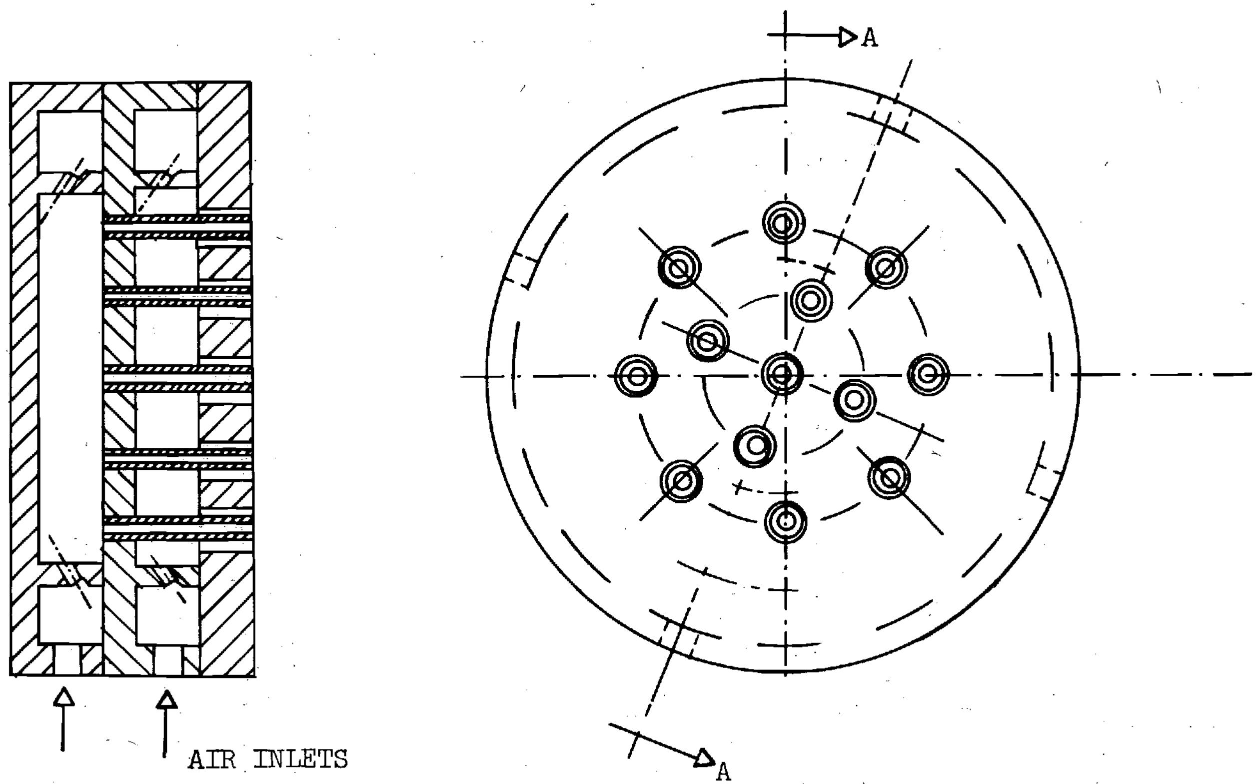

SECTION A-A

CONFIGURATION		σ (%)	L (IN.)	$V(IN.^3)$
6	1	4.7	0.875	27.6
	3	1.7	2.38	28.2

Figure 6. Description of Injector Configuration 6.

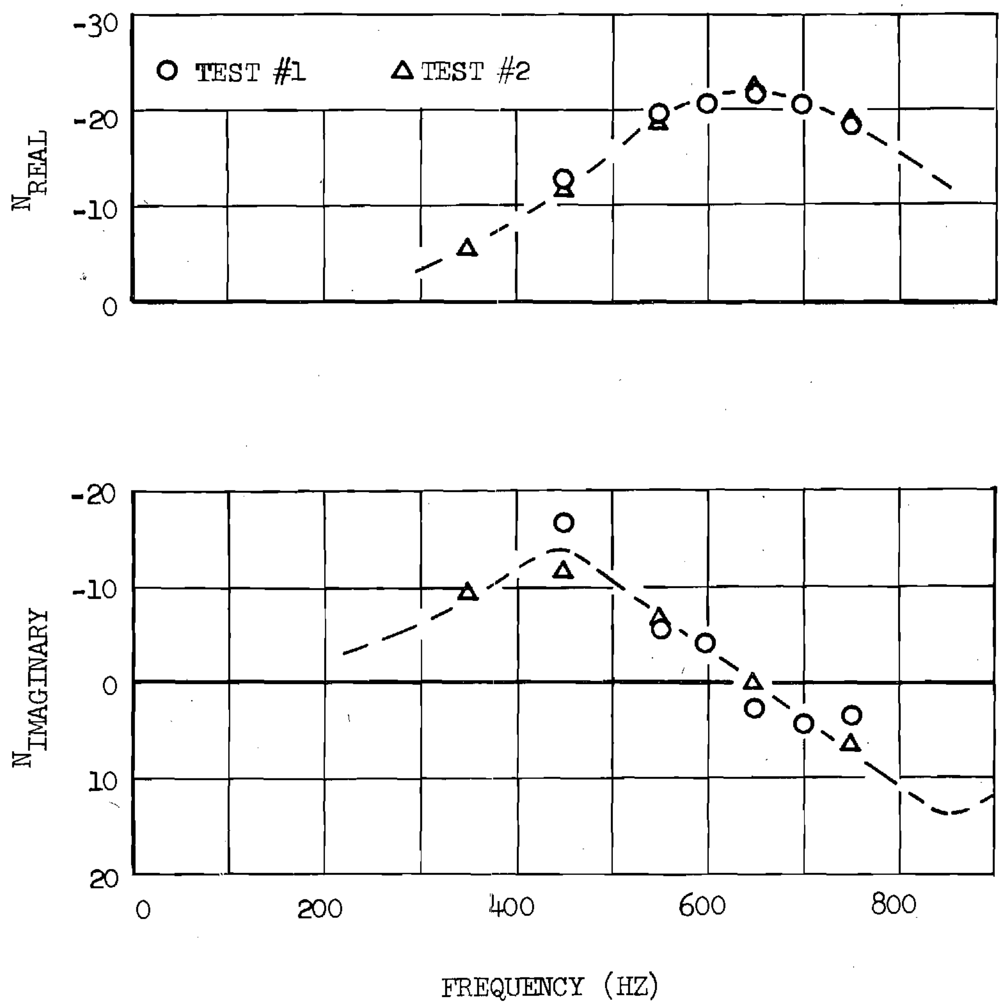

Figure 7. Repeatability of the Measured Response Factor Data.

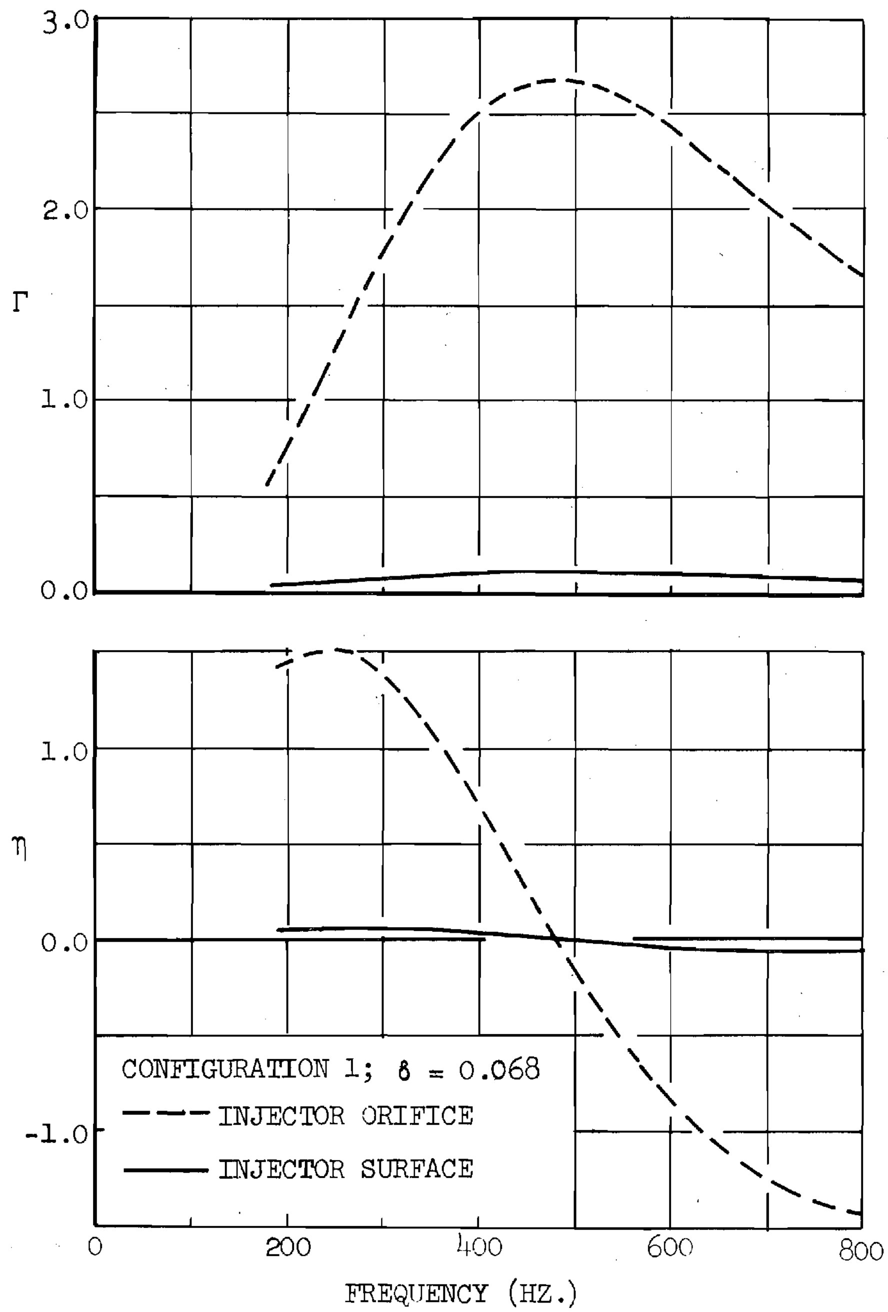

Figure 8. Predicted Admittances for the Injector Configuration 1.

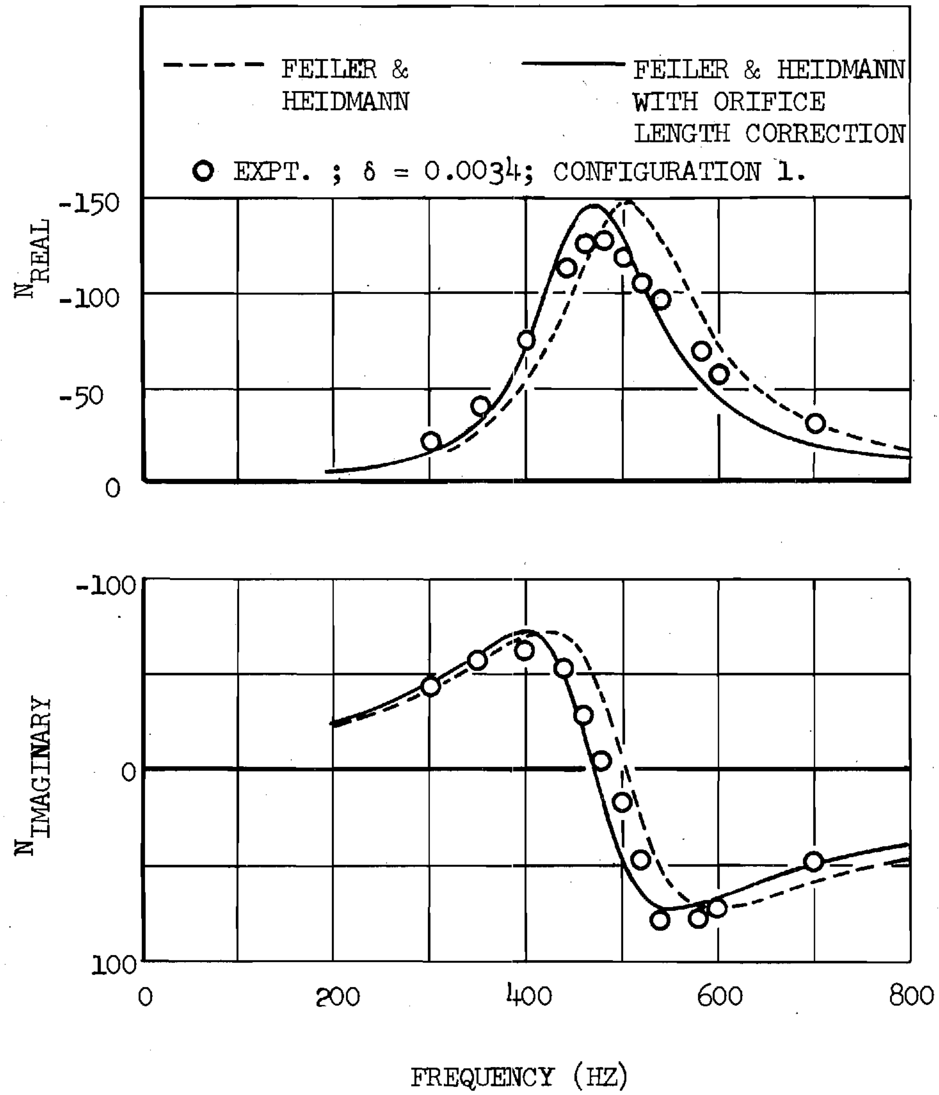

Figure 9. Feiler and Heidmann Predicted Response Factor Data with and without Orifice Length Correction.

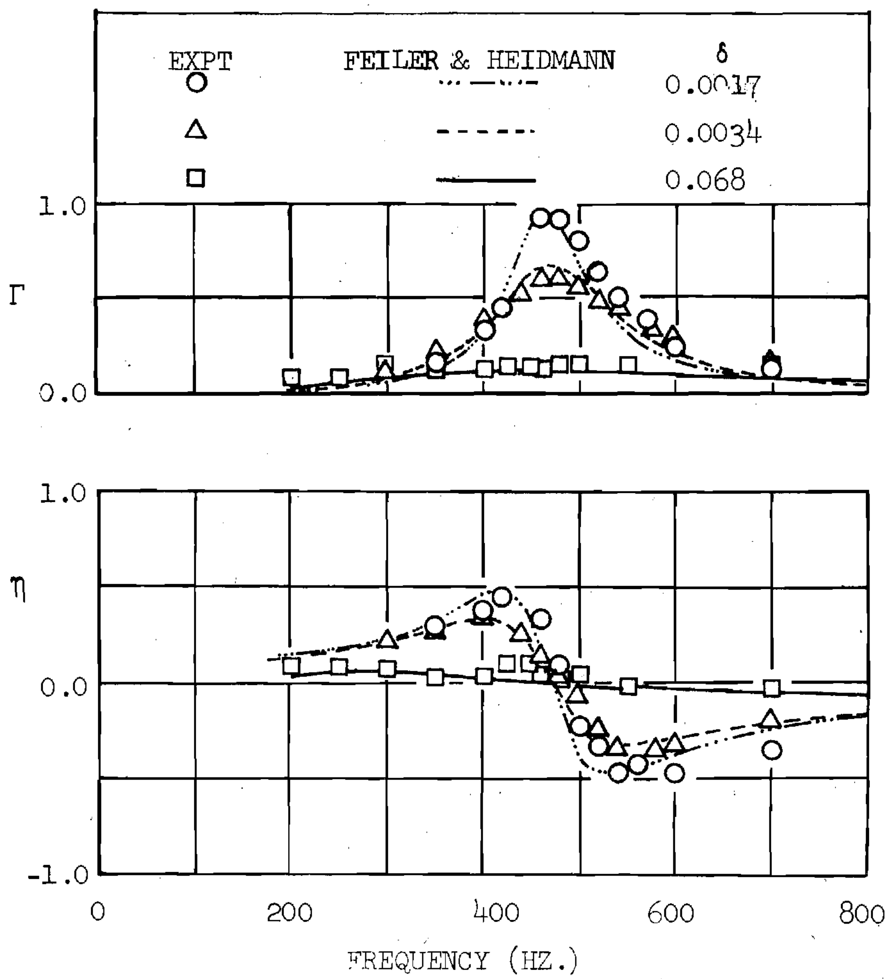

Figure 10. Frequency Dependence of the Surface Admittances of Injector Configuration 1.

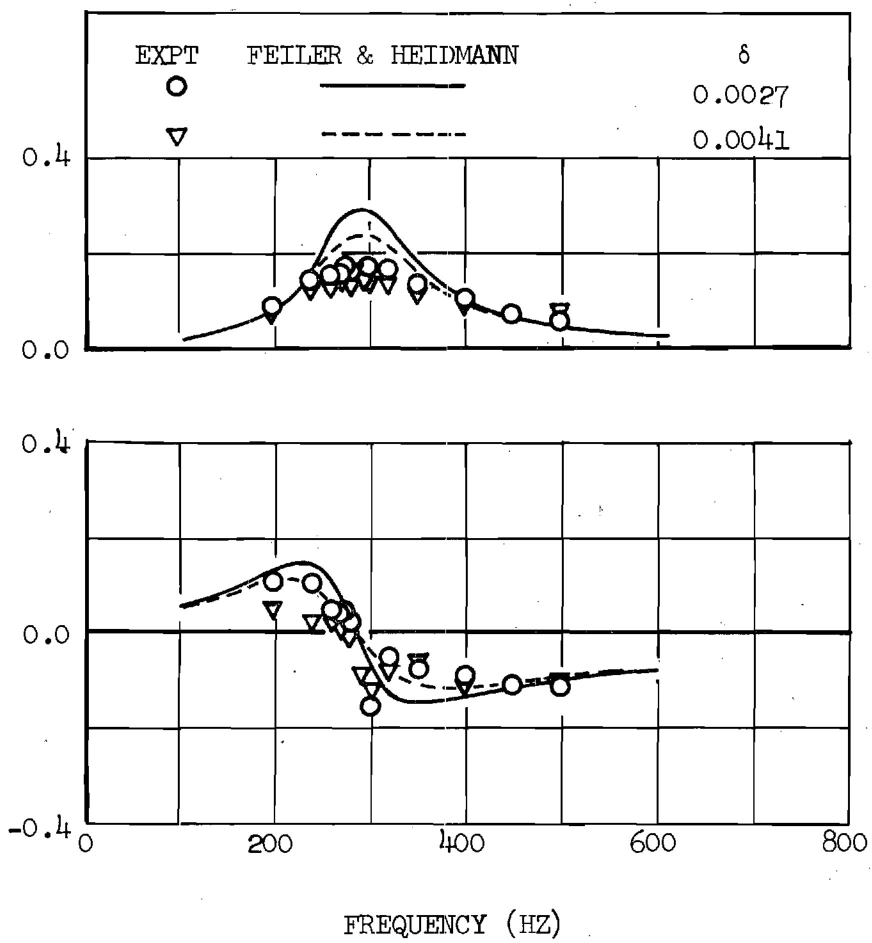

Figure 11. Frequency Dependence of the Surface Admittances of Injector Configuration 2.

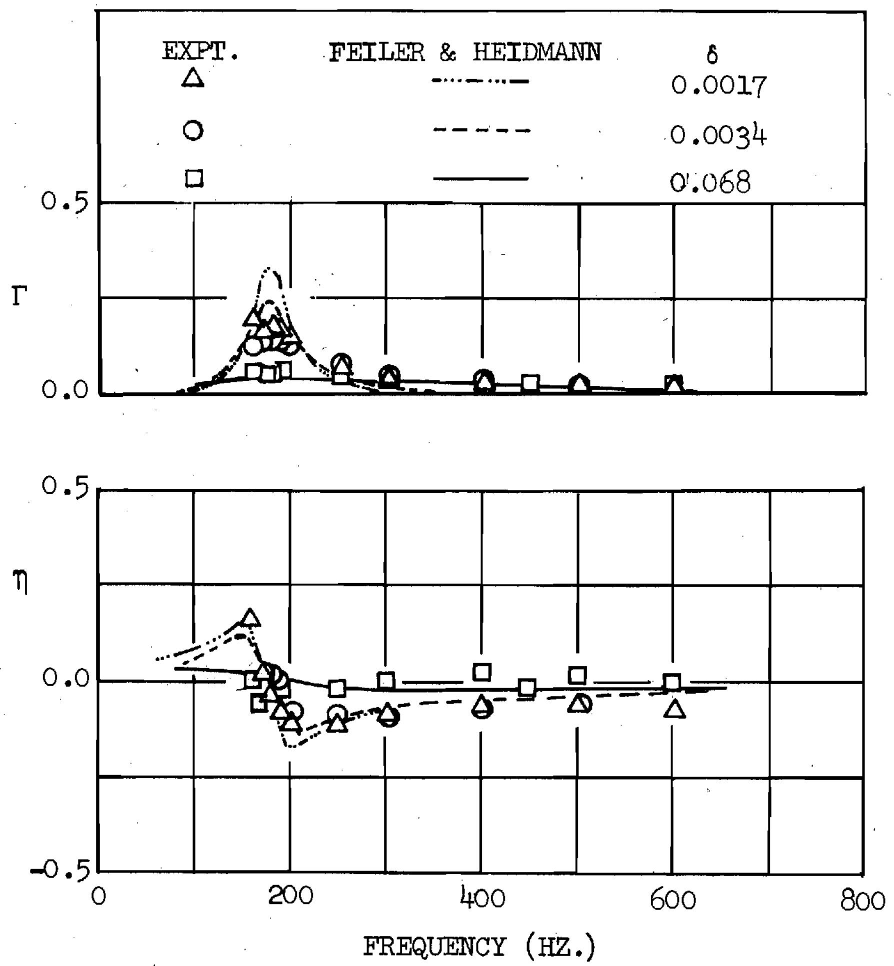

Figure 12. Frequency Dependence of the Surface Admittances of Injector Configuration 3.

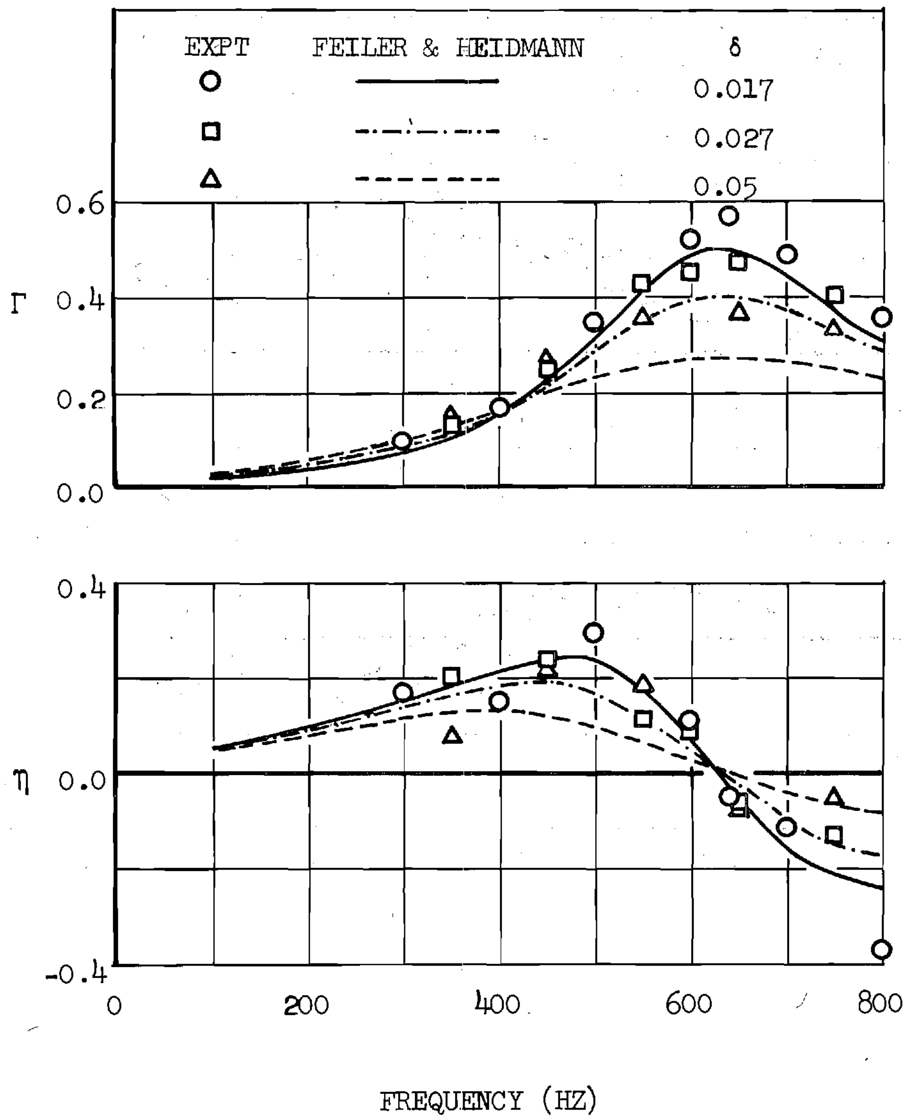

Figure 13. Frequency Dependence of the Surface Admittances of Injector Configuration 4.

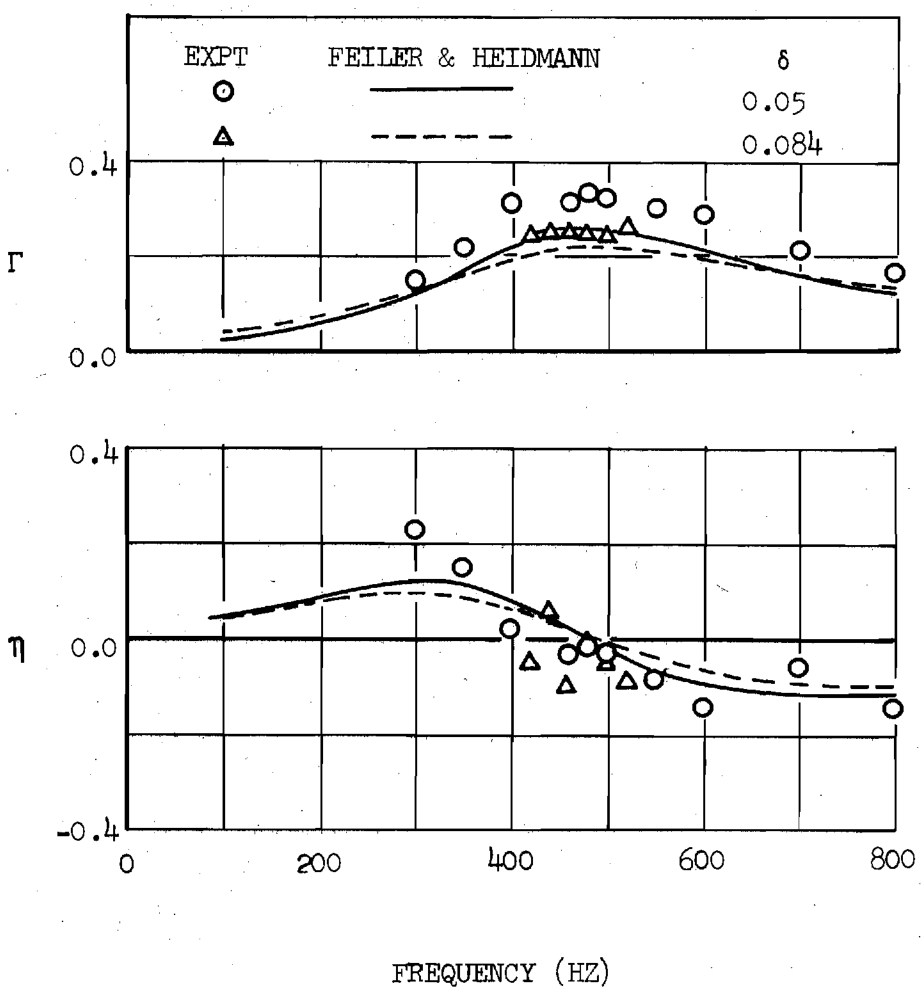

Figure 14. Frequency Dependence of the Surface Admittances of Injector Configuration 5.

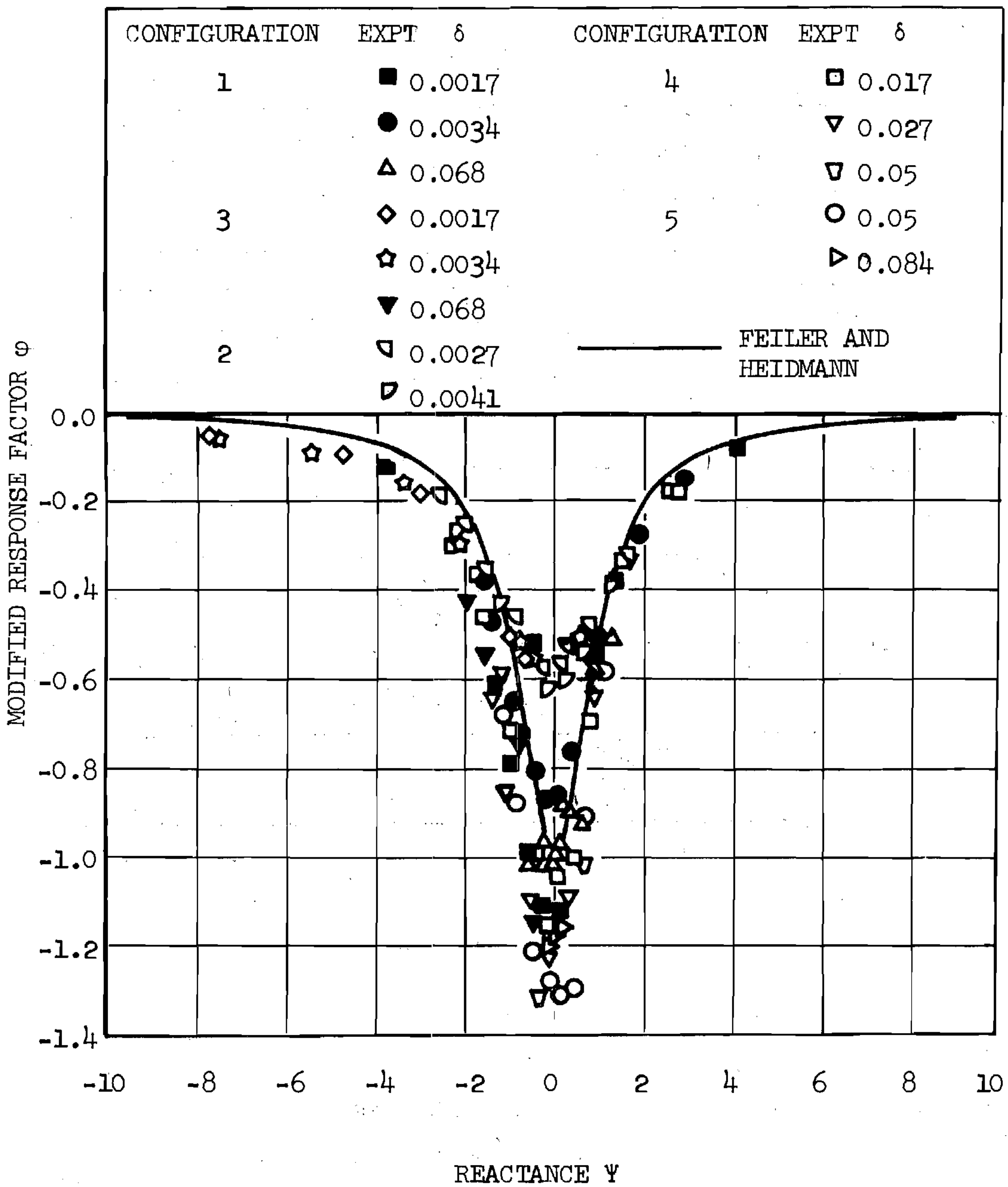

Figure 15. **Generalized Response Factor Data Plotted Against Reactance.**

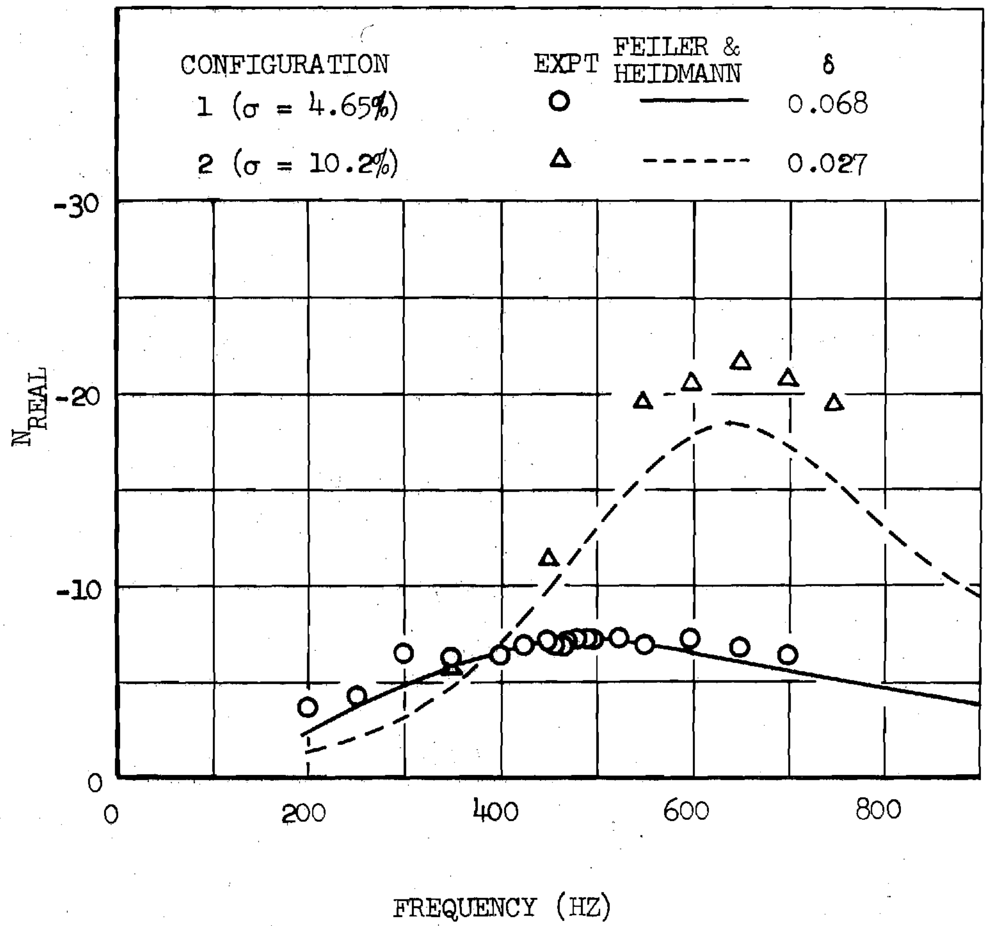

Figure 16. Effect of Open-Area Ratio on Injector Response Factor.

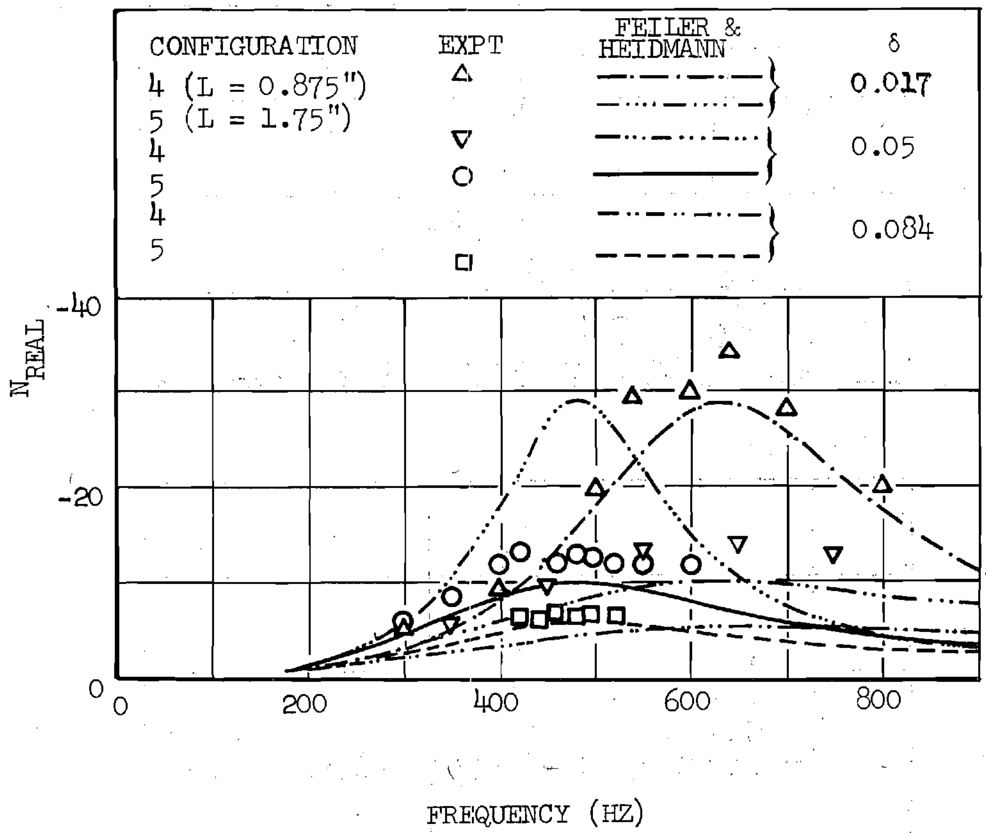

Figure 17. Effect of Orifice Length on Injector Response Factor.

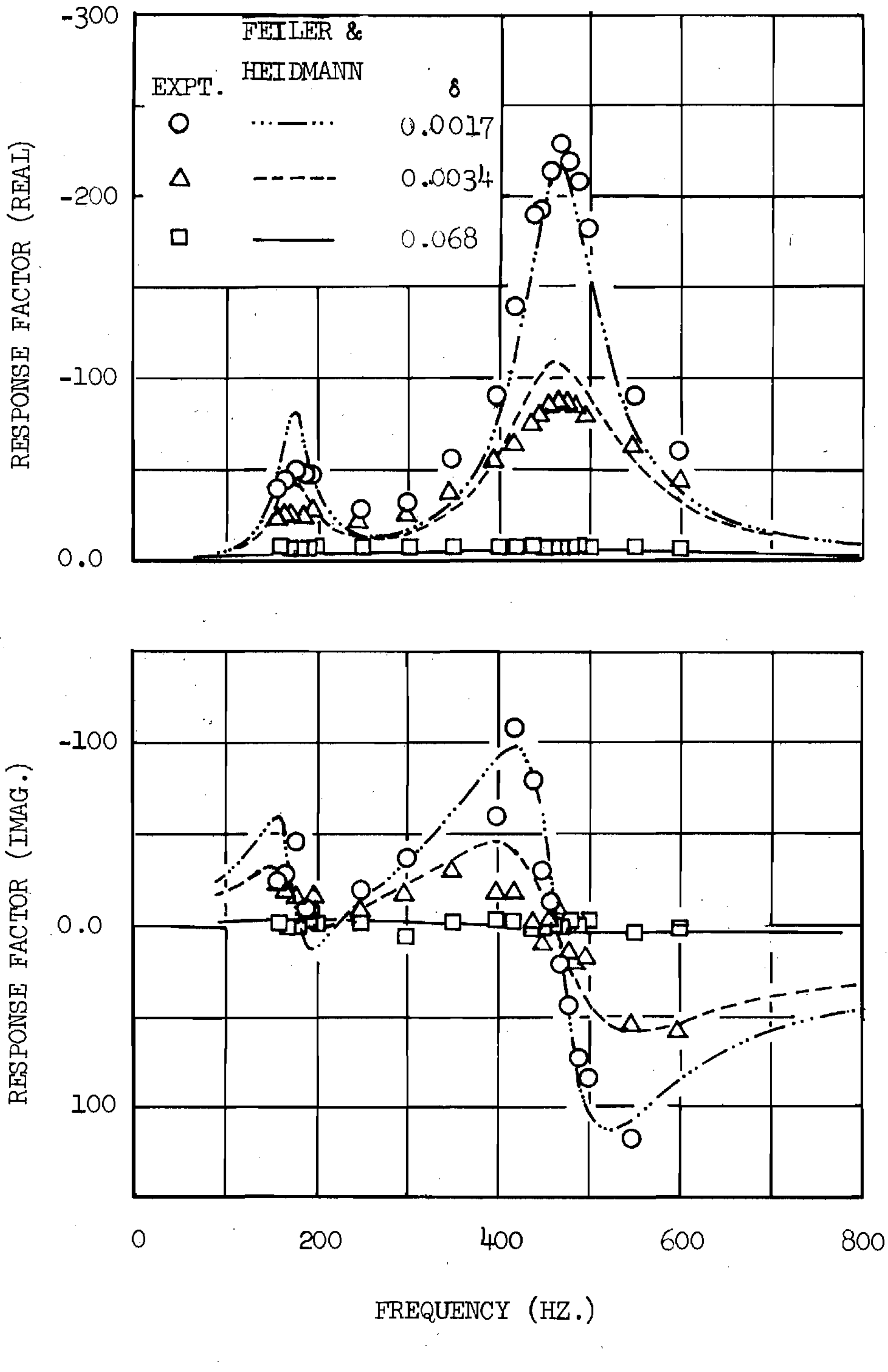

Figure 18. Frequency Dependence of Response Factors of Injector Configuration 6.

REPORT DISTRIBUTION LIST

NASA-Lewis Research Center
Attn: Dr. R. J. Priem/MS 500-204
21000 Brookpark Road
Cleveland, OH 44135
(2 copies)

NASA-Lewis Research Center
Attn: N. T. Musial/MS 500-311
21000 Brookpark Road
Cleveland, OH 44135

NASA-Lewis Research Center
Attn: Library/MS 60-3
21000 Brookpark Road
Cleveland, OH 44135

NASA-Lewis Research Center
Attn: Report Control Office/MS 5-5
21000 Brookpark Road
Cleveland, OH 44135

NASA-Lewis Research Center
Attn: E. A. Bourke/MS 500-205
21000 Brookpark Road
Cleveland, OH 44135

NASA Headquarters
Attn: RPS/Robert A. Wasel
600 Independence Ave., SW, Rm 526
Washington, DC 20546

NASA-Lewis Research Center
Attn: Procurement Section
Mail Stop 500-313
21000 Brookpark Road
Cleveland, OH 44135

NASA-Lyndon B. Johnson Space Center
Attn: EP/Joseph G. Thibodaux
Houston, TX 77058

NASA-George C. Marshall Space Flight Center
Attn: S&E-ASTN-PP/R. J. Richmond
Huntsville, AL 35812

Aerojet Liquid Rocket Company
Attn: David A. Fairchild
Bldg. 20001/Sec. 9732
P. O. Box 13222
Sacramento, CA 95813

Aerojet General Corporation
Propulsion Division
Attn: R. Stiff
P. O. Box 15847
Sacramento, CA 95803

Aerospace Corporation
Attn: O. W. Dykema
P. O. Box 92957
Los Angeles, CA 90045

Aerospace Corporation
Attn: Library-Documents
2400 E. El Segundo Boulevard
Los Angeles, CA 90045

Air Force Rocket Propulsion Lab. (RPM)
Attn. Library
Edwards, CA 93523

Air Force Office of Scientific Research
Chief Propulsion Division
Attn: Dr. J. F. Masi (NAE)
1400 Wilson Boulevard
Arlington, VA 22209

Air Force Rocket Propulsion Lab.
Attn: Daweel George
Edwards, CA 93523

AFAPL
Research & Technology Division
AF Systems Command
U. S. Air Force
Attn: Library/APRP
Wright Patterson AFB, OH 45433

NASA Scientific & Technical Information Facility - Acquisitions Br.
P. O. Box 33
College Park, MD 20740 (10 copies)

Army Ballistics Research Labs.
Attn: Austin W. Barrows
Code AMXBR-1B
Aberdeen Proving Grounds, MD 21005

Army Ballistic Research Labs.
Attn: Ingo W. May
Code AMXBR-1B
Aberdeen Proving Grounds, MD 21005

Army Material Command
Missile Systems Div.
Attn: Stephen R. Matos
Code AMCRD-MT
5001 Eisenhower Ave.
Alexandria, VA 22304

Air Force Systems Command
Arnold Engineering Development Center
Attn: Dr. H. K. Doetsch
Tullahoma, TN 37389

Aeronutronic Div. of Philco Ford Corporation
Technical Information Dept.
Ford Road
Newport Beach, CA 92663

Battelle Memorial Institute
Attn: Report Library, Room 6A
505 King Avenue
Columbus, OH 43201

Bell Aerosystems, Inc.
Attn: Library
Box 1
Buffalo, NY 14205

Bell Aerospace Company
Attn: T. F. Ferger
P. O. Box 1
Mail Zone, J-81
Buffalo, NY 14205

Air Force Rocket Propulsion Lab
Attn: Richard R. Weiss
Edwards, CA 93523

AFAPL
Attn: Frank D. Stull (RJT)
Wright Patterson AFB, OH 45433

California Institute of Technology
Jet Propulsion Laboratory
Attn: Fred E. C. Culick
4800 Oak Grove Drive
Pasadena, CA 91103

California Institute of Technology
Jet Propulsion Laboratory
Attn: Jack H. Rupe
4800 Oak Grove Drive
Pasadena, CA 91103

California State University
Sacramento School of Engineering
Attn: Frederick H. Reardon
6000 J. Street
Sacramento, CA 95819

Chemical Propulsion Information Agency
Johns Hopkins University/APL
Attn: T. W. Christian
8621 Georgia Avenue
Silver Spring, MD 20910

Colorado State University
Attn: Charles E. Mitchell
Fort Collins, CO 80521

Frankford Arsenal
Attn: Martin Visnov
NDP-R, Bldg. 64-2
Bridge & Tacony Streets
Philadelphia, PA 19137

General Electric Company
Flight Propulsion Lab. Dept.
Attn: D. Suichu
Cincinnati, OH 45215

Bureau of Naval Weapons
Department of the Navy
Attn: Library
Washington, DC

Brooklyn Polytechnic Institute
Long Island Graduate Center
Attn: V. D. Agosta
Route 110
Farmingdale, NY 11735

Marquardt Corporation
16555 Saticory Street
Box 2013 - South Annex
Van Nuys, CA 91409

Massachusetts Institute of Tech.
Department of Mechanical Engr.
Attn: T. Y. Toong
77 Massachusetts Avenue
Cambridge, MA 02139

McDonald Douglas Corporation
McDonnell Douglas Astronautics Co.
Attn: William T. Webber
5301 Bolsa Ave.
Huntington Beach, CA 92647

D. E. Mock
Advanced Research Projects Agency
Washington, DC 20525

Lockheed Aircraft Corporation
Lockheed Propulsion Co., Div.
Attn: Norman S. Cohen
P. O. Box 111
Redlands, CA 92373

Naval Postgraduate School
Department of Aeronautics
Attn: David W. Netzer
Monterey, CA 93940

Naval Underwater Systems Center
Energy Conversion Dept.
Attn: Robert S. Lazar, Code 5B331
Newport, RI 02840

Georgia Institute of Technology
School of Aerospace Engineering
Attn: Warren C. Strahle
Atlanta, GA 30332

Georgia Institute of Technology
School of Aerospace Engineering
Attn: Ben T. Zinn
Atlanta, GA 30322

Melvin Gerstein
P. O. Box 452
Altadena, CA 91001

Ohio State University
Department of Aeronautical and
Astronautical Engineering
Attn: R. Edse
Columbus, OH 43210

Pennsylvania State University
Mechanical Engineering Dept.
Attn: G. M. Faeth
207 Mechanical Engineering Bldg.
University Park, PA 16802

Princeton University
Forrestal Campus Library
Attn: Irvin Glassman
P. O. Box 710
Princeton, NJ 08450

Princeton University
Forrestal Campus Library
Attn: David T. Harrje
P. O. Box 710
Princeton, NJ 08540

Princeton University
Forrestal Campus Library
Attn: Martin Summerfield
P. O. Box 710
Princeton, NJ 08540

Propulsion Sciences, Inc.
Attn: Vito Agosta
P. O. Box 814
Melville, NY 11746

Georgia Institute of Technology
School of Aerospace Engineering
Attn: Edward W. Price
Atlanta, GA 30332

Naval Weapons Center
Attn: Charles J. Thelan, Code 4305
China Lake, CA 93555

Naval Postgraduate School
Department of Aeronautics
Attn: Allen F. Fuhs
Monterey, CA 93940

Research and Development Associates
Attn: Raymond B. Edelman
P. O. Box 3580
525 Wilshire Blvd.
Santa Monica, CA 90402

Rockwell International Corp.
Rocketdyne Division
Attn: L. P. Combs, D/991-350
Zone 11
6633 Canoga Avenue
Canoga Park, CA 91304

Rockwell International Corp.
Rocketdyne Division
Attn: James A. Nestlerode
Dept. 596-124, AC46
6633 Canoga Ave.
Canoga Park, CA 91304

Rockwell International Corp.
Rocketdyne Division
Attn: Carl L. Oberg
Dept. 589-197-SS11
6633 Canoga Ave.
Canoga Park, CA 91304

Rockwell International Corp.
Rocketdyne Division
Attn: Library Dept. 596-306
6633 Canoga Avenue
Canoga Park, CA 91304

Purdue University
Jet Propulsion Laboratory
Project Squid
Attn: Robert Goulard
West Lafayette, IN 47907

Purdue University Res. Foundation
School of Mechanical Engineering
Attn: John R. Osborn
Thermal Sci. Propulsion Center
West Lafayette, IN 47906

Purdue University Res. Foundation
School of Mechanical Engineering
Attn: Bruce A. Reese
Thermal Sci. Propulsion Center
West Lafayette, IN 47906

Tennessee Technological University
Dept. of Mech. Engrg.
Attn: Kenneth R. Purdy
P. O. Box 5014
Cookeville, TN 38501

Textron, Inc.
Bell Aerospace, Div.
Research Department
Attn: John R. Morgenthaler, C-84
P. O. Box One
Buffalo, NY 14240

TRW, Inc.
TRW Systems Gp.
Attn: A. C. Ellings
One Space Park
Redondo Beach, CA 90278

TRW Systems
Attn: G. W. Elveran
One Space Park
Redondo Beach, CA 90278

TRW Systems Group
STL Tech. Lib. Doc. Acquisitions
One Space Park
Redondo Beach, CA 90278

Stanford Research Institute
333 Ravenswood Avenue
Menlo Park, CA 94025

Susquehanna Corporation
Atlantic Research Division
Attn: Library
Shirley Highway and Edsall Rd.
Alexandria, VA 22314

TISIA
Defense Documentation Center
Cameron Station, Bldg. 5
5010 Duke Street
Alexandria, Va. 22314

United Aircraft Corporation
Pratt & Whitney Aircraft Div.
Attn: Thomas C. Mayes
P. O. Box 2691
West Palm Beach, FL 33402

United Aircraft Corporation
United Technology Center
Attn: Library
P. O. Box 358
Sunnyvale, CA 94088

University of California, Berkeley
Dept. of Mechanical Engineering
Attn: A. K. Oppenheim
Berkeley, CA 94720

University of Michigan
Attn: James A. Nicholls
P. O. Box 622
Ann Arbor, MI 48107

University of Wisconsin
Mechanical Engineering Dept.
Attn: P. S. Myers
1513 University Avenue
Madison, WI 53706

Office of Assistnat Director
(Chemical Technician)
Office of the Director of Defense
Research & Engineering
Washington, DC 20301

Tulane University
Attn: J. C. O'Hara
6823 St. Charles Ave.
New Orleans, LA 70118

Ultrasystems, Inc.
Attn: Thomas J. Tyson
500 Newport Center Dr.
Newport Beach, CA

United Aircraft Corp.
Pratt & Whitney Division
Florida Research & Development
Center
Attn: Library
West Palm Beach, FL 33402

United Aircraft Corporation
Attn: R. H. Woodward Waesche
400 Main Street
East Hartford, CT 06108

University of California
Aerospace Engineering Dept.
Attn: F. A. Williams
P. O. Box 109
LaJolla, CA 92037

University of Illinois
Aeronautics/Astronautic Eng. Dept.
Attn: R. A. Strehlow
Trans. Bldg., Room 101
Urbana, IL 61801

University of Utah
Dept. of Chemical Engineering
Attn: Alva D. Baer
Bark Bldg., Room 307
Salt Lake City, UT 84112

U. S. Naval Research Laboratory
Director (Code 6180)
Attn: Library
Washington, DC 20390

Virginia Polytechnic Institute
State University
Attn: J. A. Schetz
Blacksburg, VA 24061

E-16-601

Journal of Sound and Vibration (1973) **30**(2), 179–190

EXPERIMENTAL AND THEORETICAL DETERMINATION OF THE ADMITTANCES OF A FAMILY OF NOZZLES SUBJECTED TO AXIAL INSTABILITIES†

W. A. BELL, B. R. DANIEL AND B. T. ZINN
Georgia Institute of Technology,
School of Aerospace Engineering, Atlanta, Georgia 30332, *U.S.A.*

(*Received* 3 *March* 1973)

In combustion instability analyses of rocket engines, it is necessary to determine the interaction between the oscillations in the combustor and the wave system in the nozzle. This interaction can be specified once the nozzle admittance is known. The present paper is concerned with the experimental and theoretical determination of the admittances of practical nozzles that are subjected to axial oscillations. The impedance tube technique, modified to account for the presence of a mean flow, was used to experimentally measure the one-dimensional nozzle admittances. The modified impedance tube theory and experimental facility used to evaluate the nozzle admittance are briefly discussed in this paper. Crocco's nozzle admittance theory is used to predict the admittances of the tested nozzles for comparison with the experimental data. The theoretical and experimental nozzle admittances are obtained for a family of nozzles having Mach numbers from 0·08 to 0·28, different angles of convergence, and different radii of curvature at the throat and entrance sections. The analytical and experimental results are presented as curves showing the frequency dependence of the real and imaginary parts of the nozzle admittances. Examination of these data shows that the theoretical and experimental admittance values are in good agreement with one another which indicates that existing nozzle admittance theories may be used in practice to predict one-dimensional nozzle admittances.

1. INTRODUCTION

Combustion instability studies are concerned with analyzing the behavior of disturbances (i.e., waves) which may occur in the combustors of rocket engines as a result of such phenomena as local explosions that result from uneven distribution of unburned propellants, malfunction of the feed system in liquid rockets, turbulence, and so on. To determine the stability characteristics of a rocket engine, the interaction between the disturbance and the various processes occurring inside the combustor (e.g., the unsteady combustion process, the mean flow, etc.) and various system components (e.g., the nozzle) must be evaluated to ascertain whether the amplitude of the disturbance will grow or decay with time. Previous studies [1] of combustion instability indicate that the interaction between the nozzle and the combustor wave systems can significantly affect the stability characteristics of the rocket motor. Therefore, the influence of the nozzle on the disturbance inside the combustor is an important consideration in combustion instability analyses. This paper is concerned with both the theoretical and experimental determinations of the effects of various nozzle designs upon the stability of combustors experiencing longitudinal type of instability. Their effects on the three-dimensional instabilities are discussed in reference [2].

† Sponsored under NASA grant NGL 11-002-085; Dr R. J. Priem grant monitor.

The interaction between the combustor and nozzle wave systems may be described by specifying the nozzle admittance which is defined as the complex ratio of the axial velocity perturbation to the pressure perturbation, evaluated at the nozzle entrance. Once the nozzle admittance is known, it can be used to describe the nozzle boundary condition in analytical combustion instability studies and to evaluate the mean wave-energy flux that is crossing the nozzle entrance plane.

In linear combustion instability analyses it is generally assumed that the time dependence of the disturbance is exponential (e.g., $p \propto \exp(\lambda_1 t)$) and the analysis usually attempts to determine how various phenomena affect the magnitude and sign of λ_1. Such an analysis usually establishes the dependence of λ_1 upon the nozzle admittance. For example, Crocco's investigation [3] of linear axial instabilities in liquid propellant rocket motors yielded the following relationship:†

$$\lambda_1 z_e = -(y_r + \gamma M) + \left(\frac{\gamma}{\pi P_{00}}\right) \int_0^{z_e} \frac{dQ_r}{dz} \cos \frac{\omega r_c z}{c} dz + $$

$$+ (2-\gamma) \frac{\omega r_c}{c} \int_0^{z_e} M \sin \frac{2\omega r_c z}{c} dz.$$

In the above equation, the terms involving Q_r, M, and y_r, respectively, represent the dependence of λ_1 upon the unsteady combustion process, the mean flow Mach number and the oscillations in the nozzle. From the expression for λ_1, it can be seen that when the real part of the nozzle admittance y_r is positive the interaction between the oscillation in the combustor and the oscillation in the nozzle will tend to decrease λ_1 and thus exert a stabilizing influence on the rocket motor; the opposite occurs when y_r is negative.

The prediction of the nozzle admittance has been the subject of several theoretical analyses. In these investigations the mean flow in the nozzle is assumed to be one-dimensional, and the gas is assumed to be ideal and non-reacting. Tsien [4] was the first to study the response of a choked nozzle under the influence of axial pressure and velocity perturbations superimposed upon the steady-state flow. To account for the effect of the nozzle upon engine stability, Tsien introduced a transfer function defined as the ratio of the mass flow perturbation to the chamber pressure perturbation evaluated at the nozzle entrance. Assuming isothermal perturbations and a linear steady-state velocity distribution in the nozzle, Tsien restricted his studies to the limiting cases of very high and very low frequency oscillations. Later, Crocco [1, 5] removed the assumption of isothermal oscillations, extended Tsien's work to include the entire frequency range, and introduced the concept of admittance to study the influence of the nozzle on the combustor oscillations. By assuming a linear steady-state velocity profile and isentropic perturbations in the nozzle, Crocco obtained a hypergeometric equation which he then solved to determine the nozzle admittance. In 1967, Crocco extended his earlier analysis to consider the admittances of choked nozzles with three-dimensional flow oscillations [6]. By numerically integrating the equations governing the wave motion in the nozzle Crocco was able to evaluate the admittances of various nozzle configurations over the frequency range of interest in combustion instability studies. All of the analytical nozzle admittance investigations predict that in the range of frequencies which is of interest in longitudinal combustion instability studies, the real part of the nozzle admittance is positive, implying that the nozzle exerts a stabilizing influence on axial instabilities.

Although the predictions of reference [6] have been widely used in analyses of various axial combustion instability problems (e.g., see reference [7]), the accuracy of these predictions

† A list of nomenclature is given in the Appendix.

has never been fully determined. It is the objective of the present investigation to experimentally and theoretically determine the admittances of a variety of nozzle designs that are of interest in combustion instability studies. In the following sections, the experimental technique and apparatus used to measure nozzle admittances for longitudinal oscillations are discussed. The procedure used to numerically calculate the nozzle admittance from Crocco's theory [6] is then presented. Finally, the theoretical and experimental admittance results are presented for a family of practical nozzles having entrance Mach numbers from 0·08 to 0·24 with different convergent half-angles and different radii of curvature at the throat and entrance sections.

2. EXPERIMENTAL TECHNIQUES

Two techniques have been used previously to measure the one-dimensional nozzle admittance. In 1961, Crocco, Monti and Grey [8] determined the real and imaginary parts of the admittance from direct measurements of the pressure and velocity perturbations at the nozzle entrance. However, the accuracy of the data was limited by wave distortion at higher frequencies, a low signal-to-noise ratio, and difficulties in measuring the velocity perturbations with hot-wire anemometers. The second method, often referred to as the half-power bandwidth technique, was developed by Buffum, Dehority, Slates and Price [9]. The limitations of this technique were later discussed by Culick and Dehority [10], who in conclusion recommended that the classical impedance tube method [11, 12, 13] be adopted for nozzle admittance measurements. In an independent investigation, Bell [14] also concluded that the impedance tube method should be used in the experimental determination of nozzle admittances.

Based on the analyses of references [10] and [14], a modification of the classical impedance tube method was developed for this investigation. The apparatus used in the classical impedance tube technique consists of a smooth-walled cylindrical tube with a sound source at one end and the sample, whose admittance is to be measured, at the other end. The sound source is used to generate a standing wave pattern in the tube. The shape of the resulting standing wave pattern depends upon the admittance of the tested sample. By measuring the spatial dependence of the amplitude of the standing wave in the tube, the admittance of the sample can be determined. In this investigation, the classical impedance tube technique is extended to account for the presence of a one-dimensional mean flow in the tube.

To determine the nozzle admittance in a modified impedance tube experiment, an expression describing the behavior of the standing wave pattern in the tube must first be derived. This expression is obtained by solving the wave equation describing the behavior of a one-dimensional pressure oscillation superimposed upon an axial mean flow. This wave equation is [13]

$$\left(\frac{1}{c}\frac{\partial}{\partial t}+M\frac{\partial}{\partial z}\right)^2 p=\frac{\partial^2 p}{\partial z^2}. \tag{1}$$

The solution of equation (1) can be expressed as follows:

$$p=\exp\left\{i\left(\omega t+\frac{kMz}{1-M^2}\right)\right\}\left[A_+\exp\left\{\frac{-ikz}{1-M^2}\right\}+A_-\exp\left\{\frac{ikz}{1-M^2}\right\}\right]. \tag{2}$$

Equation (2) describes a standing wave pattern formed by a combination of two simple harmonic waves traveling along the tube; the wave with amplitude A_+ travels in the positive z direction, while the one with amplitude A_- travels in the negative z direction. In impedance tube analyses, it is convenient to express the axial dependence of the waves in terms of hyperbolic functions. Introducing the relationship

$$A_{\pm} = \tfrac{1}{2}A\exp\{\pm[\pi\alpha - i\pi(\beta + \tfrac{1}{2})]\} \tag{3}$$

into equation (2) yields

$$p = A\exp\left\{i\left(\omega t + \frac{kMz}{1 - M^2}\right)\right\}\cosh\left[\pi\alpha - i\pi\left(\beta + \tfrac{1}{2} + \frac{2z}{\lambda}\right)\right]. \tag{4}$$

By letting $z = 0$ at the nozzle entrance, the non-dimensional specific admittance y can be expressed in terms of the parameters α and β. From the definition of the specific admittance,

$$y = \rho c\frac{u}{p}\bigg|_{z=0},$$

and the axial component of the linearized momentum equation [13],

$$\rho c\left(ik + M\frac{\partial}{\partial z}\right)u = -\frac{\partial p}{\partial z},$$

the following expression for y is obtained:

$$y = \coth\pi(\alpha - i\beta) \tag{5}$$

To compute the nozzle admittance from equation (5), α and β must be determined. These parameters can be computed from either pressure amplitude or phase measurements taken axially along the tube. From equation (4) the pressure can be written in the form

$$p = |p|\,e^{i(\omega t + \delta)},$$

where the pressure amplitude $|p|$ is given by

$$|p| = A\left[\cosh^2\pi\alpha - \cos^2\pi\left(\beta + \frac{2z}{\lambda}\right)\right]^{1/2} \tag{6}$$

and the phase δ is

$$\delta = \frac{kMz}{1 - M^2} + \arctan\left[\tanh\pi\alpha\cot\pi\left(\beta + \frac{2z}{\lambda}\right)\right]. \tag{7}$$

In this study, pressure amplitude measurements are used to obtain values of α and β from which the nozzle admittance is determined. The pressure amplitude measurements are taken at several axial positions along the tube as shown in Figure 1. Knowing the Mach number from the nozzle contraction ratio, and measuring the frequency and temperature directly, one can then determine the wavelength λ from the following relation:

$$\lambda = \frac{c(1 - M^2)}{f},$$

where $c = (\gamma RT)^{1/2}$. As shown in Figure 1, increasing α decreases the difference in amplitude between the maxima and minima along the standing wave. Varying β changes the positions of the minima or maxima relative to the location of the nozzle entrance. By taking several pressure amplitude measurements along the length of the tube, it is possible to determine α and β.

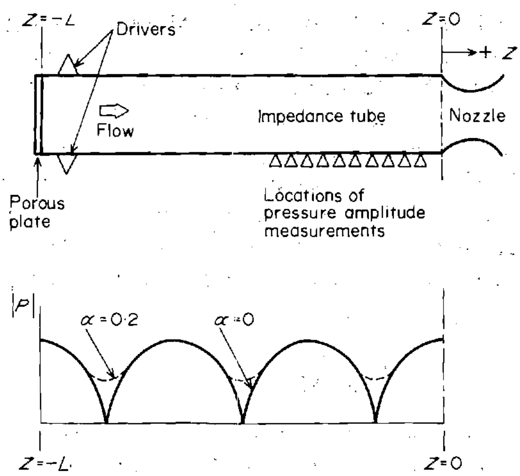

Figure 1. Modified impedance tube experiment.

In principle, only three amplitude measurements at different axial locations are required to solve for the three unknowns α, β, and A by use of equation (6). However, Gately and Cohen [15] have shown that large errors in α may result from relatively small errors in pressure amplitude measurements when only three pressure amplitudes are used. This observation was verified in this study, and it was attributed to the fact that three amplitude measurements do not yield enough information about the shape of the standing wave pattern from which α and β are determined. To improve the accuracy of the measured nozzle admittances, it is desirable to take as many pressure amplitude measurements as possible, at different axial locations, to better diagnose the shape of the standing wave pattern. In the experiments conducted in this investigation, ten pressure amplitude measurements have been taken.

To compute α and β from the measured amplitude data the method of non-linear regression [16] is used. This method consists of finding the values of α, β, and A which provide the best fit between the experimental amplitude data and equation (6). This is accomplished by computing the values of α, β, and A which minimize the r.m.s. deviation between the theoretical amplitude predictions and the corresponding experimental data. To determine the minimum r.m.s. deviation, the following function F is minimized:

$$F = \sum_{i=1}^{n} [E_i - T_i(\alpha, \beta, A)]^2. \tag{8}$$

In the above expression, n is the number of pressure amplitude measurements; $3 \leqslant n \leqslant 10$ for the present experiment. For a given pressure amplitude measurement E_i taken at a distance z_i from the nozzle entrance, the corresponding theoretical pressure amplitude is T_i, and it is obtained from equation (6); that is,

$$T_i = A\left[\cosh^2 \pi\alpha - \cos^2 \pi\left(\beta + \frac{2z_i}{\lambda}\right)\right]^{1/2}. \tag{9}$$

At the location where F is a minimum

$$\frac{\partial F}{\partial \alpha} = \frac{\partial F}{\partial \beta} = \frac{\partial F}{\partial A} = 0. \tag{10}$$

Equation (10) yields three non-linear equations which are solved numerically for the three unknowns α, β, and A.

Equation (10) is solved numerically by use of Marquardt's algorithm [16, 17]. This algorithm is an extension of the Newton–Raphson iteration scheme which keeps the rapid convergence properties of the Newton–Raphson method and improves its stability characteristics at the same time. To start the iteration, equation (8) is solved explicitly for α, β, and A, combinations of three amplitude measurements being used. For ten amplitude measurements taken axially along the tube, 120 combinations of three different pressure amplitudes can be obtained. The computed set of values of α, β, and A which gives the minimum value of F in equation (8) is then used to start the numerical iteration. The values of α and β obtained from the iteration are then used to compute the real and imaginary parts of the admittance from equation (5).

3. APPARATUS

The experimental apparatus, described in detail in reference [14], is a modified impedance tube apparatus designed to accommodate a one-dimensional mean flow through the tube. As shown in Figure 1, the regulated air flow enters the 10 ft long, 12 inch diameter impedance tube through a porous plate at the driven end and is exhausted through the nozzle under investigation, which is attached to the other end of the tube. The pressure in the impedance tube is maintained at a sufficiently high level to assure sonic flow at the nozzle throat throughout the test.

A standing wave pattern is superimposed upon the mean flow by two electropneumatic drivers which are positioned opposite to one another on the walls of the tube immediately downstream of the injector plate. To measure the pressure amplitude of the standing wave pattern in the tube, pressure transducers are located from 1 to 60 inches from the nozzle entrance along the length of the tube. Provisions have also been made for the installation of thermocouples and for static pressure monitoring.

During a test the frequency of the generated axial waves is varied linearly by a sweep oscillator. The signals from the sweep oscillator, pressure transducers, and thermocouple are continuously recorded during testing by a 14-channel tape recorder. Upon completion of a test, the pressure amplitude data is Fourier analysed (i.e., filtered), the signal from the sweep oscillator being used as a reference signal. For each frequency of interest the filtered pressure amplitude data together with the measured temperature data, used to compute the speed of sound, are input into a computer program which employs the non-linear regression method to obtain the nozzle admittance values over a range of the non-dimensional frequency S.

In this study, nozzle admittance data are obtained for a series of axisymmetric nozzles. The contour of these nozzles, shown in Figure 2, is generated by a circular arc of radius r_{cc}

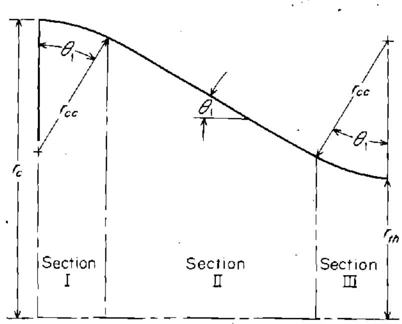

Figure 2. Nozzle contour geometry.

TABLE 1

Parameters of nozzles tested

θ_1	M 0·08	0·16	0·24
15	0·44, 1·0†	0·44	0·44
30	0·44	0·44, 1·0	0·44
45	0·44	0·44	0·44

† r_{cc}/r_c.

which starts at the impedance tube and is turned through the nozzle half-angle θ_1. This arc smoothly connects to a conical nozzle section of half-angle θ_1. This conical section then joins with a circular arc of radius r_{cc} that is also turned through an angle θ_1. The properties of the nozzles tested in this investigation are described in Table 1 which presents the value of the ratio of the radius of curvature to the chamber radius, for each nozzle with a given half-angle θ_1 and a given entrance Mach number M. By testing this group of nozzles, the dependence of the nozzle admittance upon the half-angle, entrance Mach number, and radii of curvature can be determined.

4. NOZZLE ADMITTANCE THEORY

Crocco's theory [6] was used to obtain theoretical nozzle admittance values for comparison with the experimental data. In this study Crocco developed the following expression for the nozzle admittance:

$$y = \frac{-(\rho/\rho_0)\zeta}{(c/c_0)M^2\zeta + iS}, \tag{11}$$

where ζ is a complex quantity whose behavior is governed by the non-linear Riccati equation

$$\frac{d\zeta}{d\varphi} + \zeta^2 = A(\varphi)\zeta + B(\varphi), \tag{12}$$

where

$$A(\varphi) = \left[\left(\frac{c_0}{c}\right)^2 \frac{d(q/c_0)^2}{d\varphi} + 2i\frac{\omega r_c}{c_0}\right] \Big/ \left[\left(\frac{c}{c_0}\right)^2 - \left(\frac{q}{c_0}\right)^2\right],$$

$$B(\varphi) = -\left[\left(\frac{\omega r_c}{c_0}\right)^2 - i\frac{\gamma-1}{2}\left(\frac{\omega r_c}{c_0}\right)M^2\frac{d(q/c_0)^2}{d\varphi}\right] \Big/ \left[\left(\frac{c}{c_0}\right)^2 - \left(\frac{q}{c_0}\right)^2\right]$$

and φ is the non-dimensional steady-state velocity potential. Once ζ is determined from the integration of equation (12), the specific nozzle admittance is readily obtained from equation (11).

To determine ζ for given values of the non-dimensional frequency S and a specific nozzle contour, equation (12) must be numerically integrated. The major difficulty in this integration is that ζ can assume large values over certain ranges of φ, which causes numerical difficulties in the integration scheme. Crocco and Sirignano [6] noted this behavior and developed asymptotic solutions for ζ for use when these difficulties are encountered.

Instead of using the asymptotic theory, a different approach is employed in this study. The problem is resolved by defining a new independent variable

$$\tau = \frac{1}{\zeta}.$$

Thus, as ζ takes on very large values, τ tends toward zero. Introducing the definition of τ into equation (12) gives the following Riccati equation for τ:

$$\frac{d\tau}{d\phi} + A(\phi)\,\tau + B(\phi)\,\tau^2 = 1. \tag{13}$$

At those points where ζ becomes very large, equation (13) is integrated instead of equation (12) or (13). Equations (12) and (13) are singular at the throat; consequently the numerical integration must start at that point. Following the procedure used in reference [5], ζ, the mean flow variables, and the coefficients A and B are evaluated at the throat. These values are then used to obtain initial values for the initiation of the numerical integration. Equation (12) and the equations describing the behavior of the mean flow (6) are then integrated by a modified Adams predictor–corrector scheme, a Runge–Kutta scheme of order four being used to start the integration. During the integration the value of ζ is monitored. If the magnitude of ζ exceeds a value at which instabilities can occur in the integration scheme, the integration of equation (12) is terminated, the value of τ at that point is computed, and the integration proceeds with equation (13) being used. Similarly, should the magnitude of τ become excessively large, then the value of ζ is determined at that point and the integration proceeds with equation (12) being used. This process is repeated until the nozzle entrance plane is reached. A computer program which employs this procedure was written and used to calculate the theoretical nozzle admittance values for the nozzles investigated in this study.

5. RESULTS

The experimental values of the nozzle admittance are presented as functions of non-dimensional frequency S in Figures 3 through 6. The range of S covered in this investigation is from zero to the cut-off frequency of the first tangential mode (i.e., $S \simeq 1{\cdot}8$). For values of

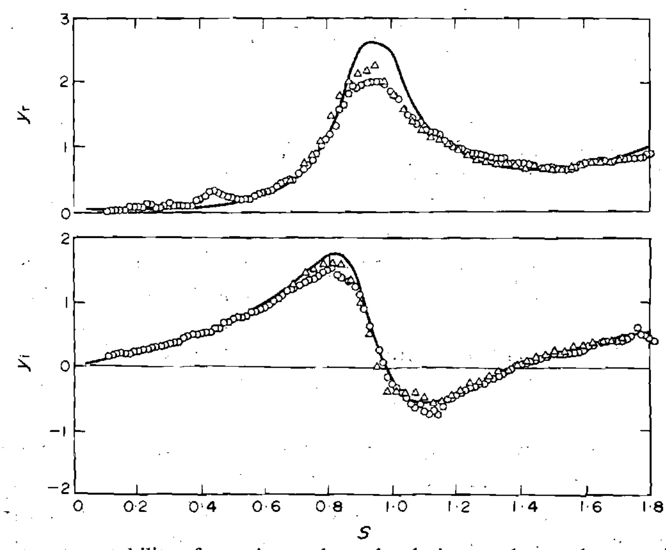

Figure 3. Test-to-test repeatability of experimental nozzle admittance data and comparison with theoretical predictions. $\theta_1 = 15°$, $M = 0{\cdot}08$, $r_{cc}/r_c = 0{\cdot}44$. ○, Experiment, test no. 1; △, experiment, test no. 2; ——, theory.

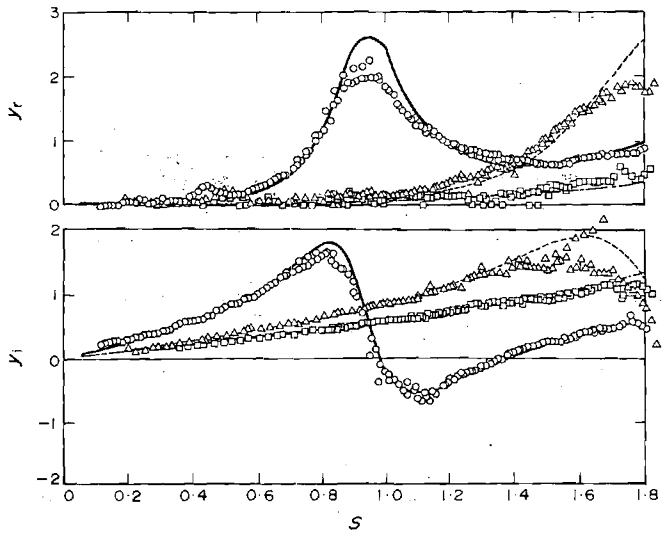

Figure 4. Effect of nozzle half-angle on the experimental and theoretical nozzle admittance values. $M = 0{\cdot}08$, $r_{cc}/r_c = 0{\cdot}44$. $\theta_1 = 15°$: ○, experiment; ——, theory. $\theta_1 = 30°$: △, experiment; ---, theory. $\theta_1 = 45°$: □, experiment; —·—, theory.

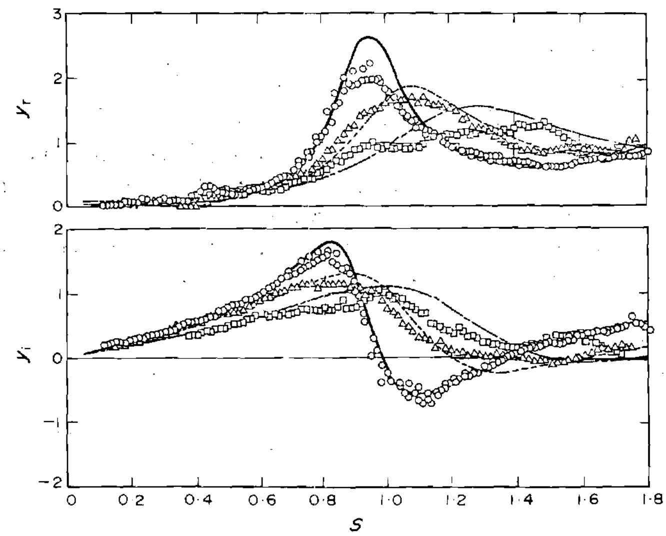

Figure 5. Effect of entrance Mach number on the experimental and theoretical nozzle admittance values. $\theta_1 = 15°$, $r_{cc}/r_c = 0{\cdot}44$. $M = 0{\cdot}08$: ○, experiment; ——, theory. $M = 0{\cdot}16$: △, experiment; ---, theory. $M = 0{\cdot}24$: □, experiment; ———, theory.

S higher than 1·8, the oscillations in the tube become three-dimensional and purely one-dimensional oscillations cannot be maintained in the impedance tube. The determination of nozzle admittances when the oscillations are three-dimensional is discussed in reference [2]. To indicate the repeatability and reliability of the experimental technique, data from two different tests are compared in Figure 3; the two sets of data are in close agreement. It is also shown in Figure 3 that the theoretical predictions compare quite well with the experimental data.

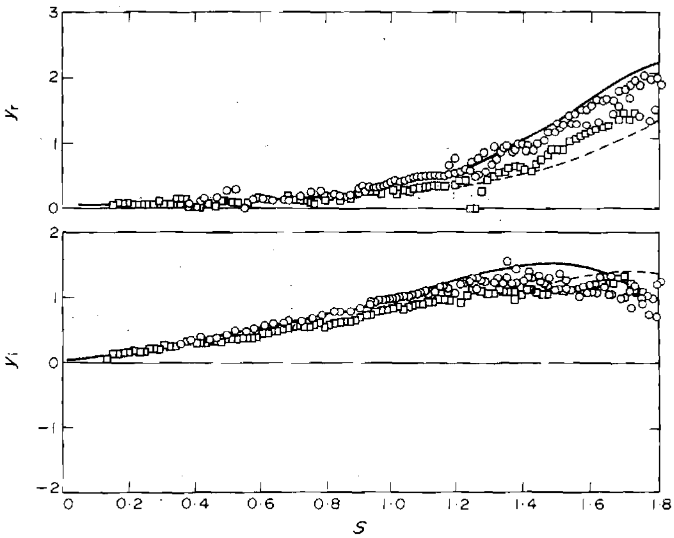

Figure 6. The effect of the ratio of the radius of curvature to chamber radius on the experimental and theoretical nozzle admittance values. $M = 0{\cdot}16$, $\theta_1 = 30°$. $r_{cc}/r_c = 1{\cdot}0$: ○, experiment; ——, theory. $r_{cc}/r_c = 0{\cdot}44$: □, experiment; ---, theory.

The effects of changing the nozzle geometry and entrance Mach number on the admittance values are presented in Figures 4, 5, and 6. For $M = 0{\cdot}08$ and $r_{cc}/r_c = 0{\cdot}44$, increasing θ_1 tends to increase the frequency at which the maximum values of the real and imaginary parts of the admittance occur, as shown in Figure 4. The effect of varying the entrance Mach number is shown in Figure 5 for $\theta_1 = 15°$ and $r_{cc}/r_c = 0{\cdot}44$. The effect of changing the ratio r_{cc}/r_c from 0·44 to 1·0 is shown in Figure 6 for nozzles with $\theta_1 = 30°$ and $M = 0{\cdot}08$. Examination of Figures 3 through 6 shows that the theoretical and experimental results are, in general, in good agreement to within experimental error and the limitations of the impedance tube theory.† These data also show that at low frequencies where the ratio of the length of the nozzle convergent section to the wavelength is small, the nozzle admittances are almost independent of frequency. At these frequencies these nozzles respond in a quasi-steady manner.

6. CONCLUSIONS

Based on the results of this investigation, the modified impedance tube technique can be used to determine the admittance of a duct termination in the presence of a mean flow. In the present study, quantitative nozzle admittance data were obtained using this technique for a family of nozzles with different entrance Mach numbers, different convergence angles, and different radii of curvature. The theoretical and experimental nozzle admittance data are in close agreement, indicating that Crocco's nozzle admittance theory can be used to predict nozzle admittances needed for longitudinal stability analyses

† For example, in the theory a uniform velocity profile across the tube is assumed, and the presence of a boundary layer near the walls is neglected. However, the good agreement between the theoretical and experimental data obtained in this study suggests that when the impedance tube diameter is large the shear flow near the wall has little effect upon the measured data.

REFERENCES

1. L. Crocco and S. I. Cheng 1956 *AGARDograph No.* 8, *Chapter* I *and Appendix B.* Theory of combustion instability and its experimental verification. London: Butterworth Publications.
2. B. T. Zinn, W. A. Bell, B. R. Daniel and A. J. Smith, Jr. 1973 *American Institute of Aeronautics and Astronautics Journal* **11**, 267. Experimental determination of three-dimensional liquid rocket nozzle admittances.
3. L. Crocco 1965 *Tenth Symposium (International) on Combustion, Pittsburgh, Pennsylvania: Combustion Institute*, 1101–1128. Theoretical studies on liquid-propellant rocket instability.
4. H. S. Tsien 1952 *American Rocket Society Journal* **22**, 139. The transfer function of rocket motors.
5. L. Crocco 1953 *Aerotecnica Roma* **33**, 46. Supercritical gaseous discharge with high frequency oscillations.
6. L. Crocco and W. A. Sirignano 1967 *AGARDograph No.* 117. Behavior of supercritical nozzles under three-dimensional oscillatory conditions. London: Butterworth Publications.
7. A. J. Smith and F. H. Reardon 1968 *Aerojet-General Technical Report No. AFRPL-TR*-67-314, *Vol.* I. The sensitive time lag theory and its application to liquid rocket combustion instability problems.
8. L. Crocco, R. Monti and J. Grey 1961 *American Rocket Society Journal* **31**, 771. Verification of nozzle admittance theory by direct measurement of the admittance parameter.
9. F. G. Buffum, G. L. Dehority, R. O. Slates and E. W. Price 1966 *China Lake, California: Naval Ordnance Test Station, NOTS TP* 3932. Acoustic losses of a subscale cold-flow rocket motor for various "J" values.
10. F. E. C. Culick and G. L. Dehority 1968 *China Lake, California: Naval Weapons Center, NWC Report No.* 4544. An analysis of axial acoustic waves in a cold-flow rocket.
11. R. A. Scott 1946 *Proceedings of the Physical Society* **58**, 253. An apparatus for accurate measurement of the acoustic impedance of sound absorbing materials.
12. W. K. R. Lippert 1953 *Acustica* **3**, 153. The practical representation of standing waves in an acoustic impedance tube.
13. R. M. Morse and K. U. Ingard 1968 *Theoretical Acoustics.* New York: McGraw-Hill Book Company, Inc. See pp. 467 ff.
14. W. A. Bell 1972 *Ph.D. Thesis, Georgia Institute of Technology.* Experimental determination of three-dimensional liquid rocket nozzle admittances.
15. W. S. Gately and R. Cohen 1969 *Journal of the Acoustical Society of America* **46**, 6. Methods for evaluating the performance of small acoustic filters.
16. R. C. Pfahl and B. J. Mitchel 1970 *American Institute of Aeronautics and Astronautics Journal* **8**, 1046. Nonlinear regression methods for simultaneous property measurement.
17. D. W. Marquardt 1963 *Journal of the Society for Industrial and Applied Mathematics* **11**, 431. An algorithm for least-squares estimation of nonlinear parameters.

APPENDIX

NOMENCLATURE

- A constant defined by equation (3), lbf/in^2
- A_+ amplitude of a pressure wave moving in the positive z direction, lbf/in^2
- A_- amplitude of a pressure wave moving in the negative z direction, lbf/in^2
- $A(\varphi)$, $B(\varphi)$ variable coefficients defined in equation (12)
- c steady-state speed of sound, ft/s
- E_i experimentally measured pressure amplitude at the ith location along the impedance tube, lbf/in^2
- f frequency, Hz
- i $\sqrt{-1}$, imaginary unit
- k wave number $= \omega/c$, radian/ft